Part II:
Introduction to Interferometric Synthetic Aperture Radar

Zhong Lu
US Geological Survey
Email: lu@usgs.gov
http://volcanoes.usgs.gov/activity/methods/insar/zhong.php

Acknowledgement
- Contribution by many colleagues.
- Funding from USGS and NASA.
- Original SAR data are copyrighted ESA, CSA, JAXA , or DLR

InSAR : How It Works

- About InSAR
- InSAR processing steps
- InSAR artifacts
- Multi-interferogram processing

Synthetic aperture radar is an active microwave sensor

- The electromagnetic wave is transmitted from the satellite. The wave propagates through the atmosphere, interacts with the Earth surface. Part of the energy is returned back and recorded by the satellite.

- By sophisticated image processing technique, both the intensity and phase of the reflected (or backscattered) signal can be calculated. So, essentially, a complex-valued SAR image represents the reflectivity of the ground surface.

- The amplitude or intensity of the SAR image is primarily controlled by terrain slope, surface roughness, and dielectric constants, while the phase of the SAR image is primarily controlled by the distance from satellite antenna to ground targets and partially controlled by the atmospheric delays as well as the interaction of microwave with ground surface.

Interferometric SAR (InSAR)

• **InSAR** combines two or more SAR images of the same area acquired from similar vantage points at different times to produce an **interferogram**.

• The **interferogram**, depicting the changes in distance between the radar and the ground, can be further processed to

i) image **ground deformation** at a horizontal resolution of tens of meters over large areas with centimeter to sub-centimeter precision under favorable conditions.

<u>or</u>

ii) generate **digital elevation model** at a horizontal resolution of tens of meters with a few meters accuracy.

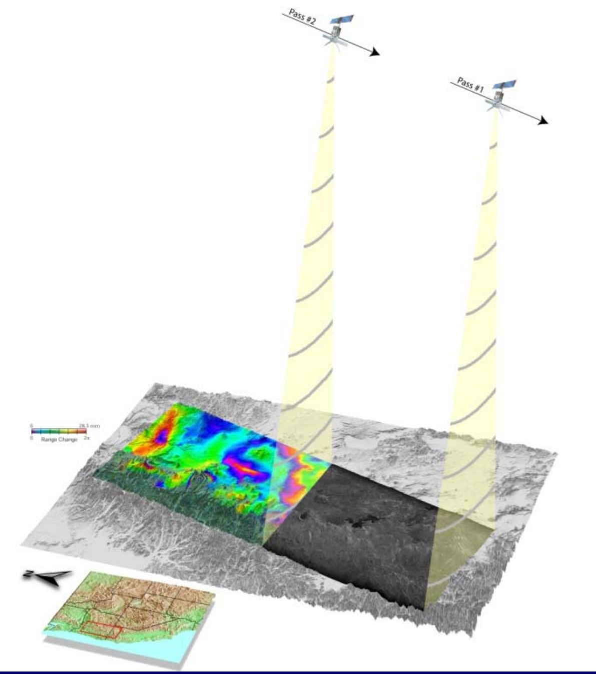

Courtesy of C. Wicks

InSAR is all about interference fringes

Interferometric fringes are daily phenomena

Interferometric fringes on an oil film

InSAR is all about interference fringes

Interferometric fringes are daily phenomena

Interferometric fringes on a CD

InSAR is all about interference fringes

Interferometric fringes are daily phenomena

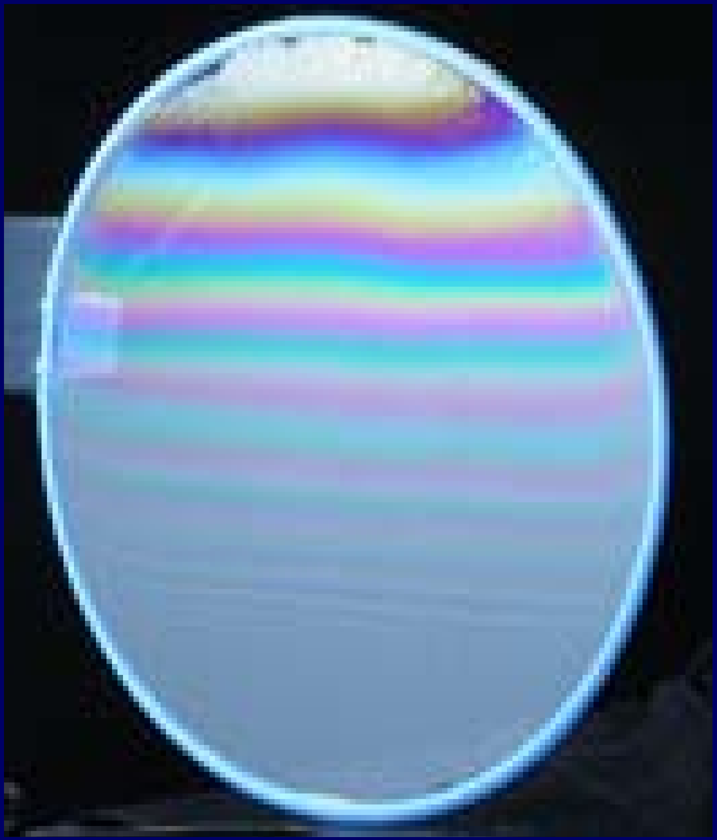

Interferometric fringes on a soap bubble

Thomas Young – Discovered interferometric phenomenon in 1801 and coined the term of “interference fringes” to describe the color bands

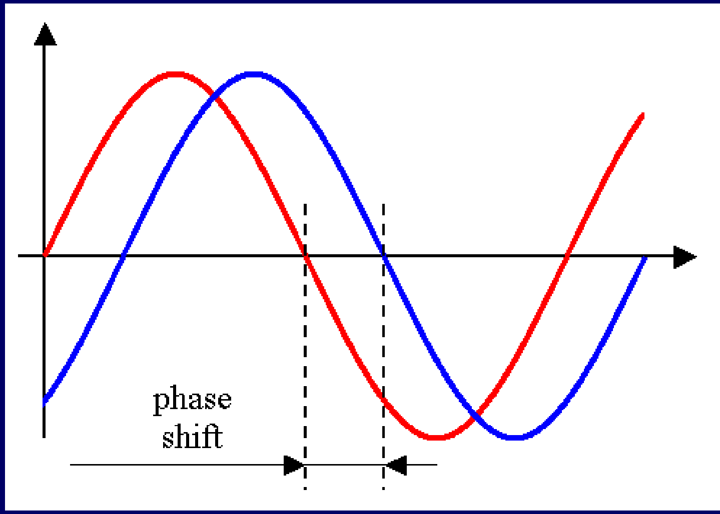

Two waves are said to be in phase when corresponding points of each reach maximum or minimum displacements at the same time. If the crests of two waves pass the same point at the same time, they are in phase for that position. If the crest of one and the trough of the other pass the same point at the same time, the phase angles differ by 180° and the waves are said to be of opposite phase.

InSAR is all about interference fringes

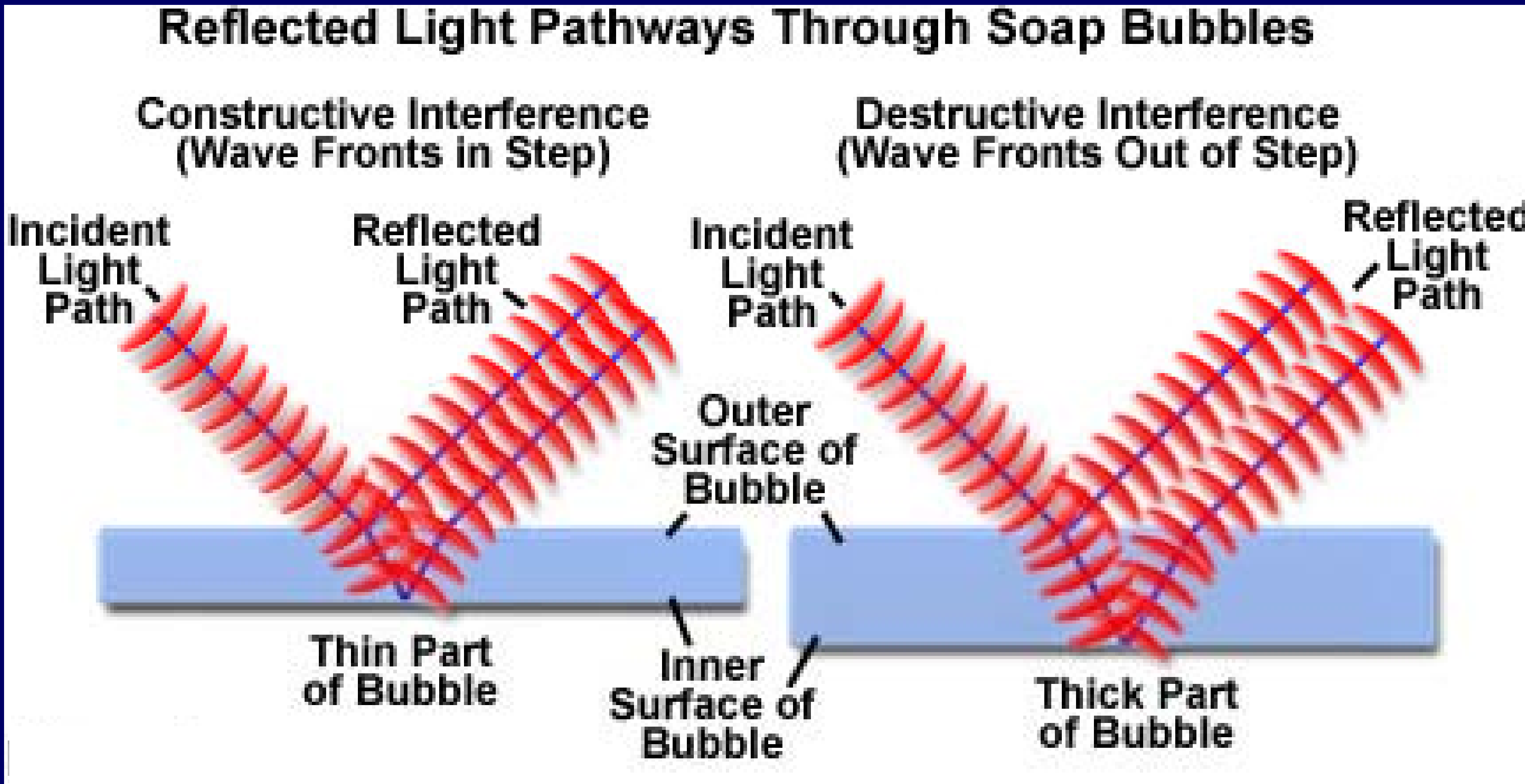

Interferometric fringes on soap bubbles

Interference colors on a soap bubble

White light is made up of all colors of different wavelengths. If one of these colors is subtracted from white light, the complementary color is seen.

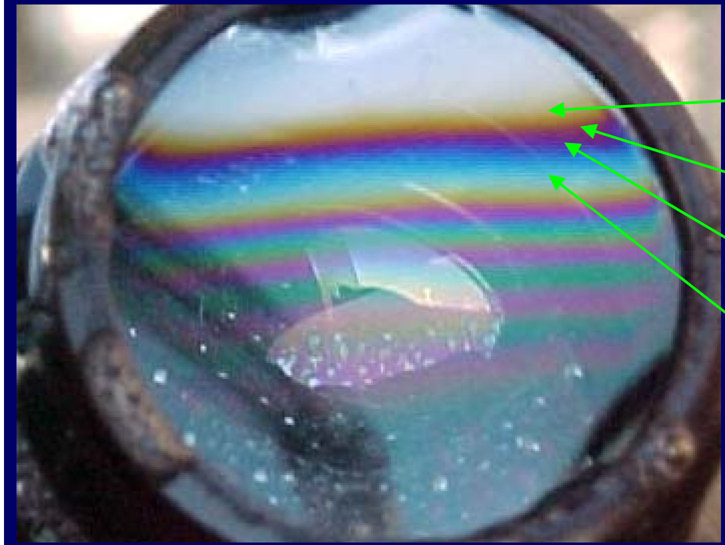

- **blue is cancelled, leaving yellow**
- **green is cancelled, leaving magenta**
- **yellow is cancelled, leaving blue**
- **red is cancelled, leaving a blue-green**

How InSAR Works

- Traditionally, distance measurement is done by precise timing.
- Accuracy is several meters for spaceborne sensors.

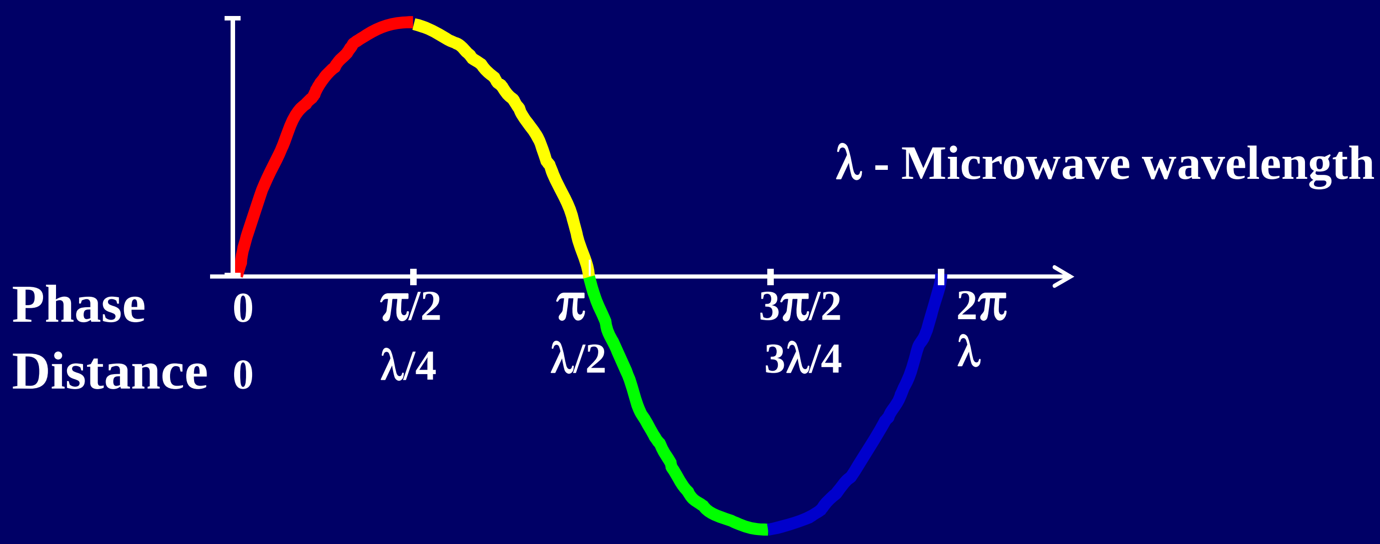

- In interferometry, the <u>distance</u> from the satellite to the ground is achieved by measuring the <u>phase</u> of the electromagnetic wave.
- Accuracy is centimeters to sub-centimeters.

How InSAR Works

- InSAR utilizes phase information of radar wave to achieve high-accuracy measurement
- Phase is a function of distance from satellite to ground (range)

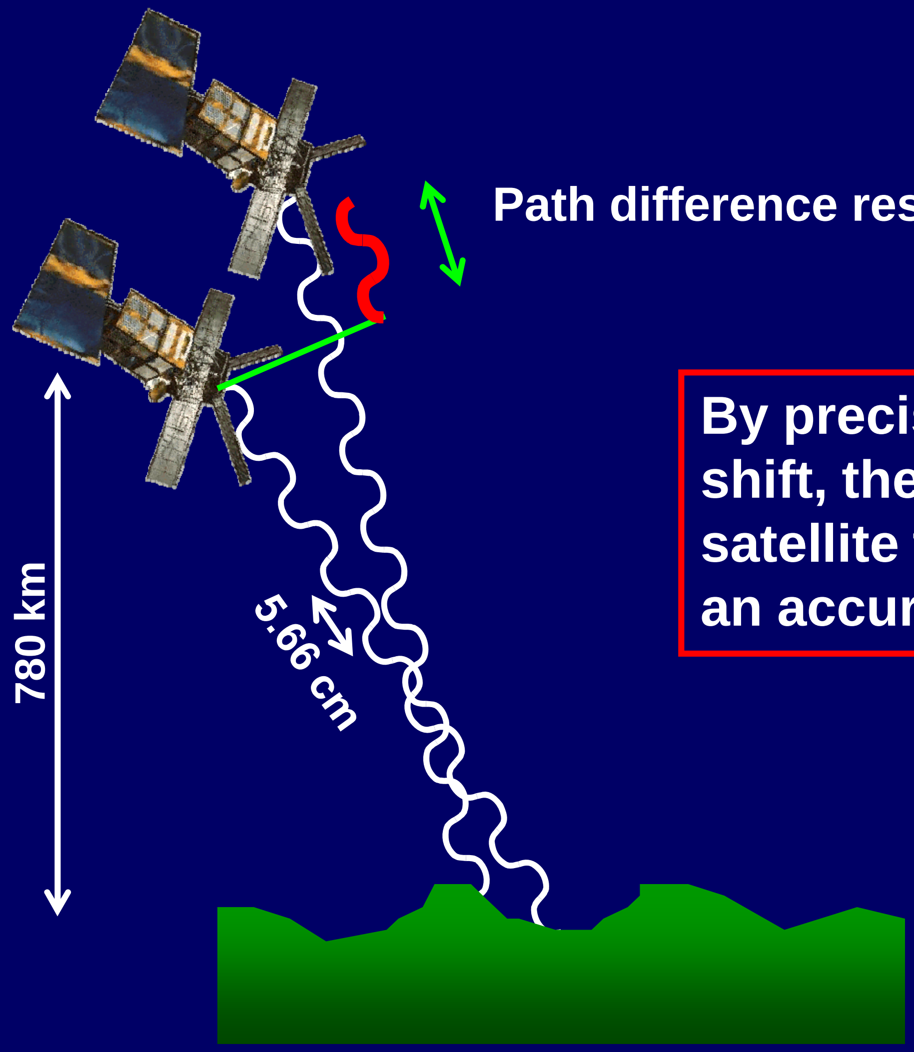

By precisely measuring the phase shift, the change in distance from satellite to ground can be calculated to an accuracy of sub-wavelength.

How InSAR Works

- InSAR utilizes phase information of radar wave to achieve high-accuracy measurement
- Phase is a function of distance from satellite to ground (range)

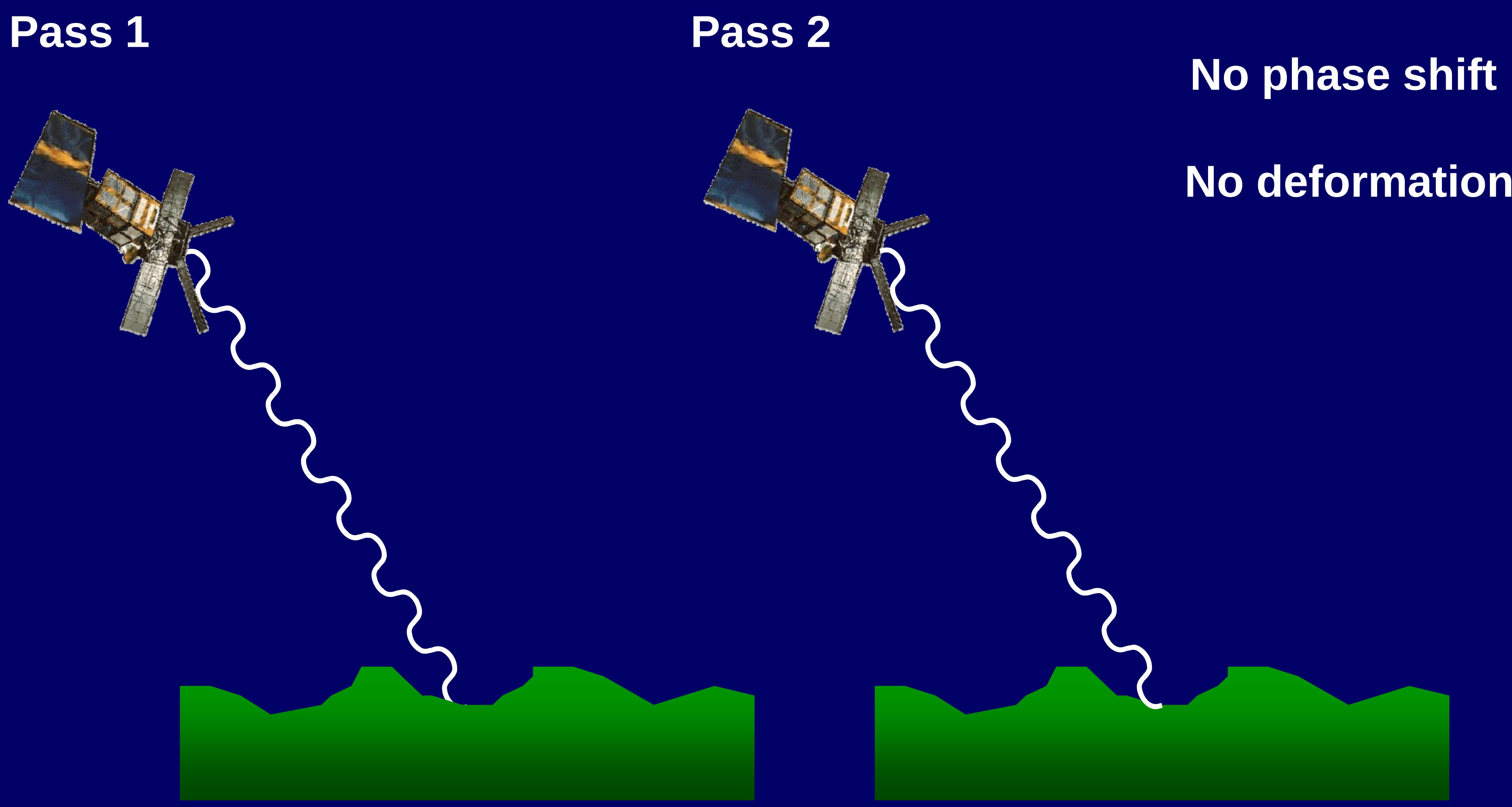

How InSAR Works

- InSAR utilizes phase information of radar wave to achieve high-accuracy measurement
- Phase is a function of distance from satellite to ground (range)

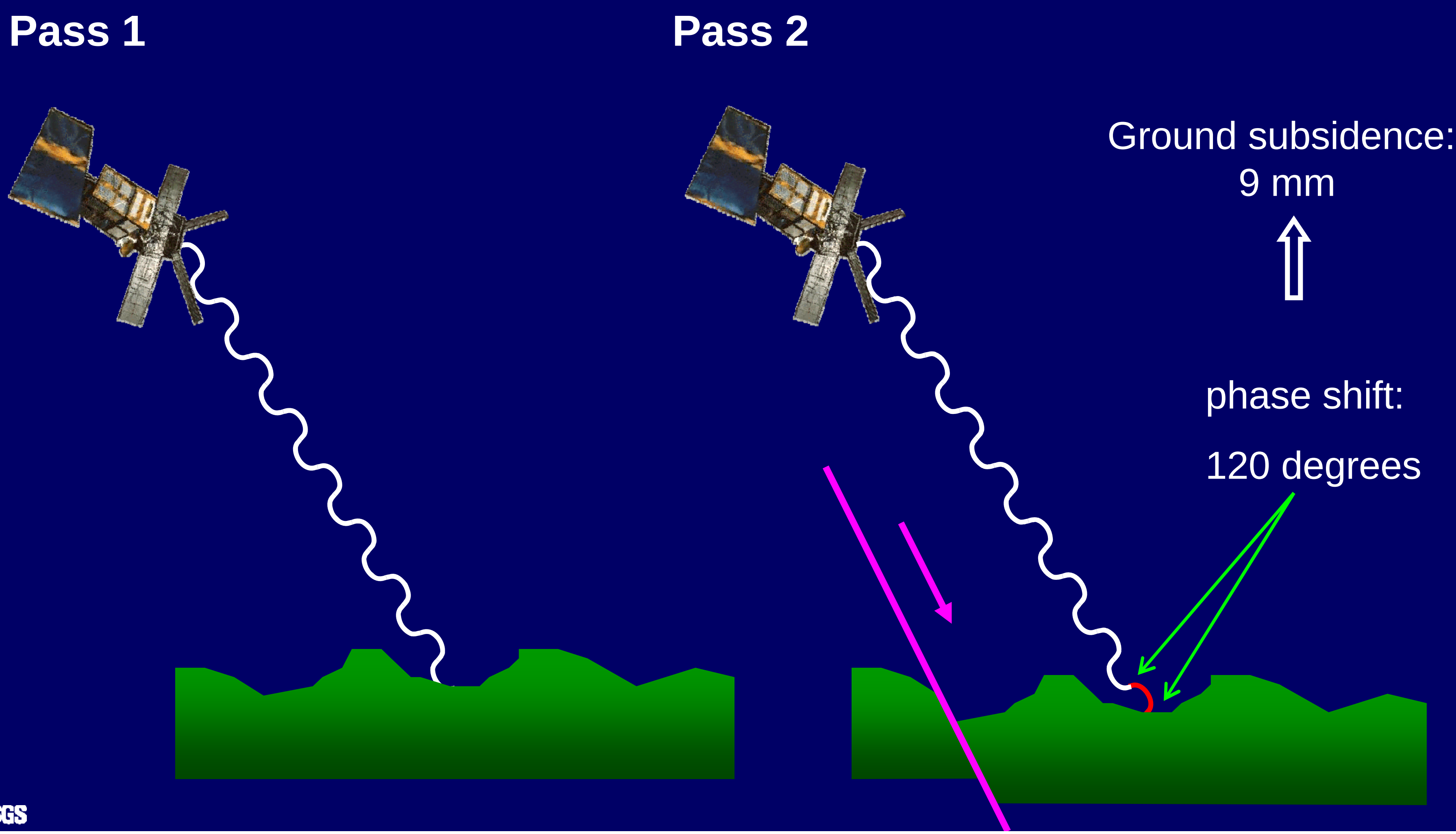

InSAR Processing Step 1 - Two SAR images

Image 1: Oct. 4, 1995 | **Image 2: Oct. 9, 1997**

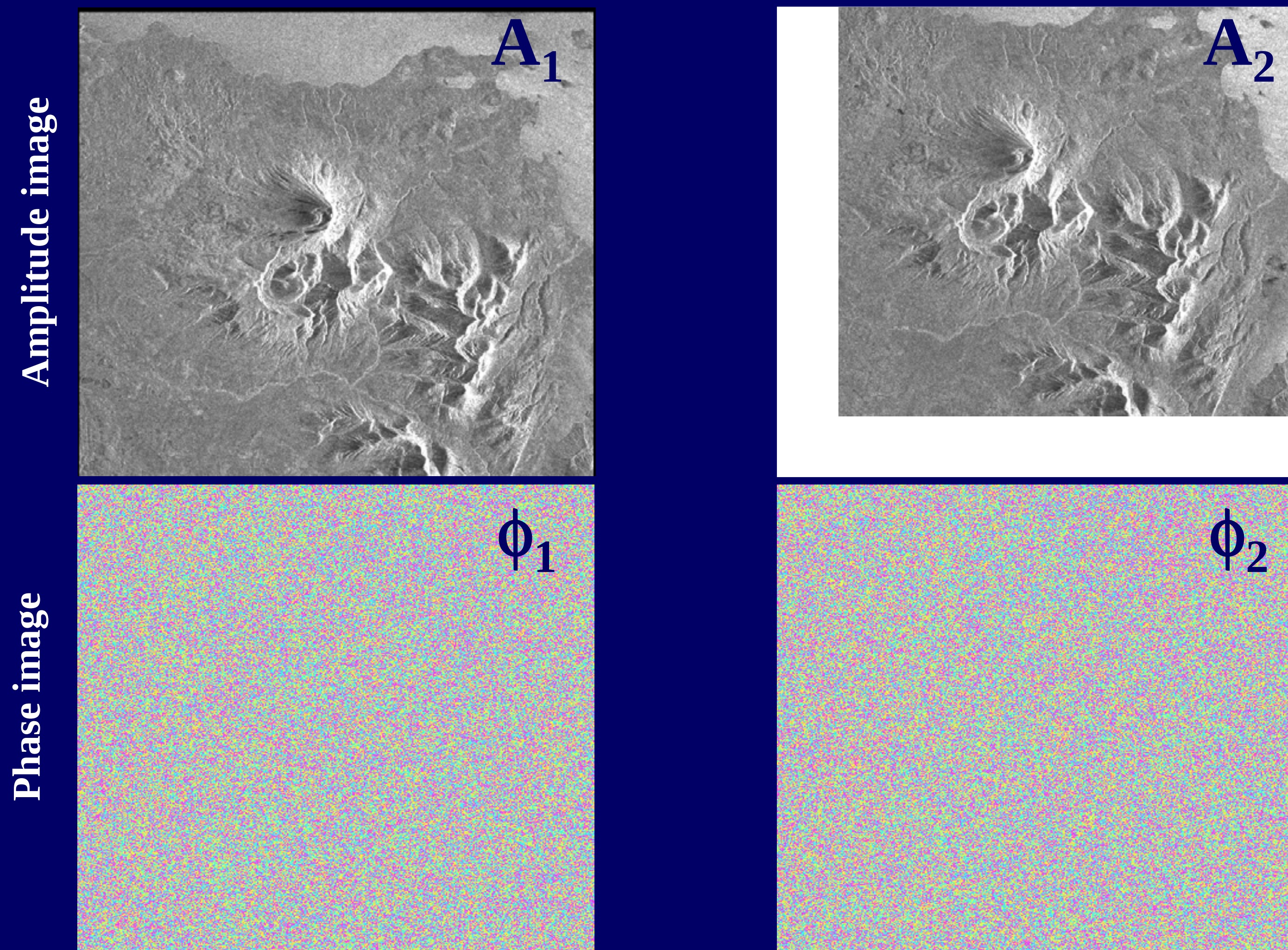

$$\phi_1 = -\frac{4\pi}{\lambda} r_1 + \varepsilon_1$$

$$\phi_2 = -\frac{4\pi}{\lambda} r_2 + \varepsilon_2$$

0 — 360°

Images are ~28 km by 25 km

InSAR Processing Step 1 - Two SAR images

Image 1: Oct. 4, 1995

$$\phi_1 = -\frac{4\pi}{\lambda} r_1 + \varepsilon_1$$

Image 2: Oct. 9, 1997

$$\phi_2 = -\frac{4\pi}{\lambda} r_2 + \varepsilon_2$$

- **ε is the sum of phase shift due to the interaction between the incident radar wave and scatterers within the resolution cell.**
- **Because the backscattering phase (ε) is a randomly distributed (unknown) variable, the phase value (ϕ) in a single SAR image cannot be used to calculate the range (r) and is of no practical use**

InSAR Processing Step 2 - SAR images co-registration

Image 1: Oct. 4, 1995 | **Image 2: Oct. 9, 1997**

Amplitude image

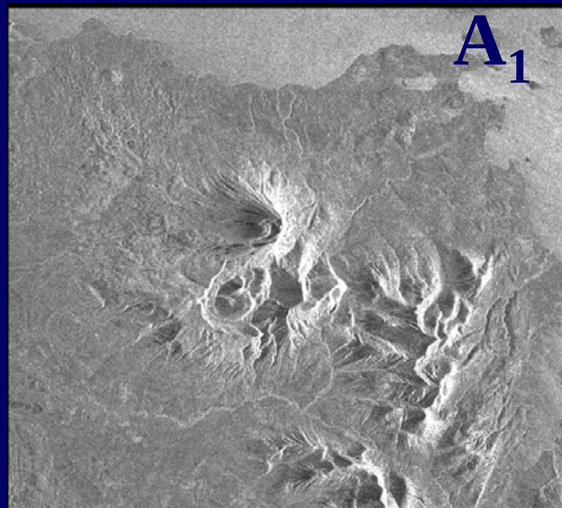

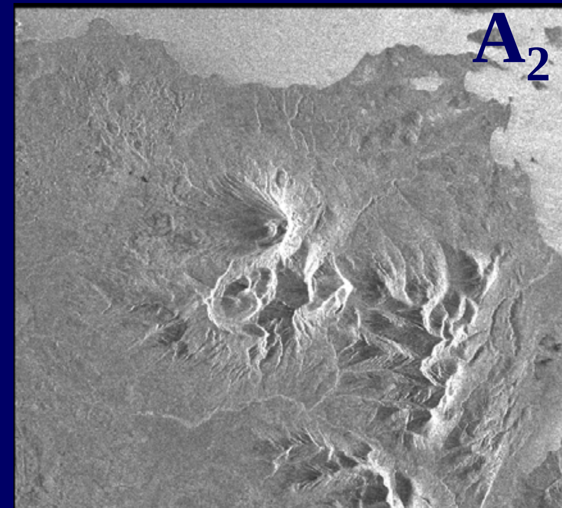

Phase image

$$\phi_1 = -\frac{4\pi}{\lambda} r_1 + \varepsilon_1$$

$$\phi_2 = -\frac{4\pi}{\lambda} r_2 + \varepsilon_2$$

0 — 360°

Images are ~28 km by 25 km

InSAR Processing Step 3 - Original interferogram: $\Delta\phi_{init} = \phi_1 - \phi_2$

$$\phi = \phi_1 - \phi_2 = -\frac{4\pi(r_1 - r_2)}{\lambda} + (\varepsilon_1 - \varepsilon_2)$$

Original interferogram

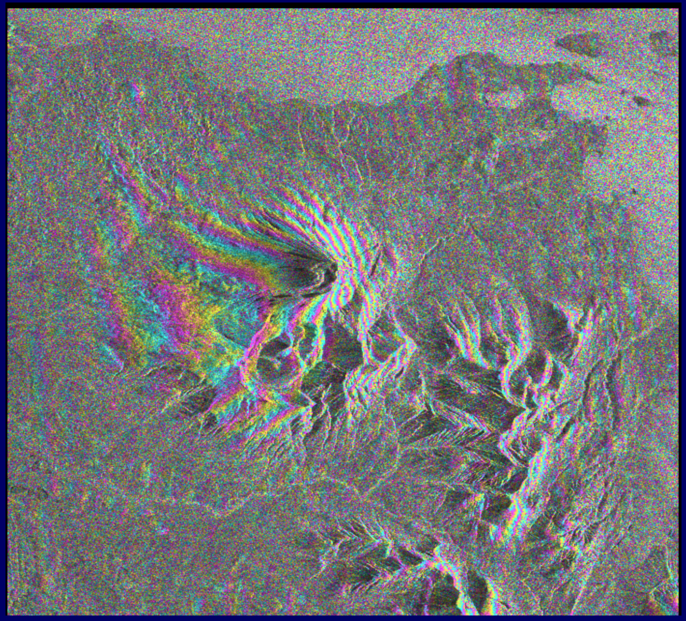

0 360°

The fundamental assumption in repeat-pass InSAR is that the scattering characteristics of the ground surface remain undisturbed.

Assume $\varepsilon_1 \approx \varepsilon_2$

$$\phi = \phi_1 - \phi_2 = -\frac{4\pi(r_1 - r_2)}{\lambda}$$

InSAR Processing Step 3 - Original interferogram: $\Delta\phi_{init} = \phi_1 - \phi_2$

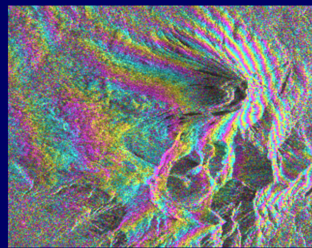

$$\phi = \phi_1 - \phi_2 = -\frac{4\pi(r_1 - r_2)}{\lambda}$$

- Nominal values for the range difference, $(r_1 - r_2)$, extend from a few meters to several hundred meters.

- The SAR wavelength (λ) is of the order of several centimeters.

- Because the measured interferometric phase value (ϕ) is modulated by 2π, ranging from $-\pi$ to π, there is an ambiguity of many cycles (i.e., numerous 2π values) in the interferometric phase value. Therefore, the phase value of a single pixel in an interferogram is of no practical use.

- However, the change in range difference, $\delta(r_1 - r_2)$, between two neighboring pixels that are a few meters apart is normally much smaller than the SAR wavelength. So the phase difference between two nearby pixels, $\delta\phi$, can be used to infer the range distance difference ($r1 - r2$) to a sub-wavelength precision.
- This explains how InSAR uses the phase difference to infer the change in range distance to an accuracy of centimeters or millimeters.

InSAR Processing Step 4 - Phase difference caused by difference of satellite positions over a flat earth: $\phi_{flat\text{-}earth}$

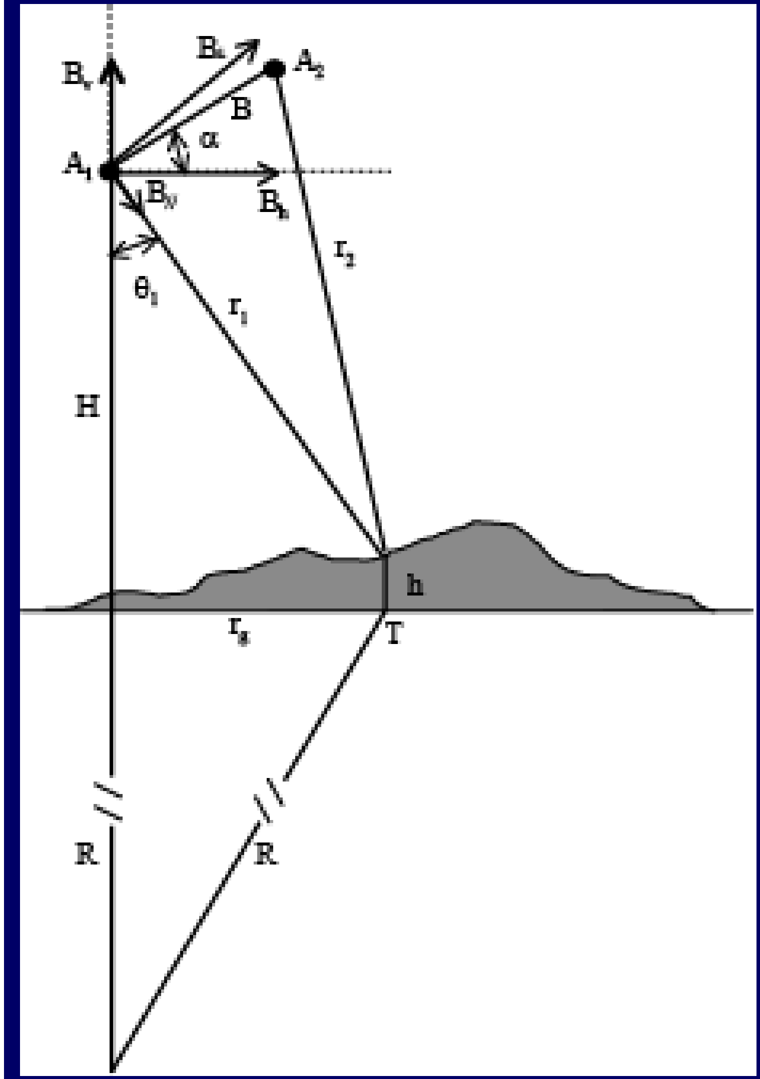

$$r_1 = \sqrt{(H+R)^2 + (R+h)^2 - 2(H+R)(R+h)\cos(\frac{r_g}{R})}$$

$$\theta_1 = \arccos\left[\frac{(H+R)^2 + r_1^2 - (R+h)^2}{2(H+R)r_1}\right]$$

h = 0

$$\phi_{flat-earth} = -\frac{4\pi}{\lambda}(r_1 - r_2) = \frac{4\pi}{\lambda}(\sqrt{r_1^2 - 2(B_h \sin\theta_1 - B_v \cos\theta_1)r_1 + B^2} - r_1)$$

USGS

InSAR Processing Step 4 - Phase difference caused by difference of satellite positions over a flat earth: $\phi_{flat-earth}$

Flat-earth interferogram

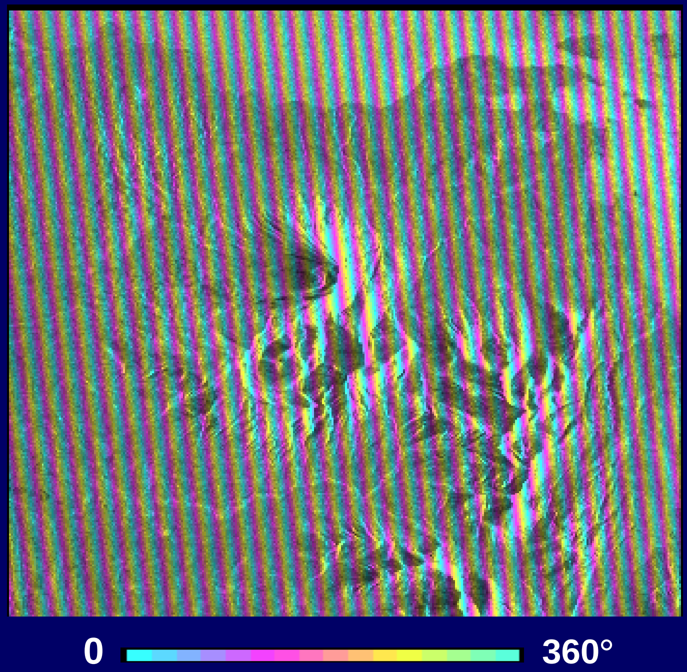

InSAR Processing Step 5 - Flattened interferogram: $\Delta\phi_{init} - \phi_{flat\text{-}earth}$

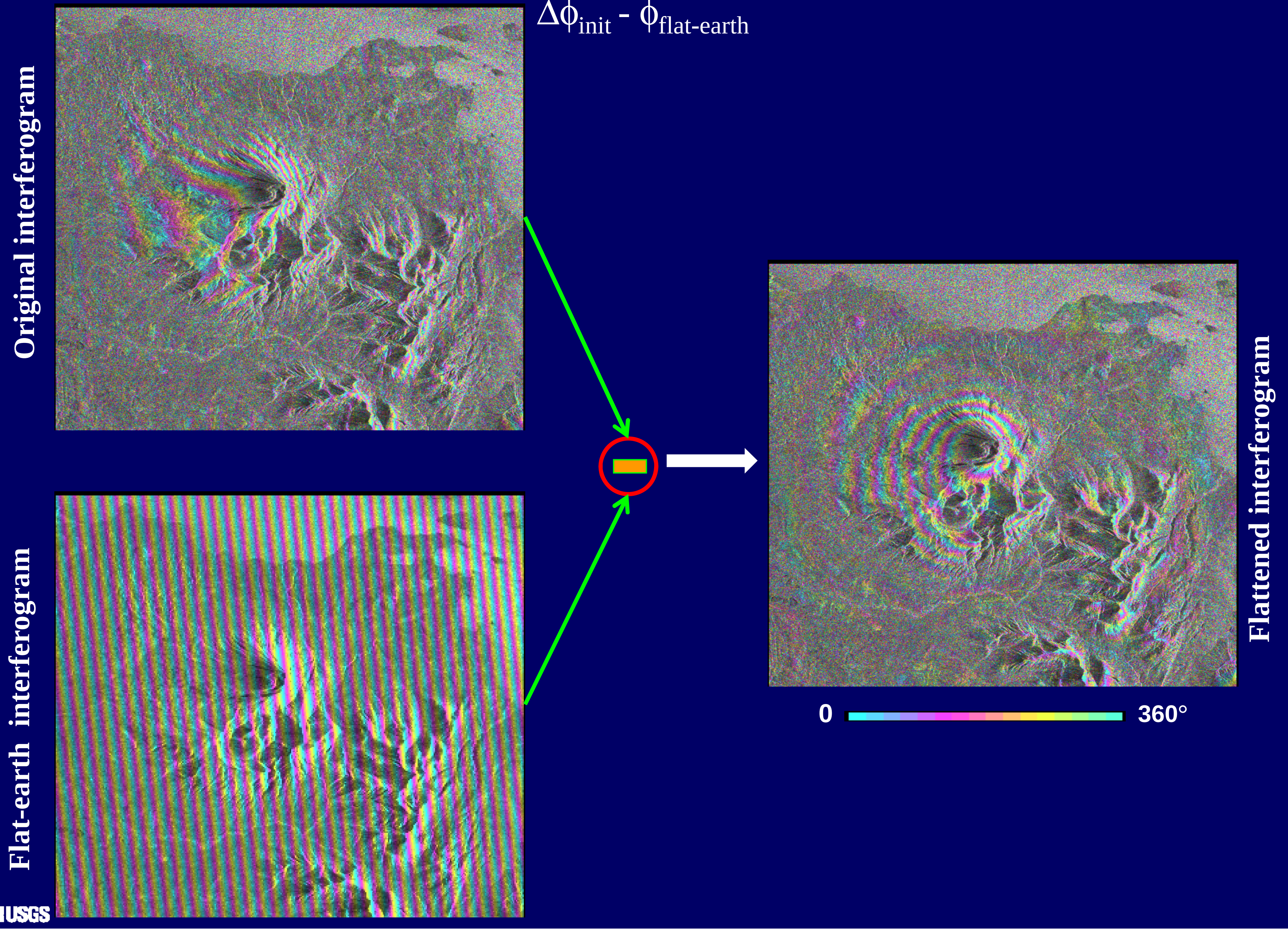

USGS

InSAR Processing Step 5 - Flattened interferogram: $\Delta\phi_{init} - \phi_{flat\text{-}earth}$

Flattened interferogram

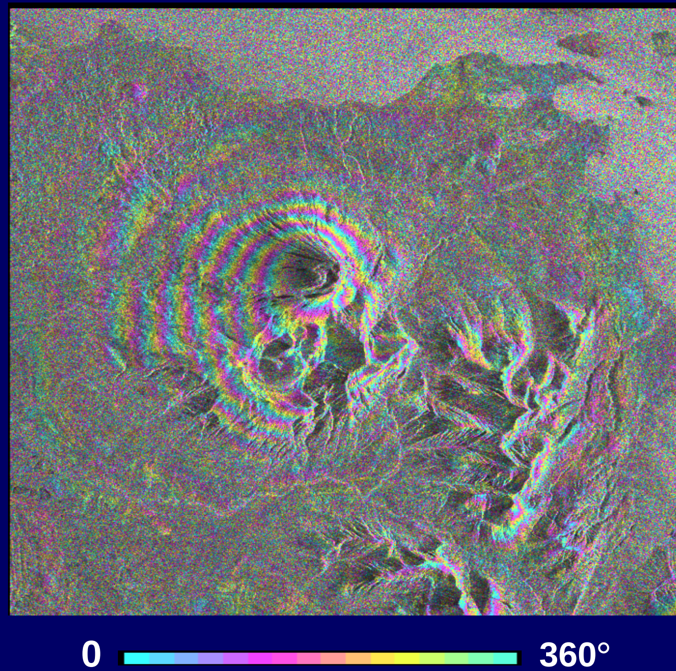

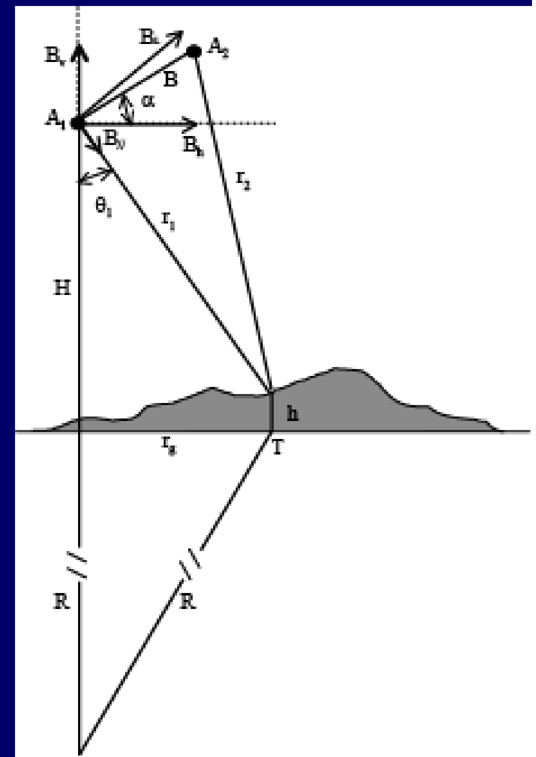

$$\Delta\phi_{init} - \phi_{flat-earth} = -\frac{4\pi}{\lambda}\frac{B\cos(\theta_1-\alpha)}{r_1\sin\theta_1}h + \phi_{def} = -\frac{4\pi}{\lambda}\frac{B_\perp}{H\tan\theta_1}h + \phi_{def}$$

For the ERS-1/-2 satellites, *H* is about 800 km, θ_1 is about 23° ±3°, λ is 5.66 cm, and $B_\perp$ should be less than 1,100 m for a coherent interferogram.

$$\Delta\phi_{init} - \phi_{flat-earth} \approx -\frac{2\pi}{9600}B_\perp h + \phi_{def}$$

InSAR Processing Step 5 - Flattened interferogram: $\Delta\phi_{init} - \phi_{flat\text{-}earth}$

For the ERS-1/-2 satellites, H is about 800 km, θ_1 is about 23° ±3°, λ is 5.66 cm, and $B_\perp$ should be less than 1,100 m for a coherent interferogram.

$$\Delta\phi_{init} - \phi_{flat-earth} \approx -\frac{2\pi}{9600} B_\perp h + \phi_{def}$$

If ϕ_{def} is negligible in the above equation, the phase value can be used to calculate height h.

$$\Delta\phi_{init} - \phi_{flat-earth} \approx -\frac{2\pi}{9600} B_\perp h$$

This explains how InSAR can be used to produce an accurate DEM over with a vertical resolution of meters over a large region.

InSAR Processing Step 5 - Flattened interferogram: $\Delta\phi_{init} - \phi_{flat\text{-}earth}$

$$\Delta\phi_{init} - \phi_{flat-earth} \approx -\frac{2\pi}{9600} B_{\perp} h - \frac{4\pi}{\lambda} d_{def}$$

- For an interferogram with $B\perp$ of 100 m, 1 m of topographic relief produces a phase value of about 4°.
- However, producing the same phase value requires only 0.3 mm of surface deformation.
- Therefore, it is evident that the interferogram phase value can be much more sensitive to changes in topography (i.e., the surface deformation d_{def}) than to the topography itself (i.e., h).
- This explains why repeat-pass InSAR is capable of detecting surface deformation at a theoretical accuracy of sub-centimeters.

InSAR Processing Step 6 - Topography-only interferogram: ϕ_{topo}

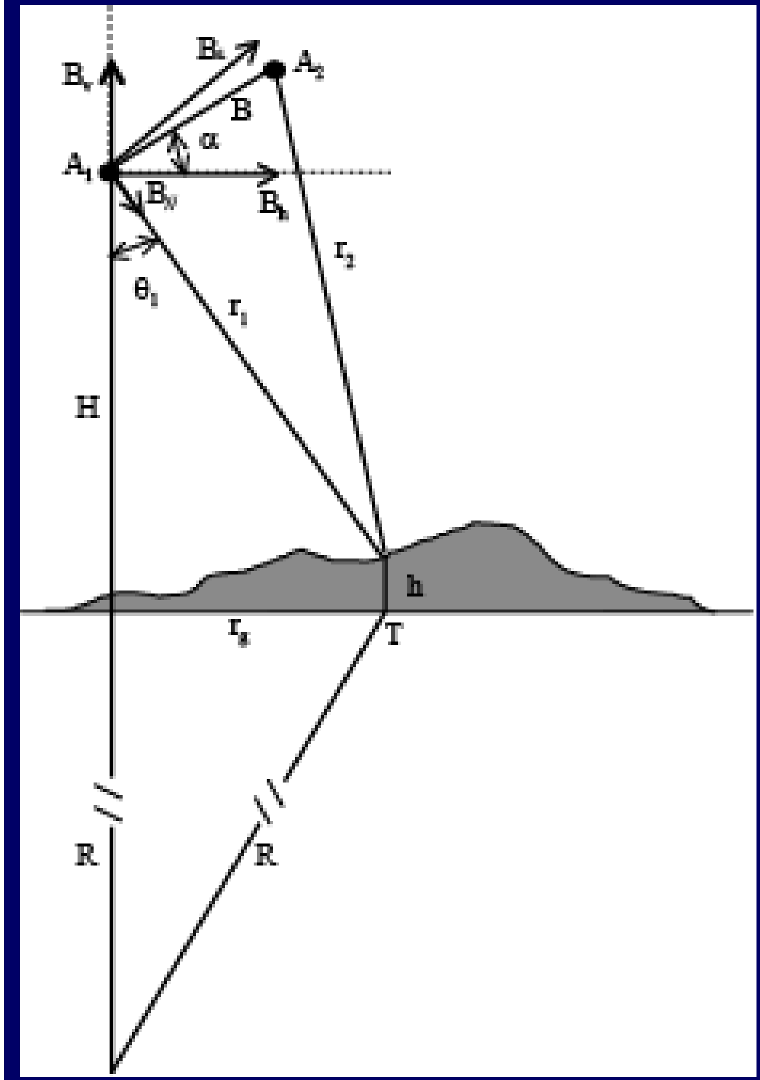

$$r_1 = \sqrt{(H+R)^2 + (R+h)^2 - 2(H+R)(R+h)\cos(\frac{r_g}{R})}$$

$$\theta_1 = \arccos\left[\frac{(H+R)^2 + r_1^2 - (R+h)^2}{2(H+R)r_1}\right]$$

$$\phi_{topo} = -\frac{4\pi}{\lambda}(r_1 - r_2) = \frac{4\pi}{\lambda}(\sqrt{r_1^2 - 2(B_h \sin\theta_1 - B_v \cos\theta_1)r_1 + B^2} - r_1)$$

USGS

InSAR Processing Step 6 - Topography-only interferogram: ϕ_{topo}

DEM

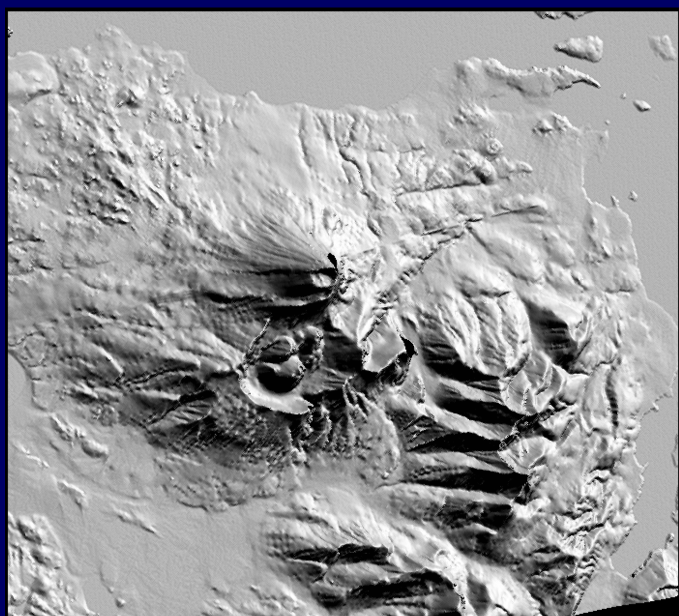

InSAR Imaging Geometry & Parameters

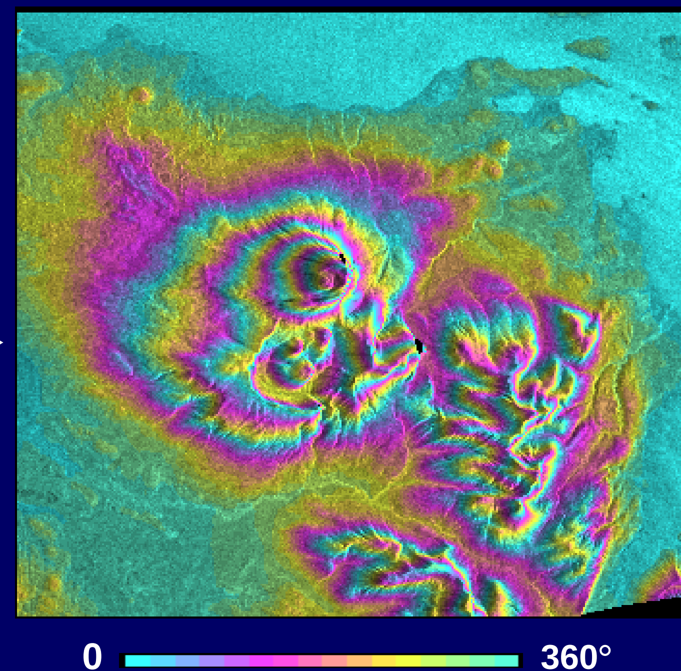

Topography-only interferogram

InSAR Processing Step 7 - Deformation interferogram (+noise):

$$\Delta\phi_{def} = \Delta\phi_{init} - \phi_{flat\text{-}earth} - \phi_{topo}$$

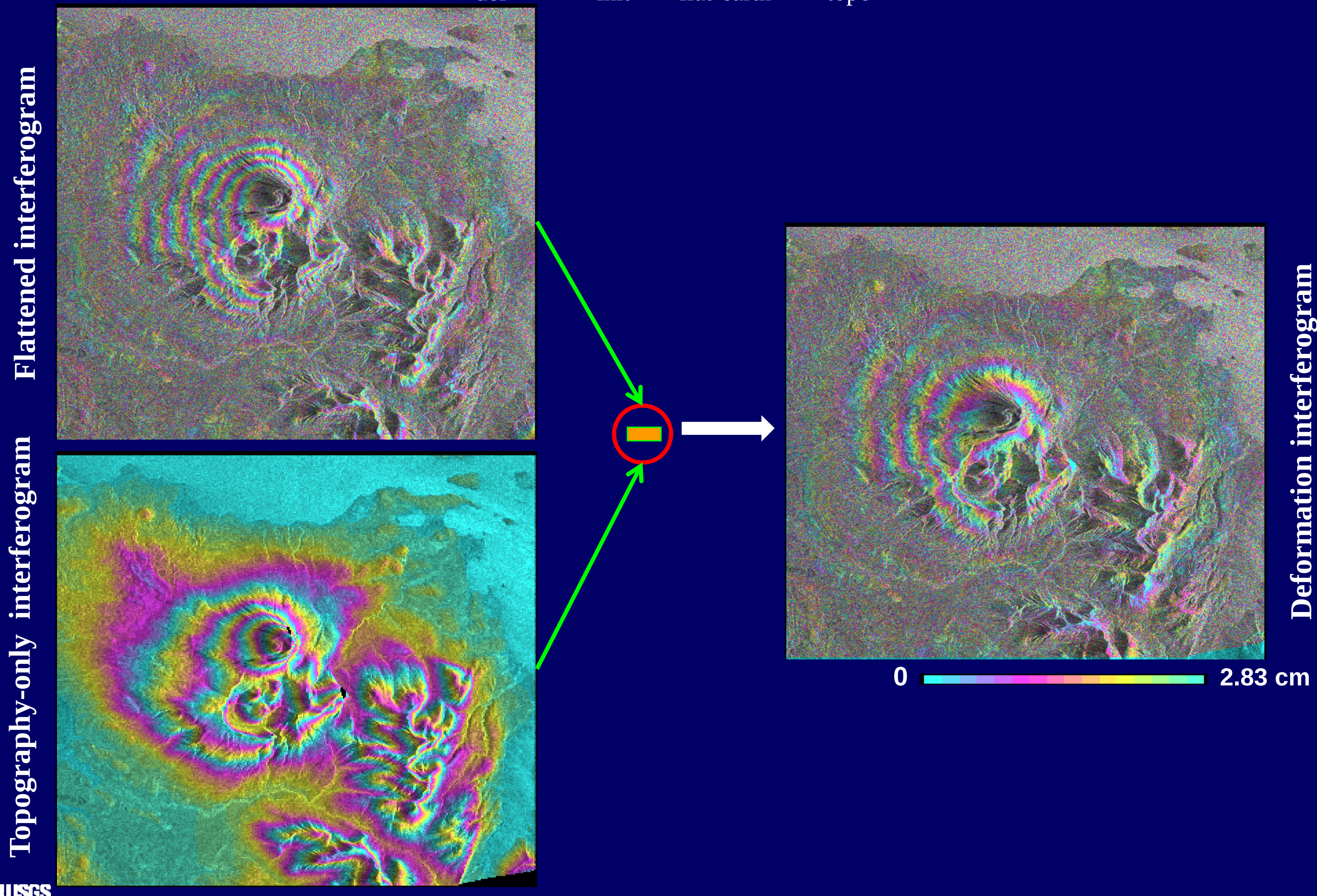

InSAR Processing Step 8 - Deformation interferogram with noise reduction:

$$\Delta\phi_{def} = \Delta\phi_{init} - \Delta\phi_{flat} - \Delta\phi_{topo}$$

Filtered deformation interferogeram

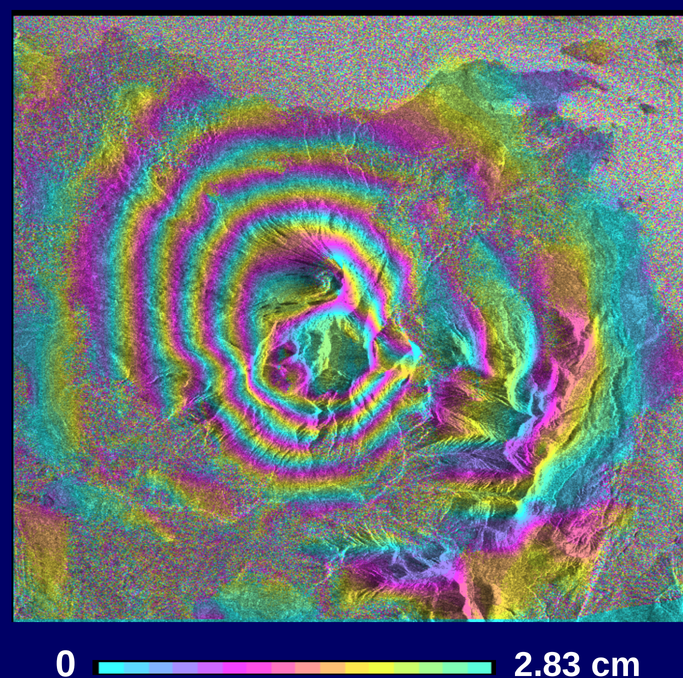

InSAR Processing Step 9 - Deformation interferogram in map projection (including phase unwrapping and geocoding)

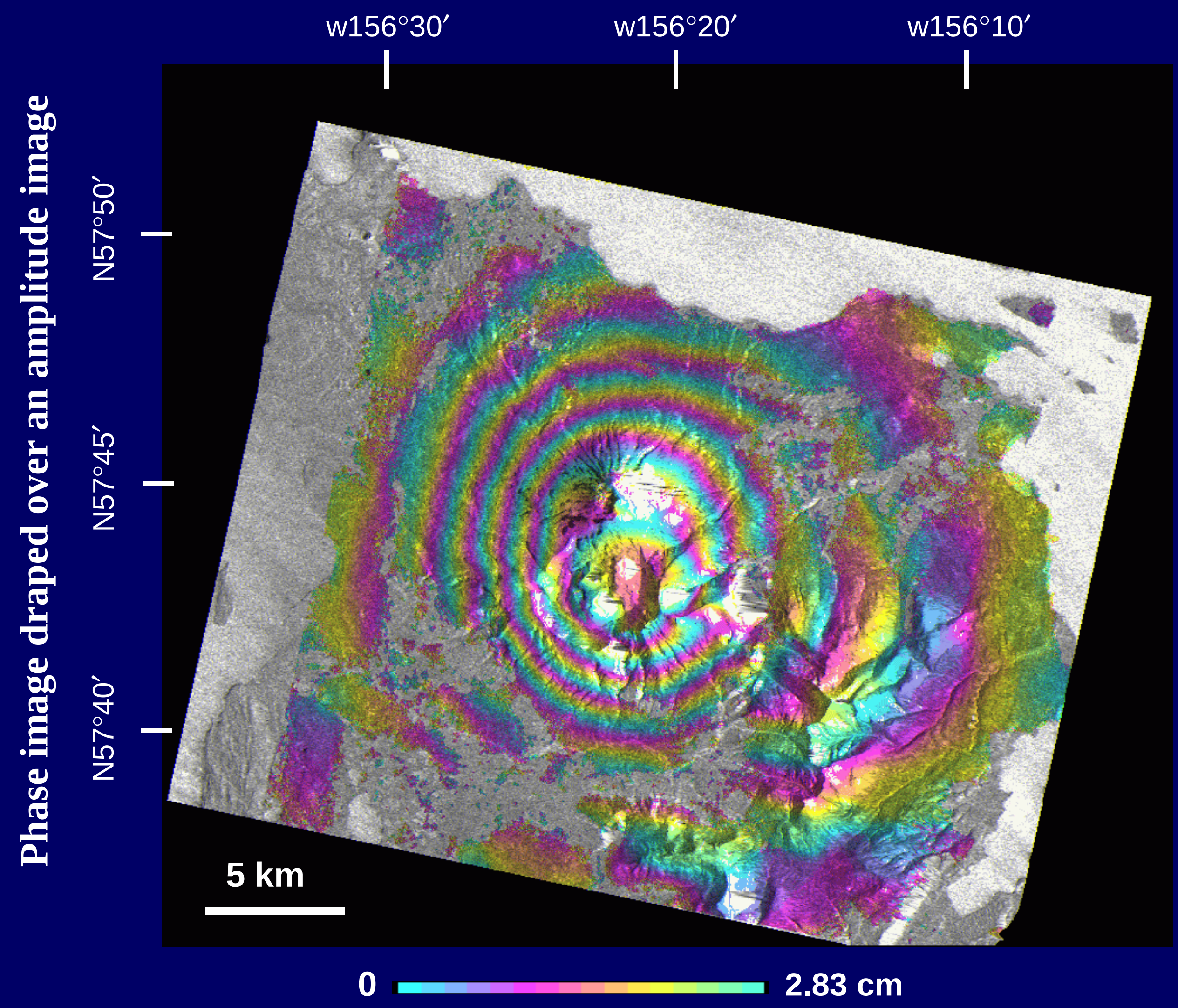

InSAR Processing Step 9 - Deformation interferogram in map projection

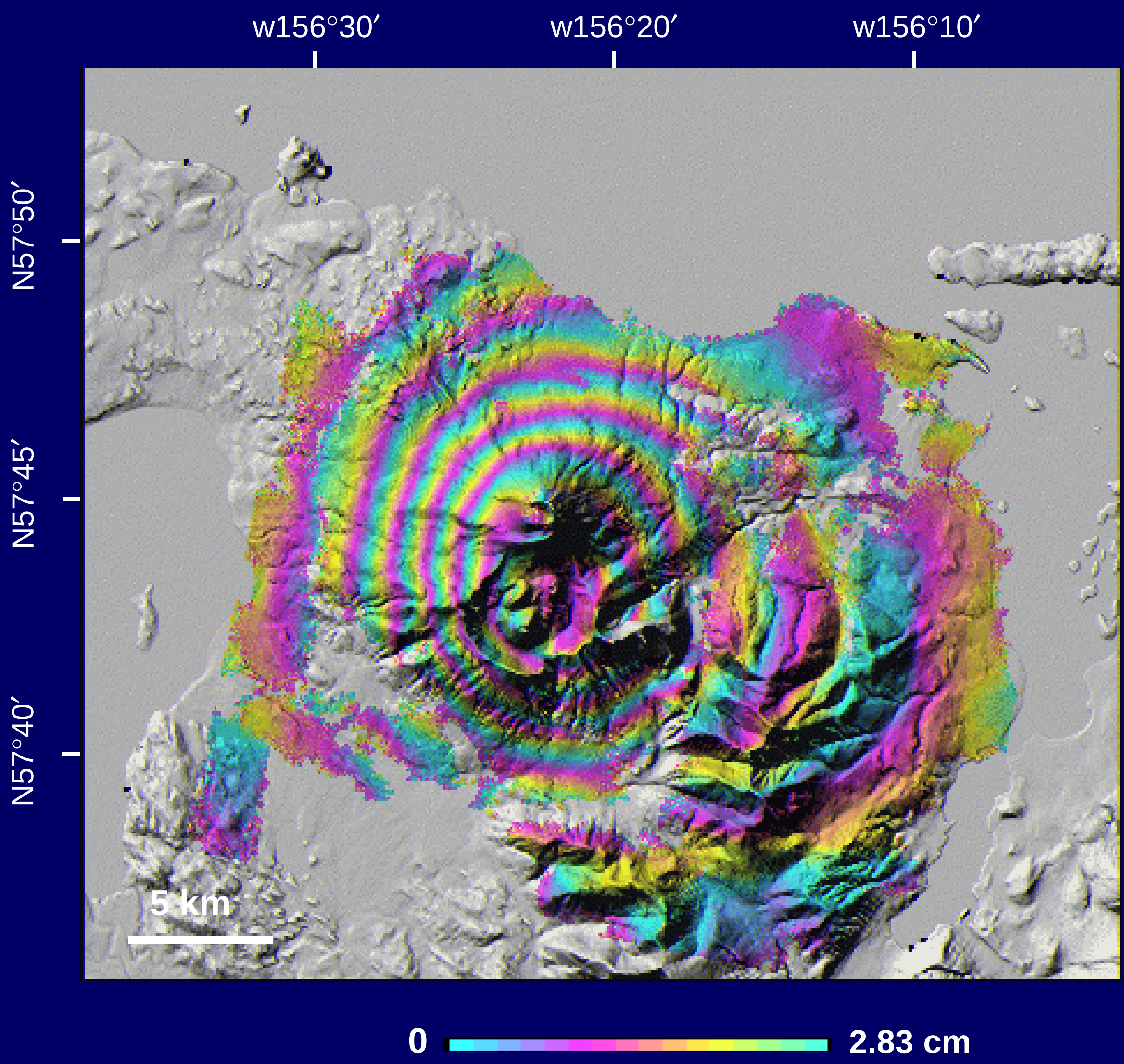

Phase image draped over a DEM image

InSAR Processing Step 10 – Deformation interpretation

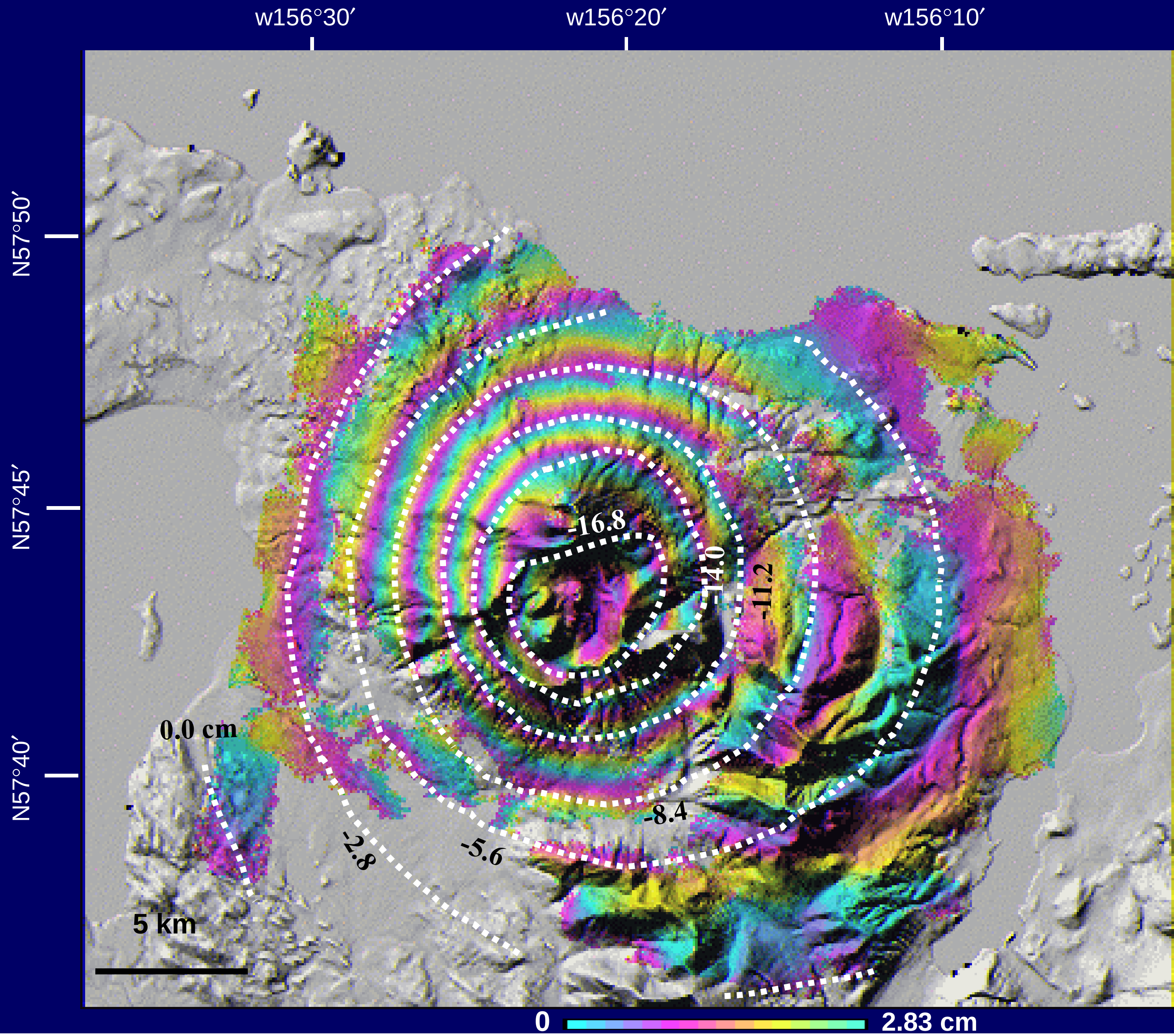

InSAR Processing Step 11 - Deformation modeling

4 Oct. 95 - 9 Oct. 97

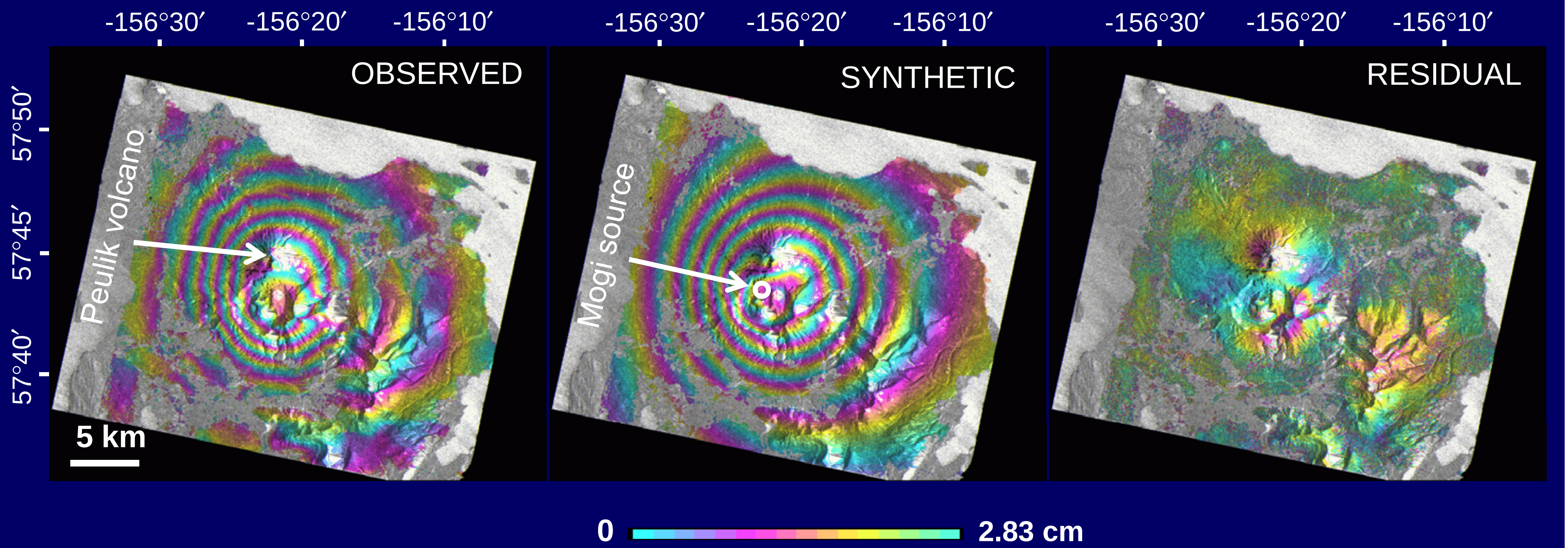

Best-fit source parameters:
- Spherical point source (Mogi source)
- The model source is located at a depth of 6.5 ± 0.2 km.
- The calculated volume change of magma reservoir is 0.043 ± 0.002 km^{3}.

Representation of Interferometric Data

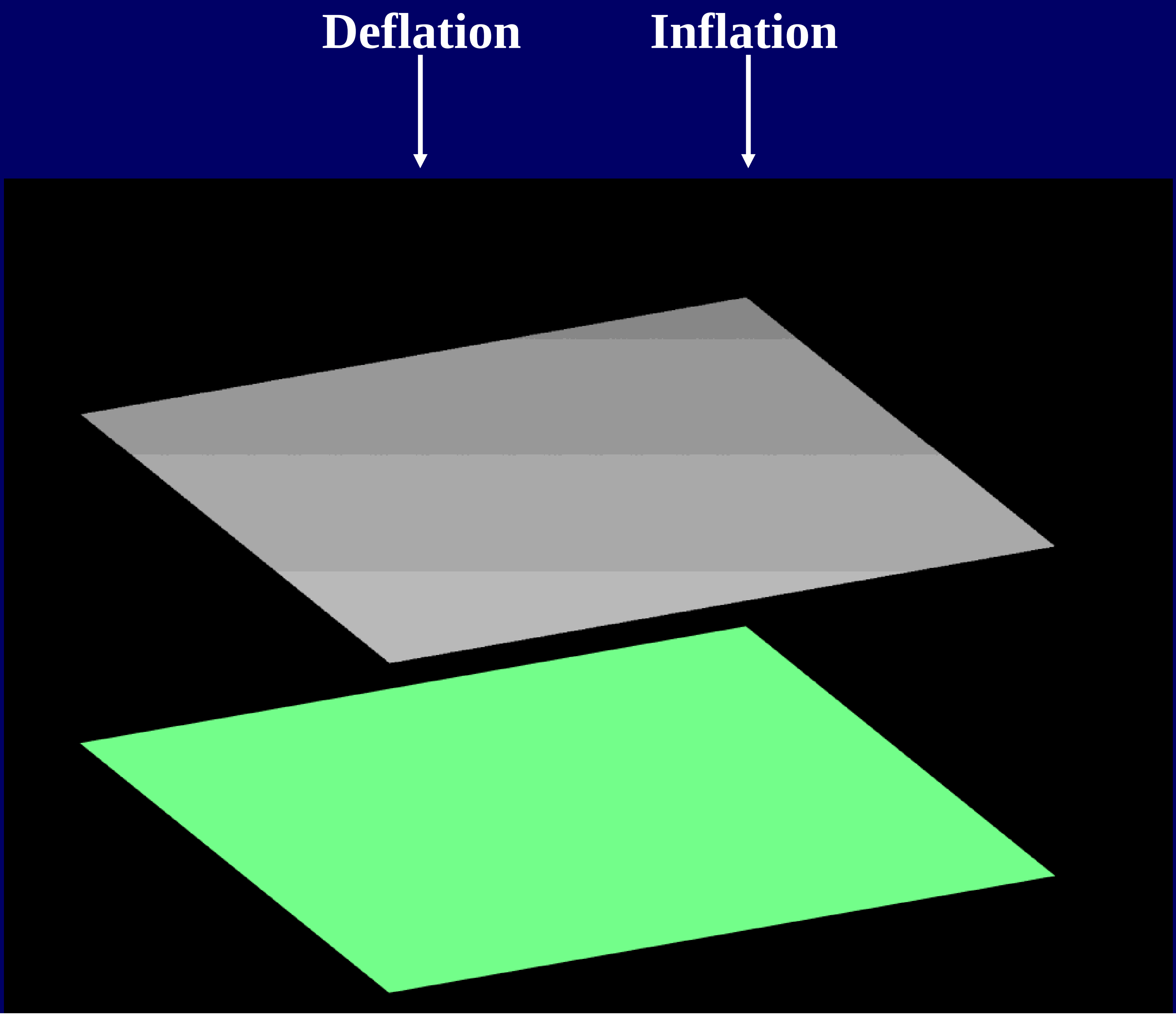

USGS

8.5-cm Deformation Produces ~3 Fringes (干涉条纹)

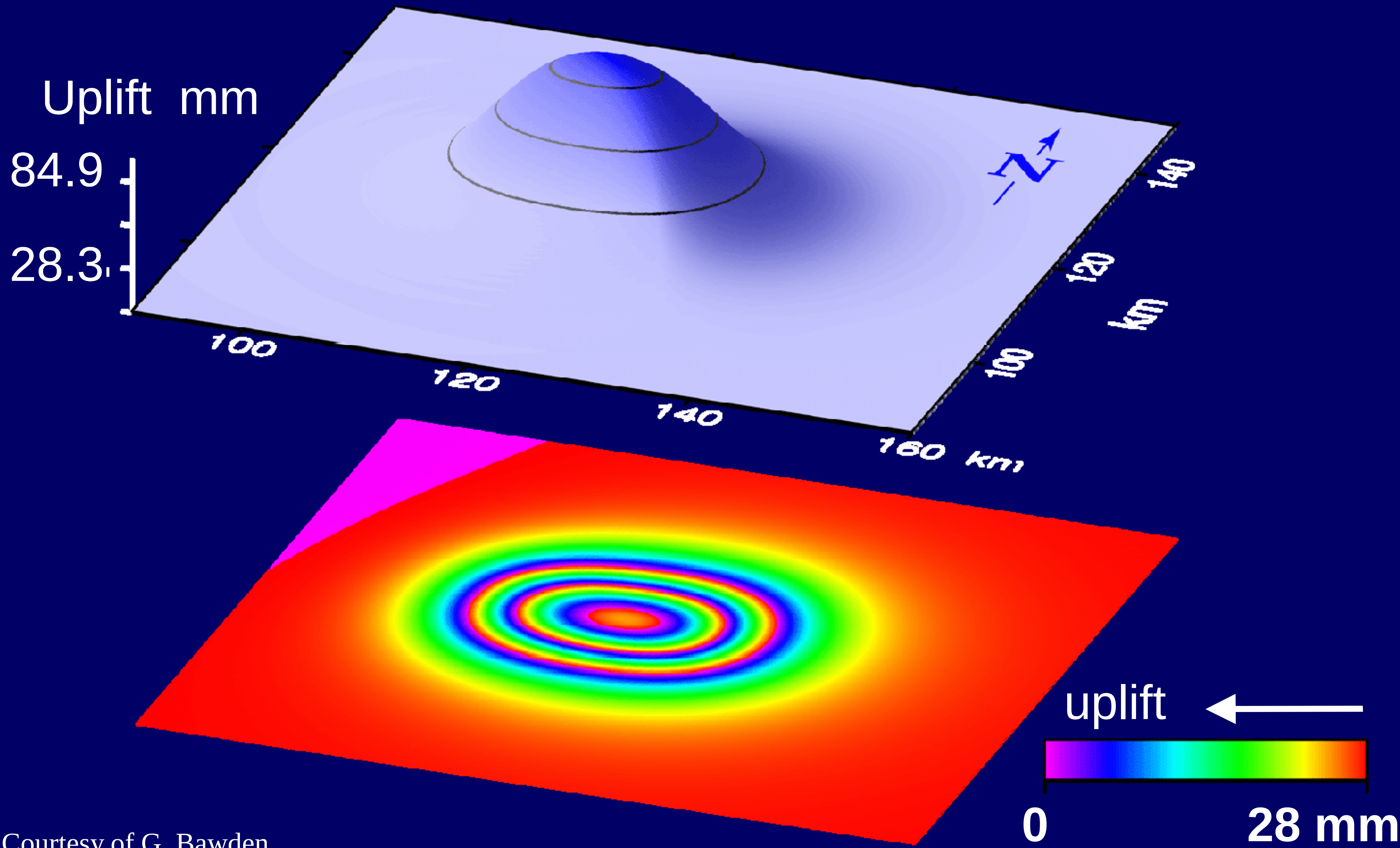

Courtesy of G. Bawden

USGS

Representation of Interferometric Data

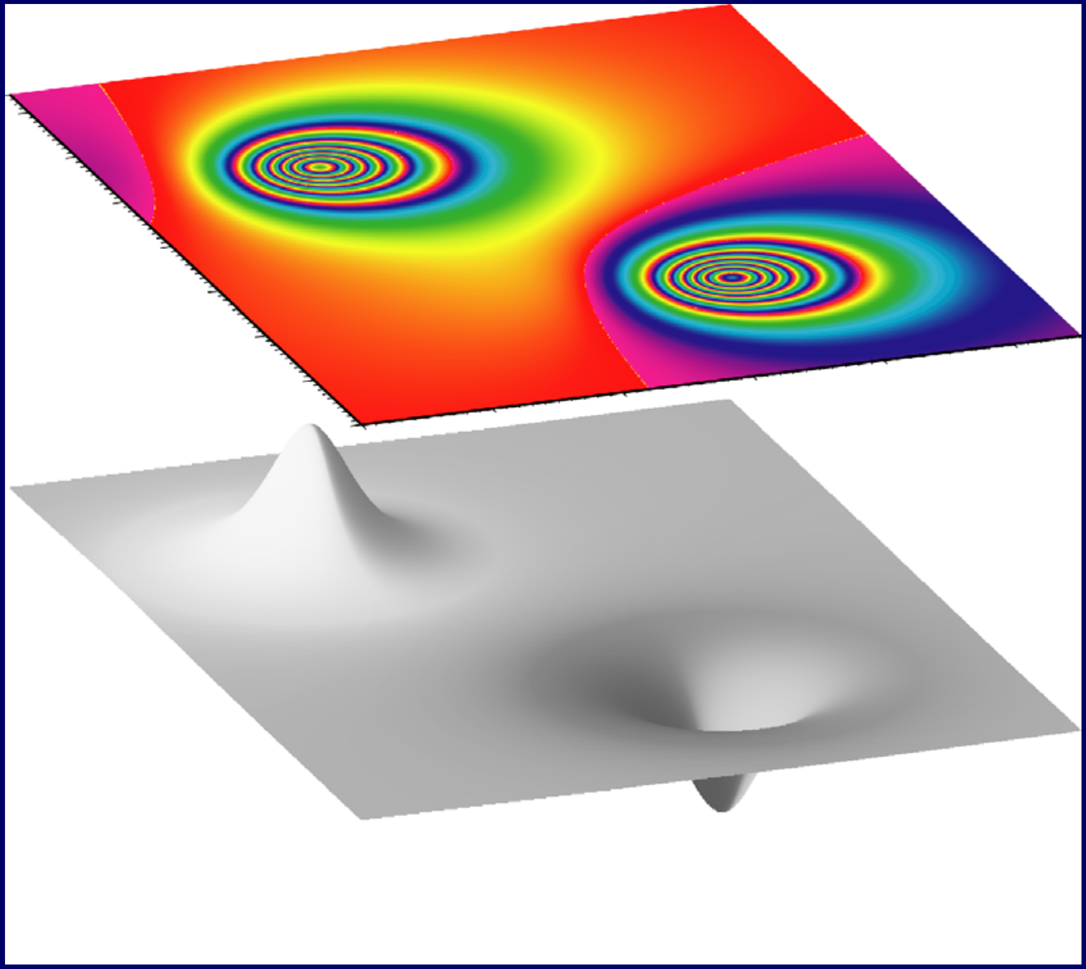

Inflation and deflation in an interferogram

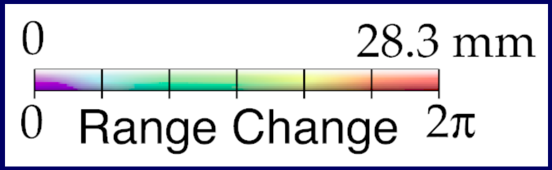

Courtesy of C. Wicks

USGS

Representation of Interferometric Data

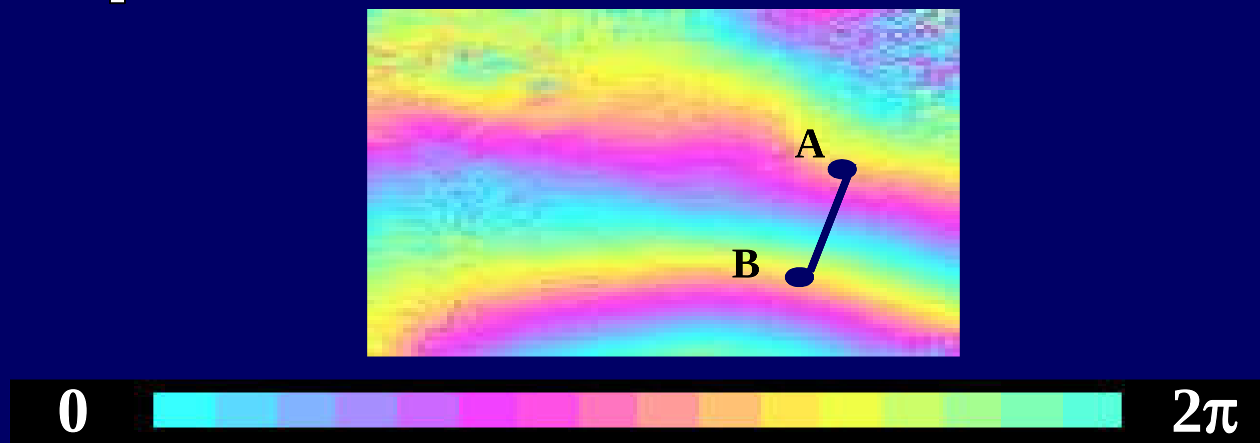

- **<u>Phase Difference from A to B</u>: -2π (one fringe)**
- **<u>Deformation</u>: B inflates 2.83 cm relative to A.**

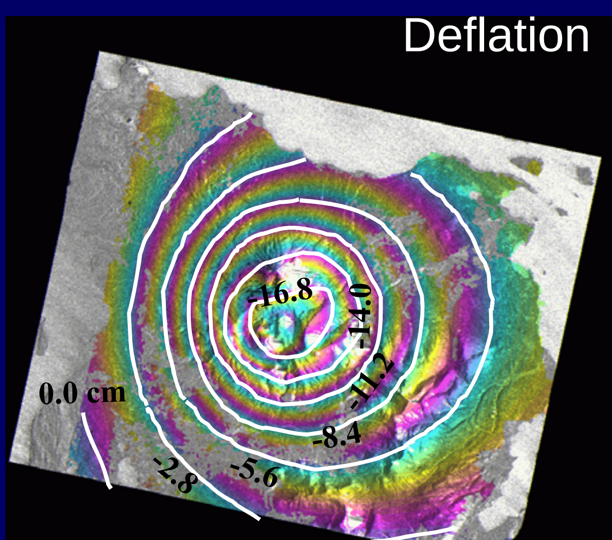

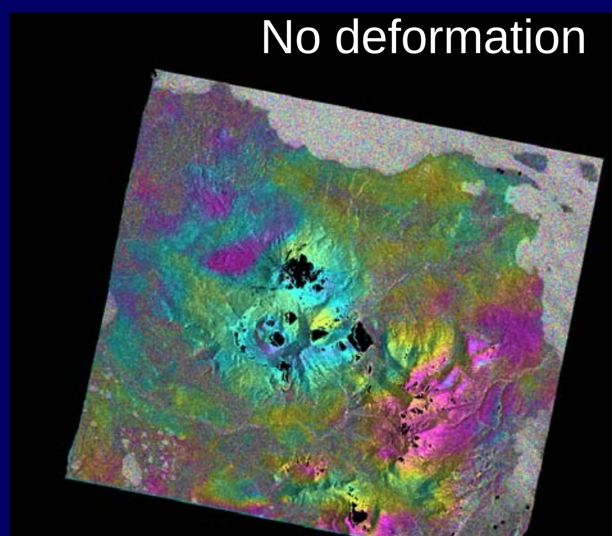

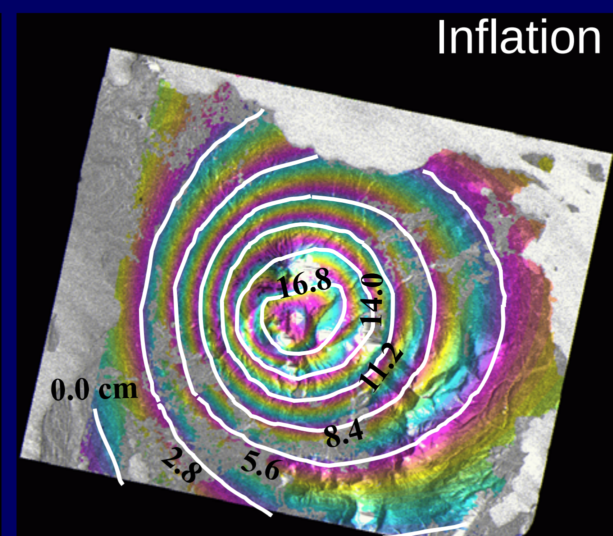

Atmospheric Artifacts in InSAR Imagery

InSAR Artifact: Atmospheric Delays

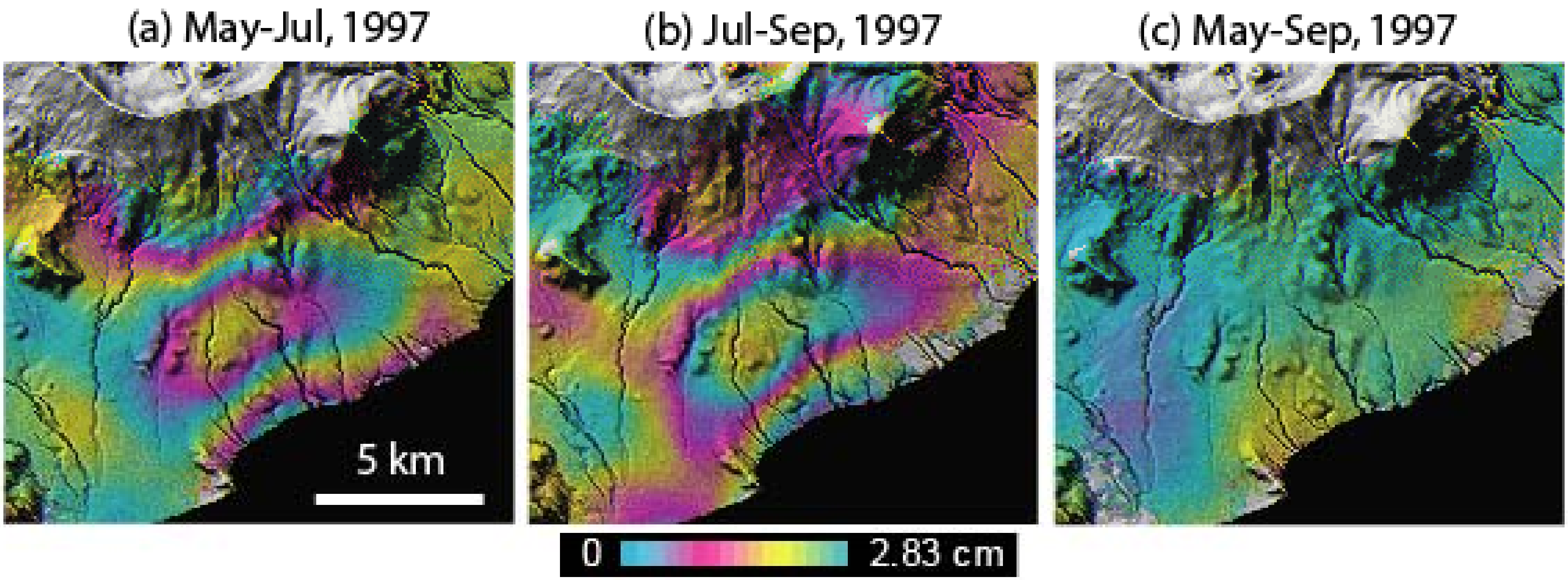

Atmospheric Anomalies

Topography-removed interferogram, 990801-000924

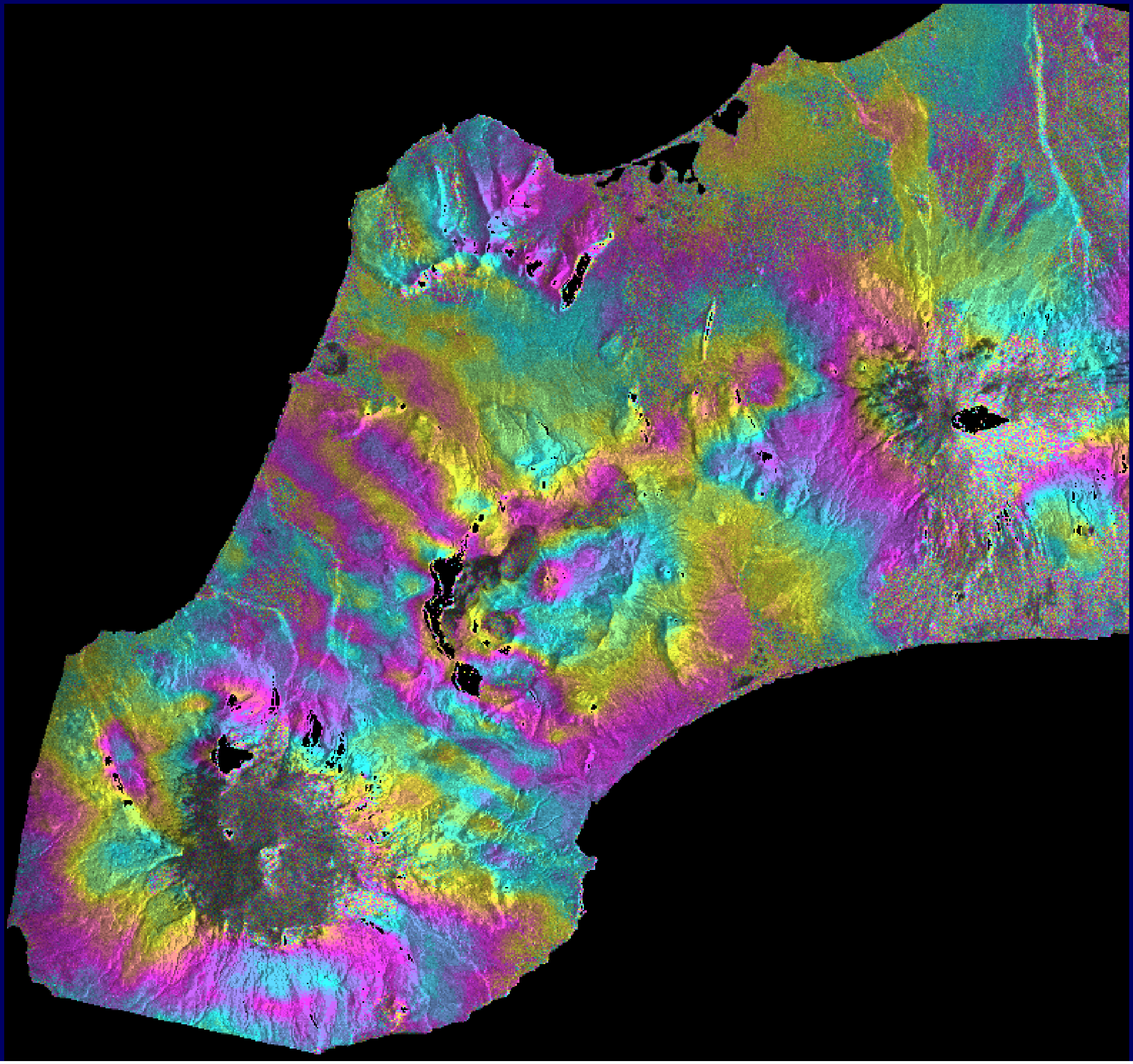

Atmospheric artifacts

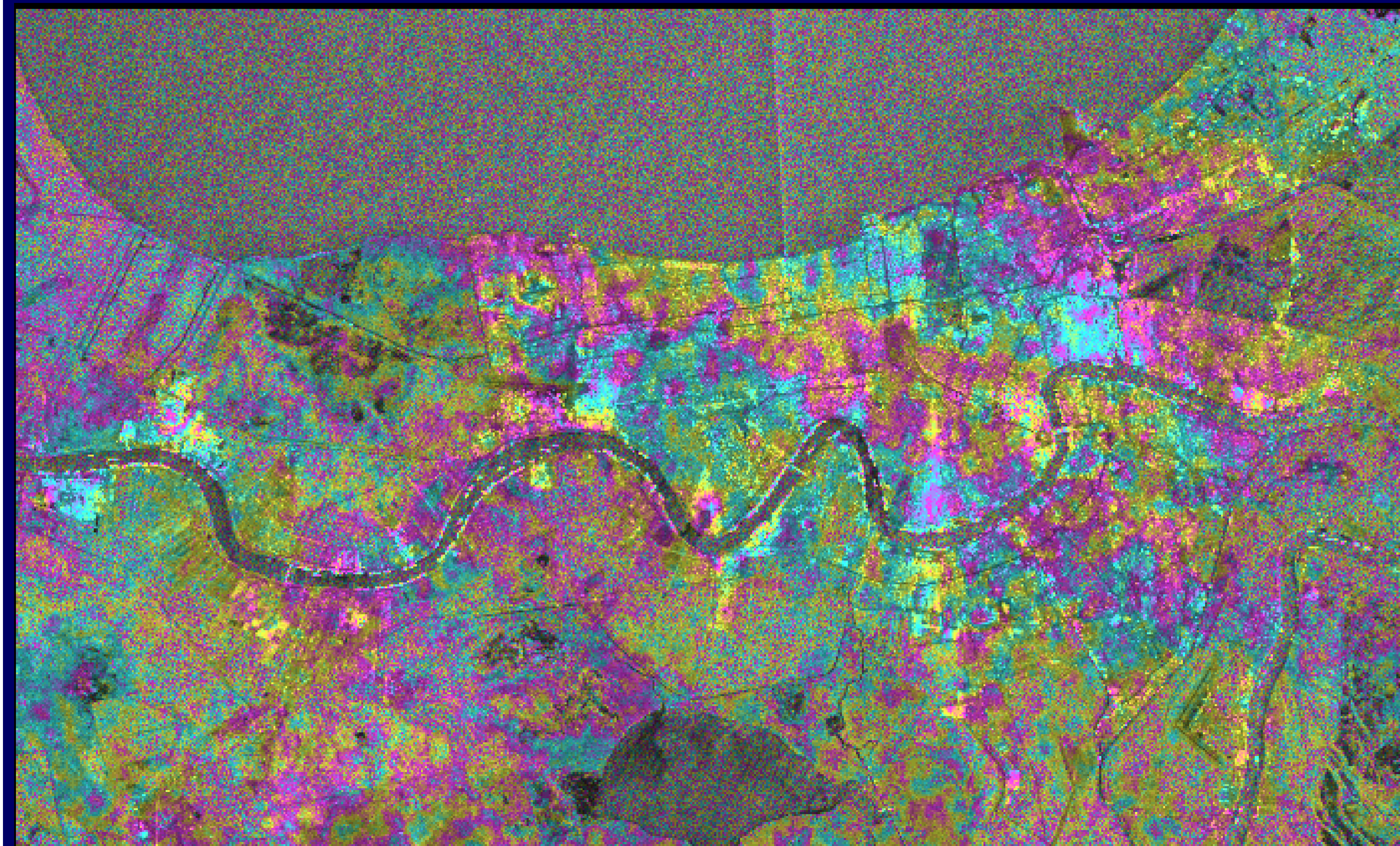

range change

0 2.83 cm

1995/09/18 – 1995/09/19

USGS

Atmospheric artifacts

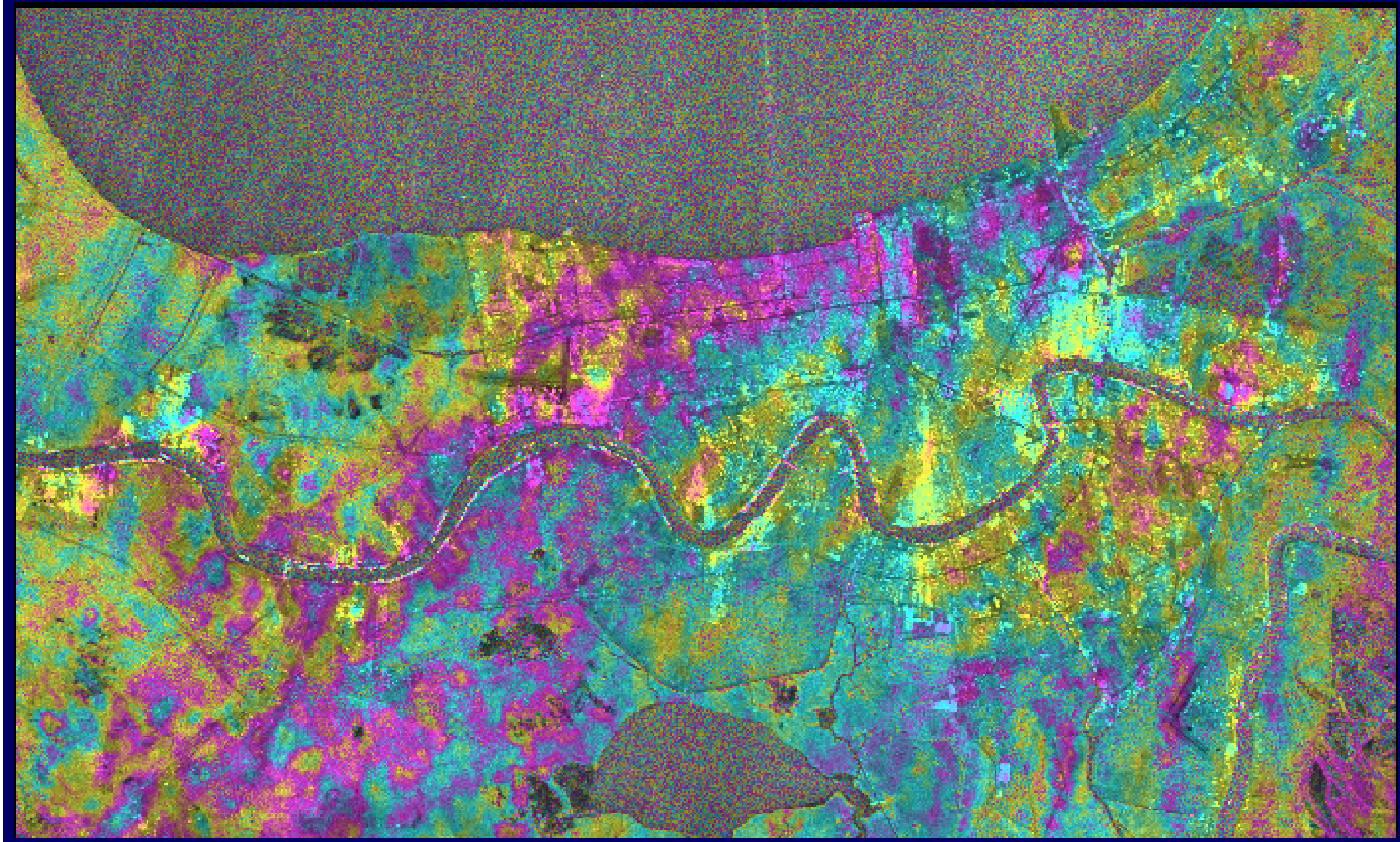

1995/11/27 – 1995/11/28

USGS

Reducing Atmospheric Artifacts

Estimate water-vapor concentrations from

- operational weather models
- continuous GPS measurements
- optical satellite sensors (MODIS, ASTER, and MERIS)
- multi-interferogram InSAR processing

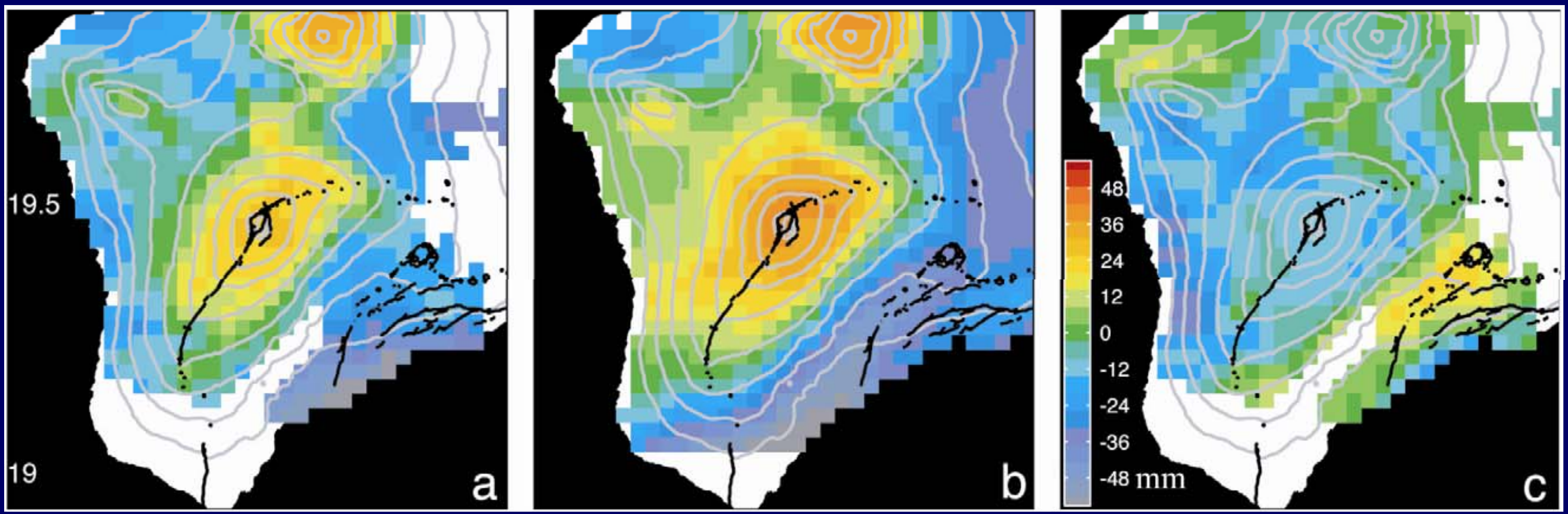

Observed interferogram

Weather-model derived interferogram

Atmosphere-reduced interferogram

Foster et al., GRL, 2006

Ionospheric Artifacts in InSAR Imagery

Signal Propagation Through the Ionosphere

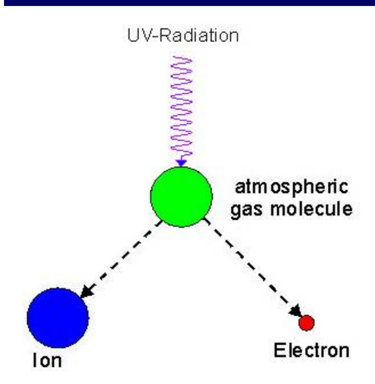

EUV radiation of the sun ionizes neutral atoms and molecules

Typical vertical profiles of the plasma density

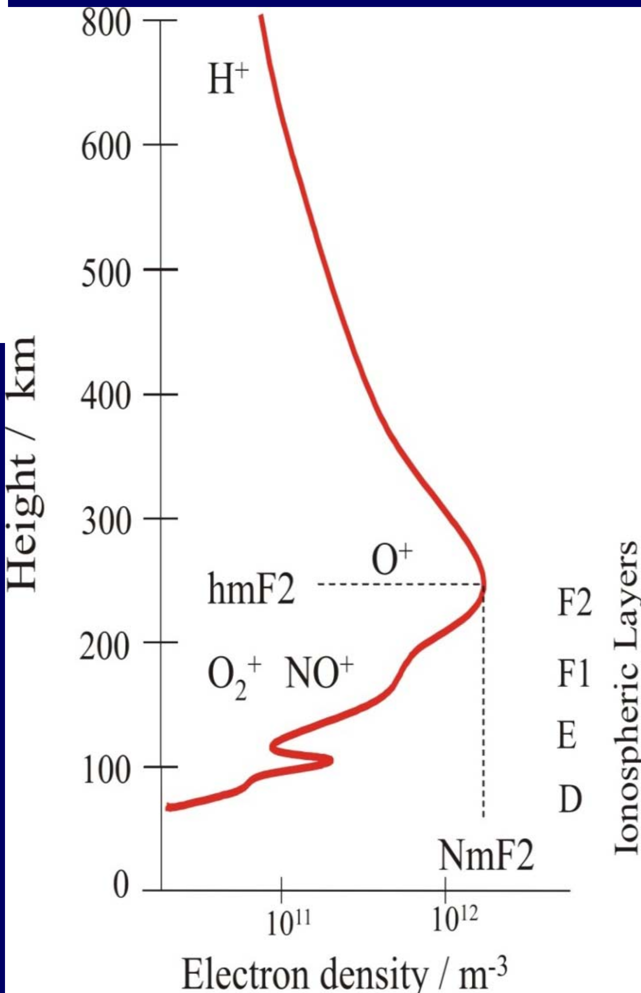

Refractive Index:

$$N_{iono} = (n_{iono} - 1) \cdot 10^6 = -K \cdot 10^6 \frac{n_e}{f^2}$$

Two-way phase shift of frequency *f* due to the ionosphere (nadir looking Radar):

$$\phi(f) = -2\pi f \frac{2}{10^6} \int_0^H \frac{N_{iono}(f,h)}{c} dh \approx 2\pi \frac{2K}{cf} TEC$$

TEC = Total Electron Content

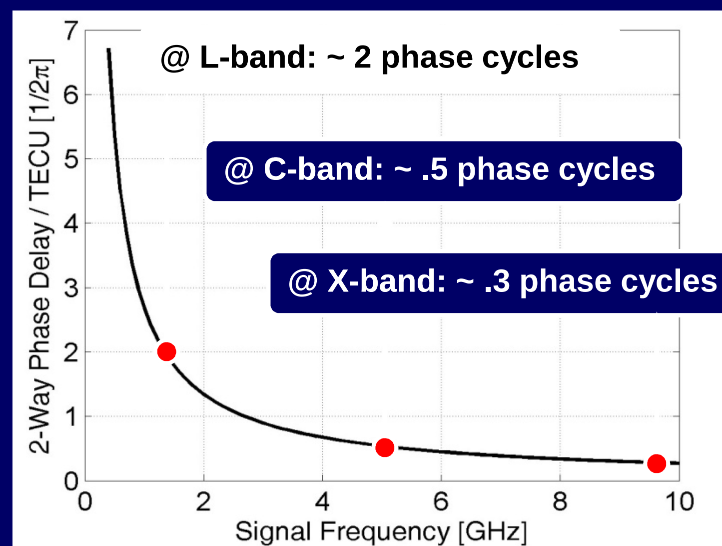

Courtesy of F. Meyer

Ionospheric Effects on InSAR

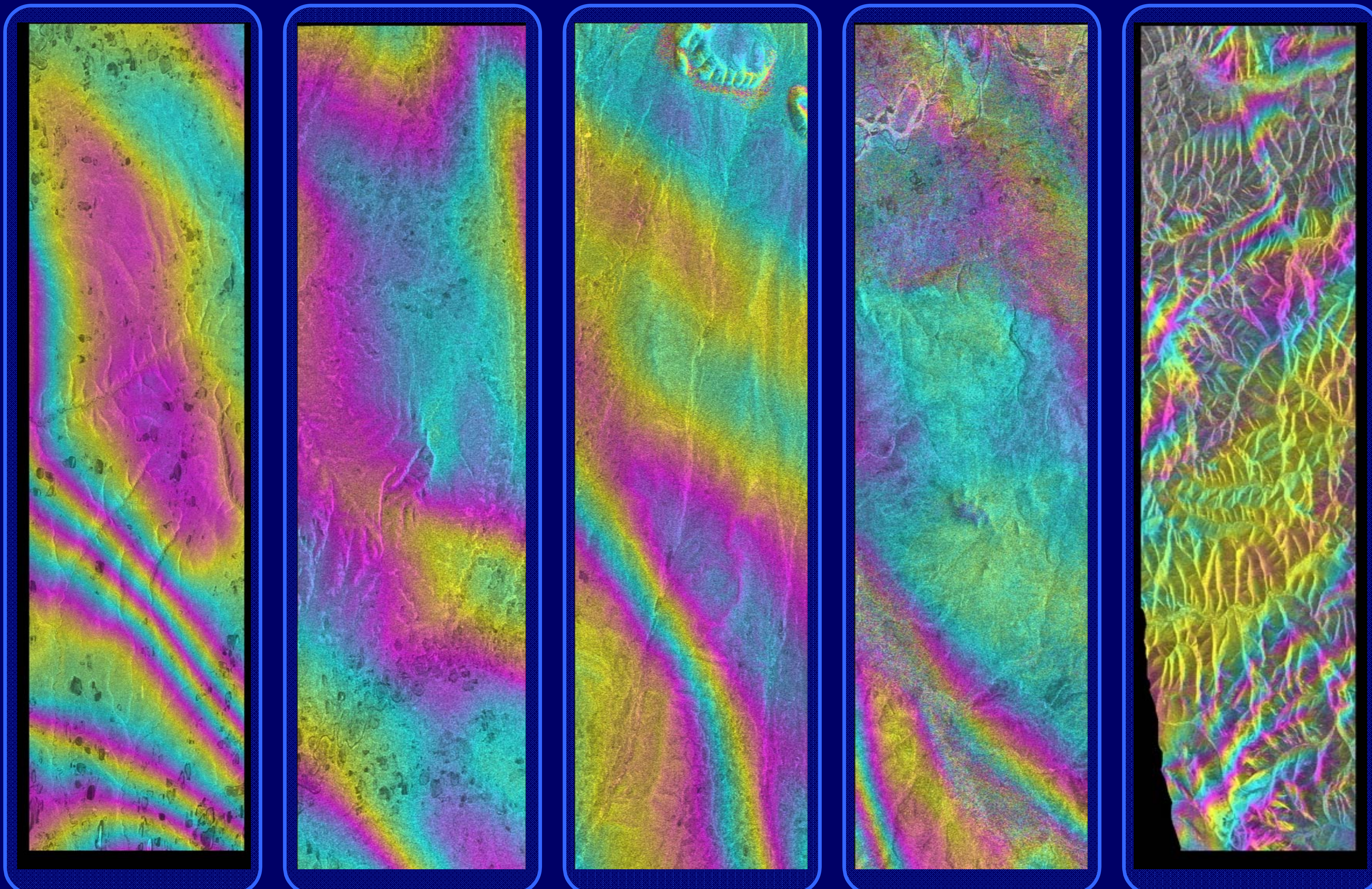

Courtesy of F. Meyer

Ionospheric Effects on SAR/InSAR

- **Potential effects on SAR**
  - ✓**Reduction of geolocation accuracy in azimuth**
  - ✓**Image distortion**
  - ✓**Reduction of image focus in azimuth**

- **Potential effects on InSAR**
  - ✓**Phase ramps in range direction**
  - ✓**Ionospheric phase screens**
  - ✓**Local or global decorrelation**

Methods for Ionospheric Correction

Faraday Rotation (FR) Based Correction

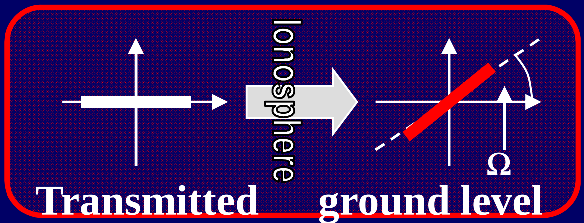

- FR estimation from quad-pol data — *Freeman, 2004; Quegan, 2010*
- FR estimation from HH-HV correlation — *Nicoll & Meyer, 2008*

Range Split-Spectrum Based Correction

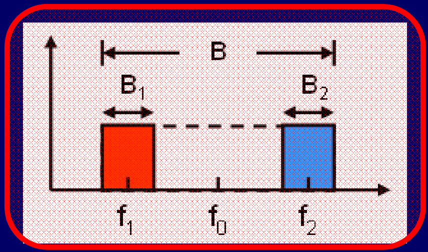

- **Distributed targets in Repeat-pass InSAR** — ***Rosen, 2009, 2010***
- **Coherent Targets in single image** — ***Papathanassiou, 2009***
- **Amplitude correlation of sub-looks** — ***Meyer & Bamler, 2005***

Methods for Ionospheric Correction

Azimuth Autofocus Based Correction

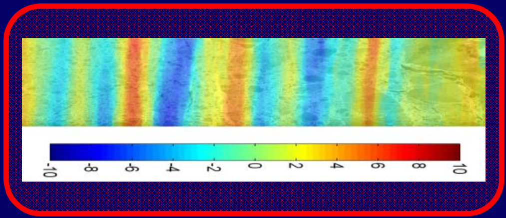

- Contrast maximization for point targets – *several authors*
- Coherent AF: Phase Curvature analysis – *Papathanassiou, 2008*
- Incoherent AF: Sub-look co-registration (MLR) – *Meyer & Nicoll, 2008*

Hybrid Methods

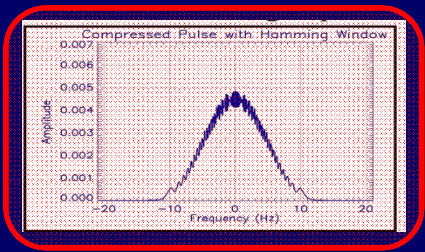

- **Combination of range and phase offsets in InSAR** ***– Meyer, 2005***
- **Two dimensional phase signature of point targets** ***– Papathanassiou***
- **…**

Baseline Artifacts in InSAR Imagery

Artifacts due to errors in satellite positioning

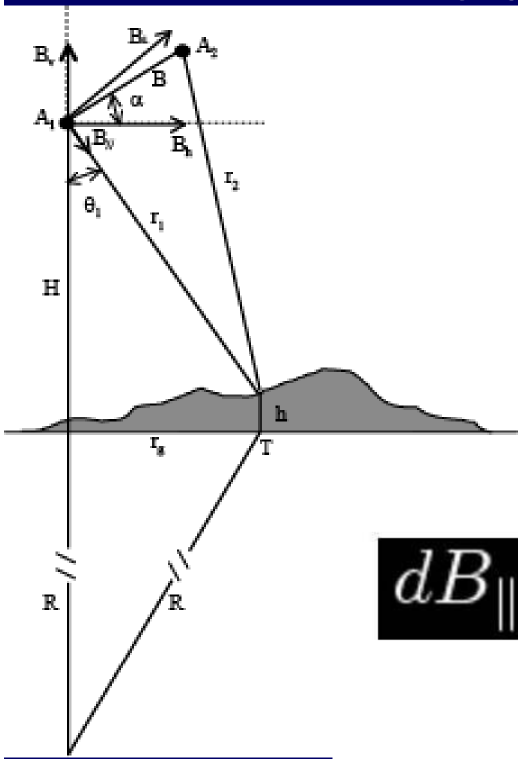

$dB_\parallel$

$dB_\perp$ (nearly linear)

2 m

$d\frac{\partial B_\parallel}{\partial t}$ (linear)

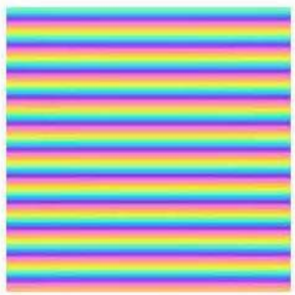

$d\frac{\partial B_\perp}{\partial t}$

2 cm/s

$d\frac{\partial^2 B_\parallel}{\partial t^2}$

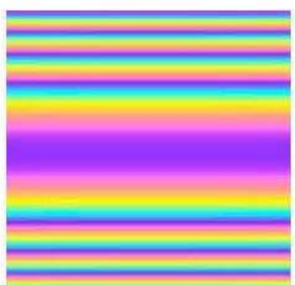

$d\frac{\partial^2 B_\perp}{\partial t^2}$

2 mm/s²

Courtesy of
A. Hooper

USGS

Artifacts due to errors in satellite positioning

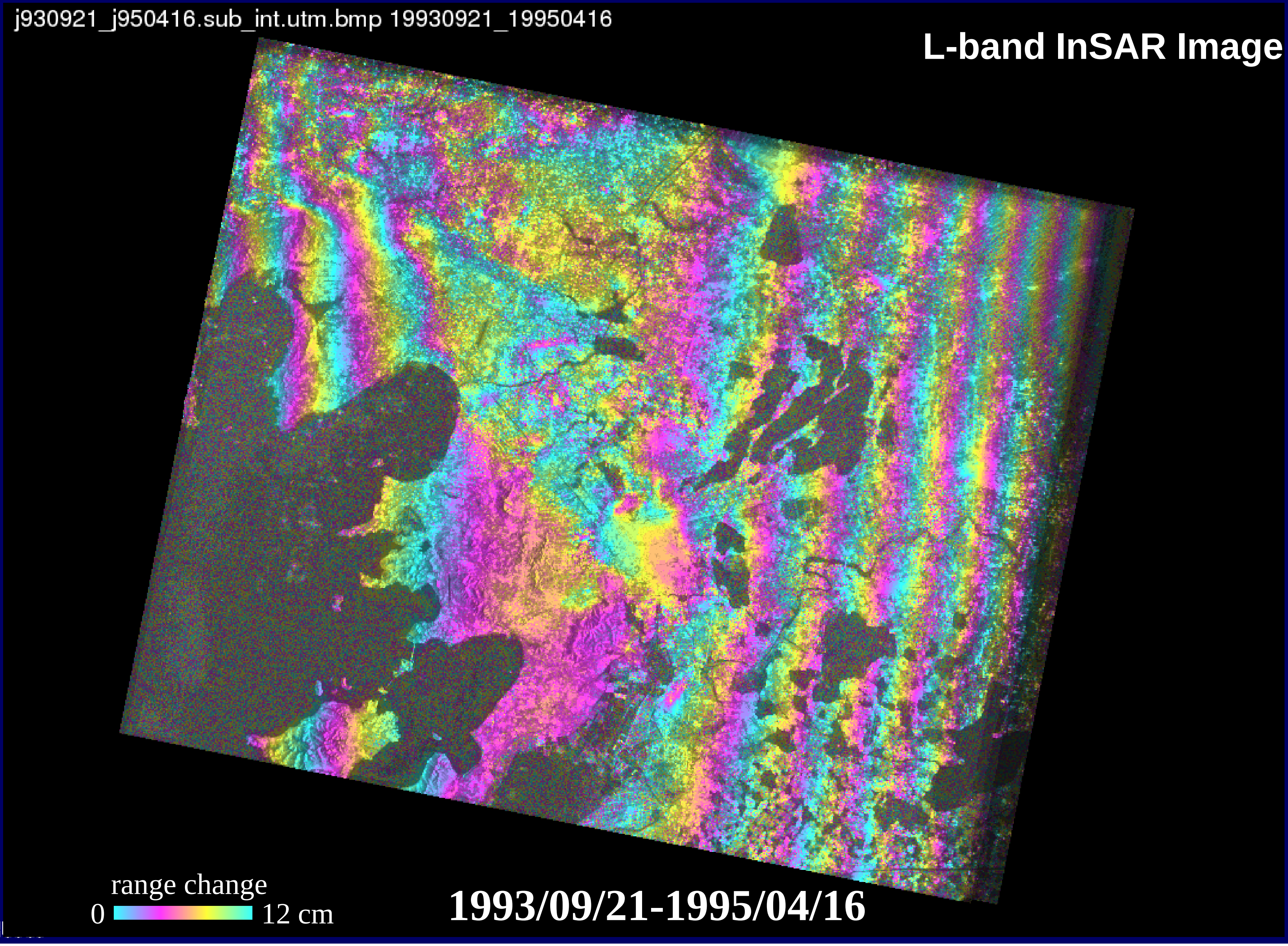

Artifacts due to errors in satellite positioning

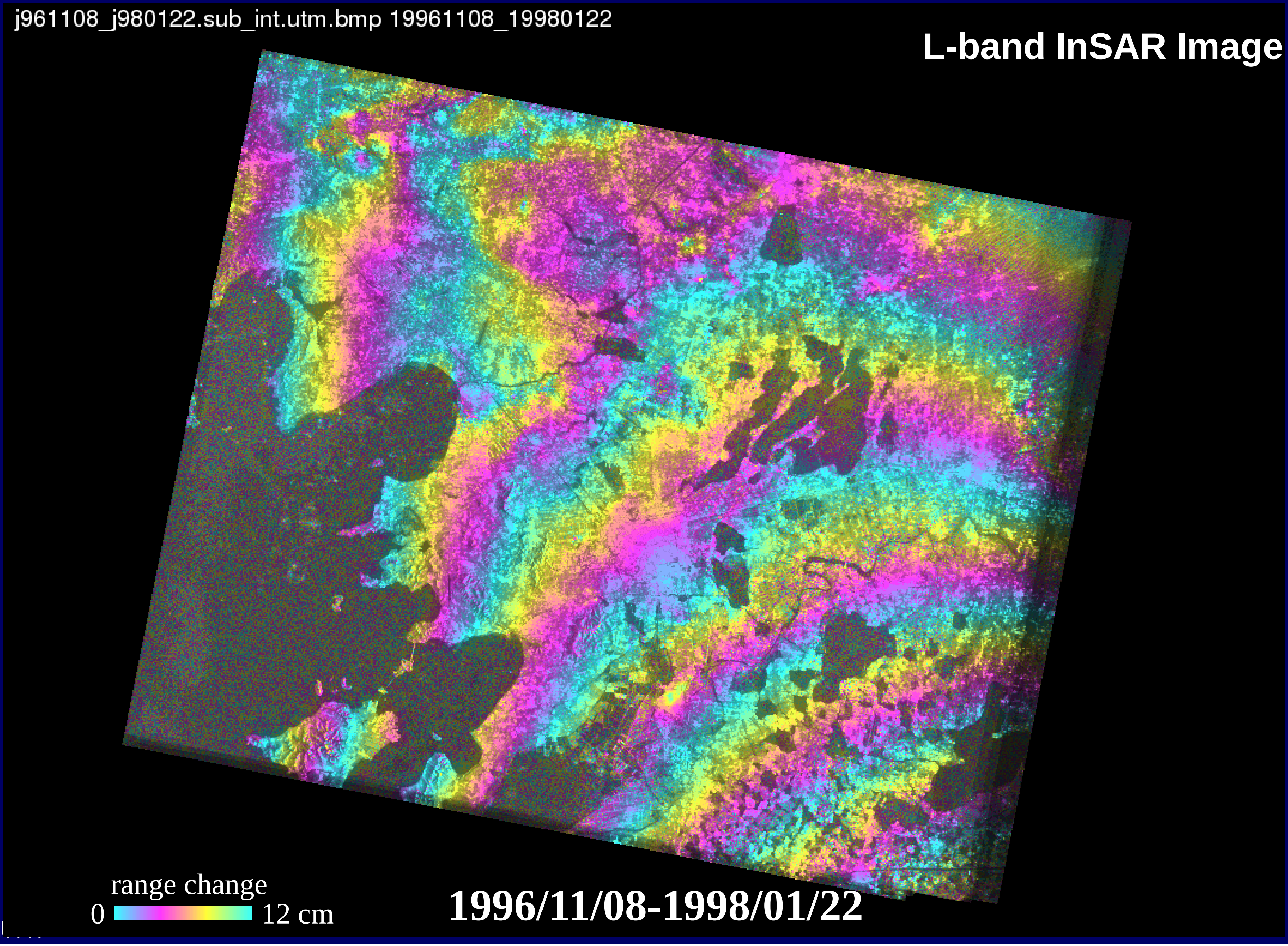

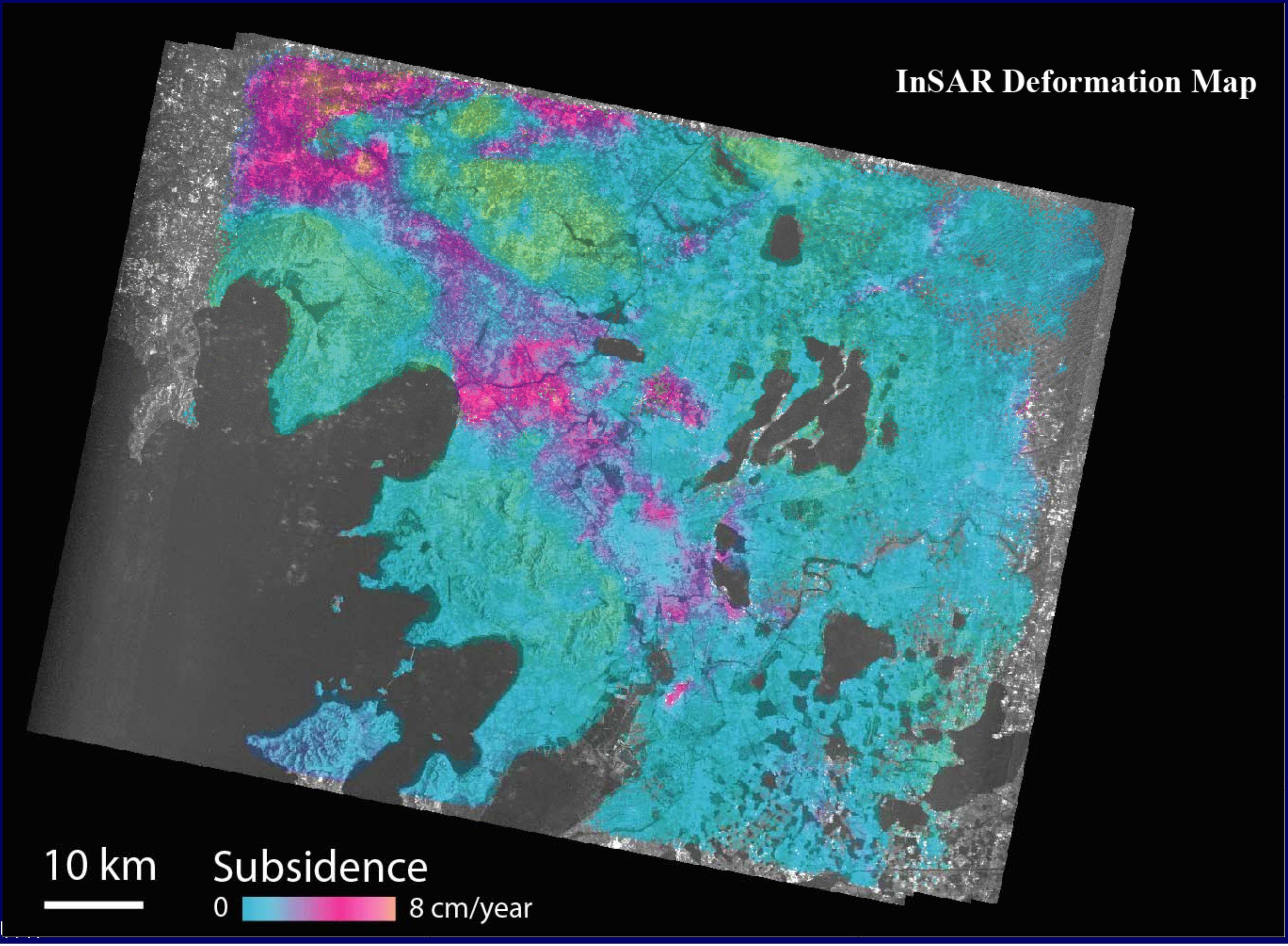
InSAR Deformation Map
10 km
Subsidence
0
8 cm/year

InSAR Artifact: errors in satellite positioning

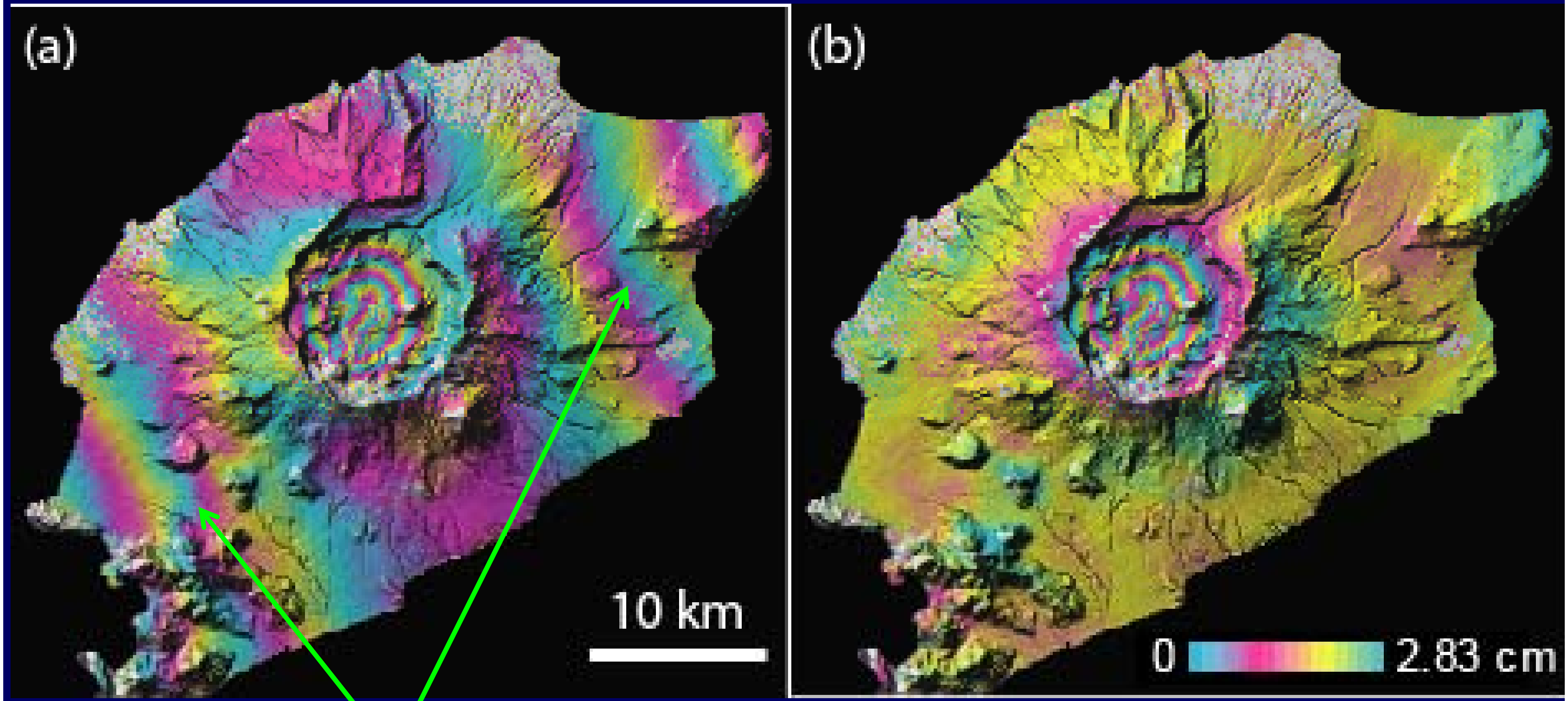

Artifacts due to baseline errors

InSAR deformation image with refined baseline

InSAR artifact due to errors in satellite positioning & DEM

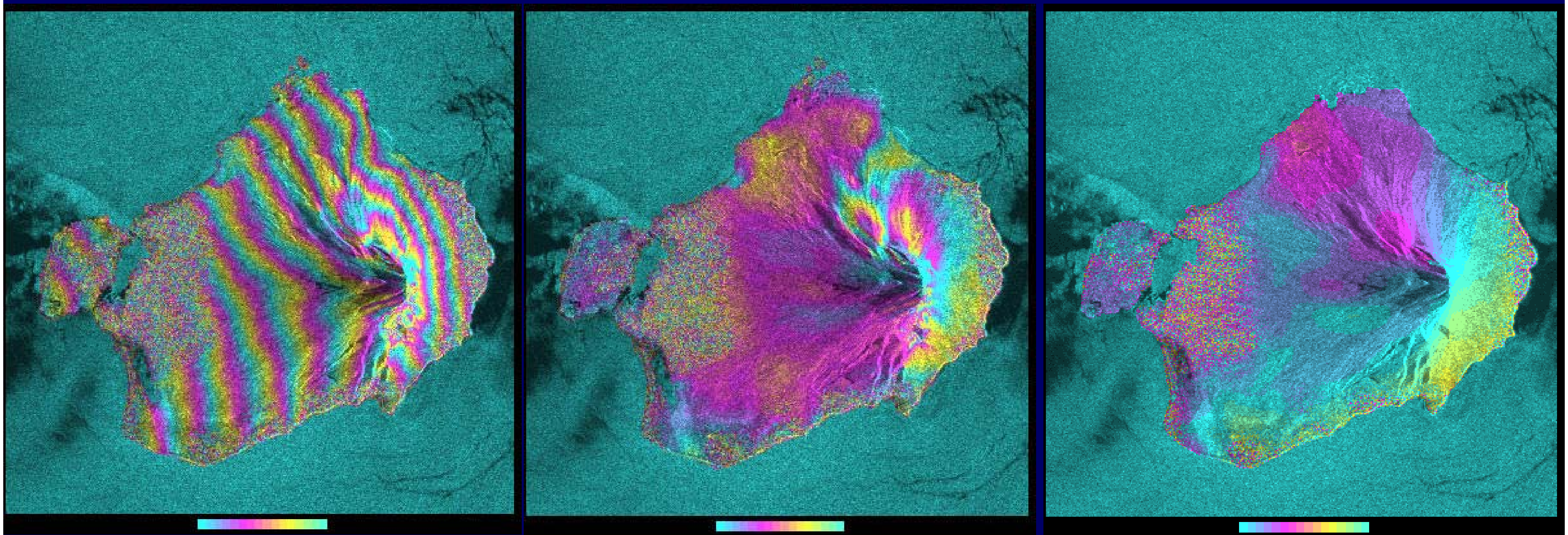

Original Satellite restitute vectors + 60-m DEM

Precision Satellite restitute vectors + 60-m DEM

Precision Satellite restitute vectors + 10-m DEM

SAR-processor Artifacts in InSAR Imagery

Imperfect SAR Processor

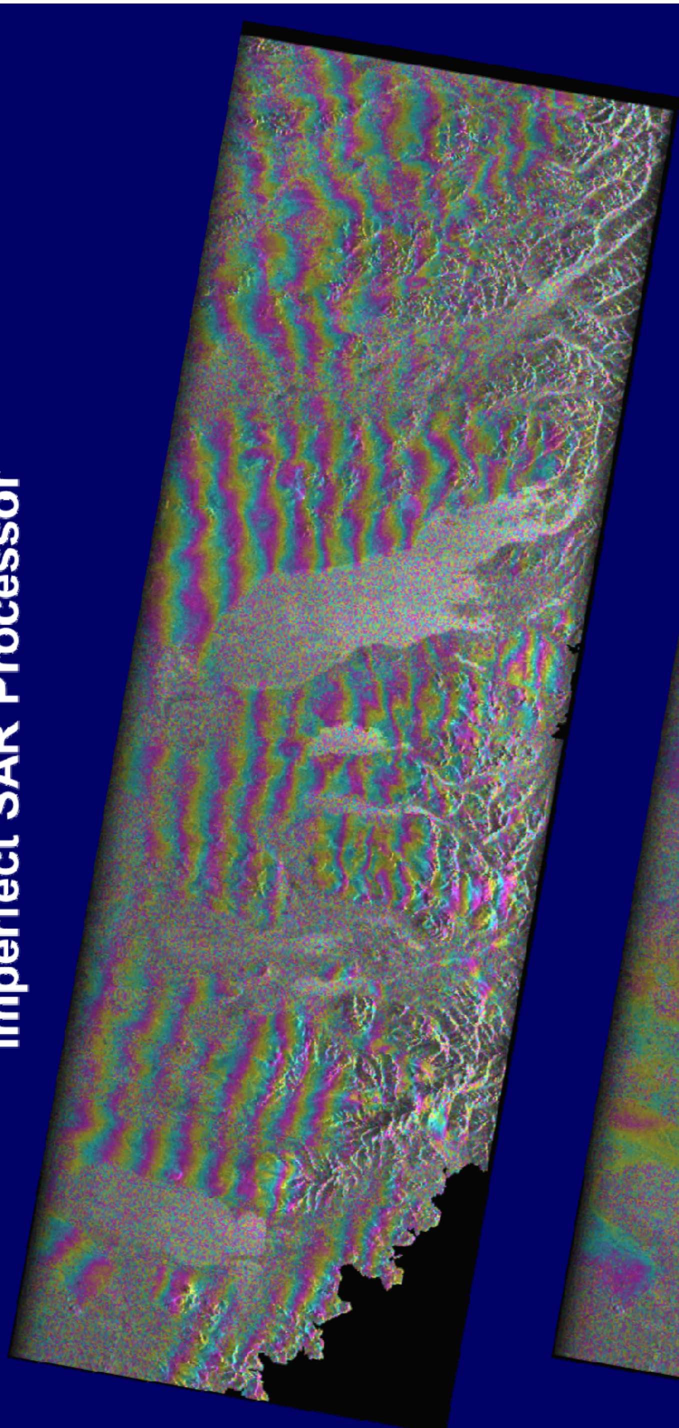

Precision SAR Processor

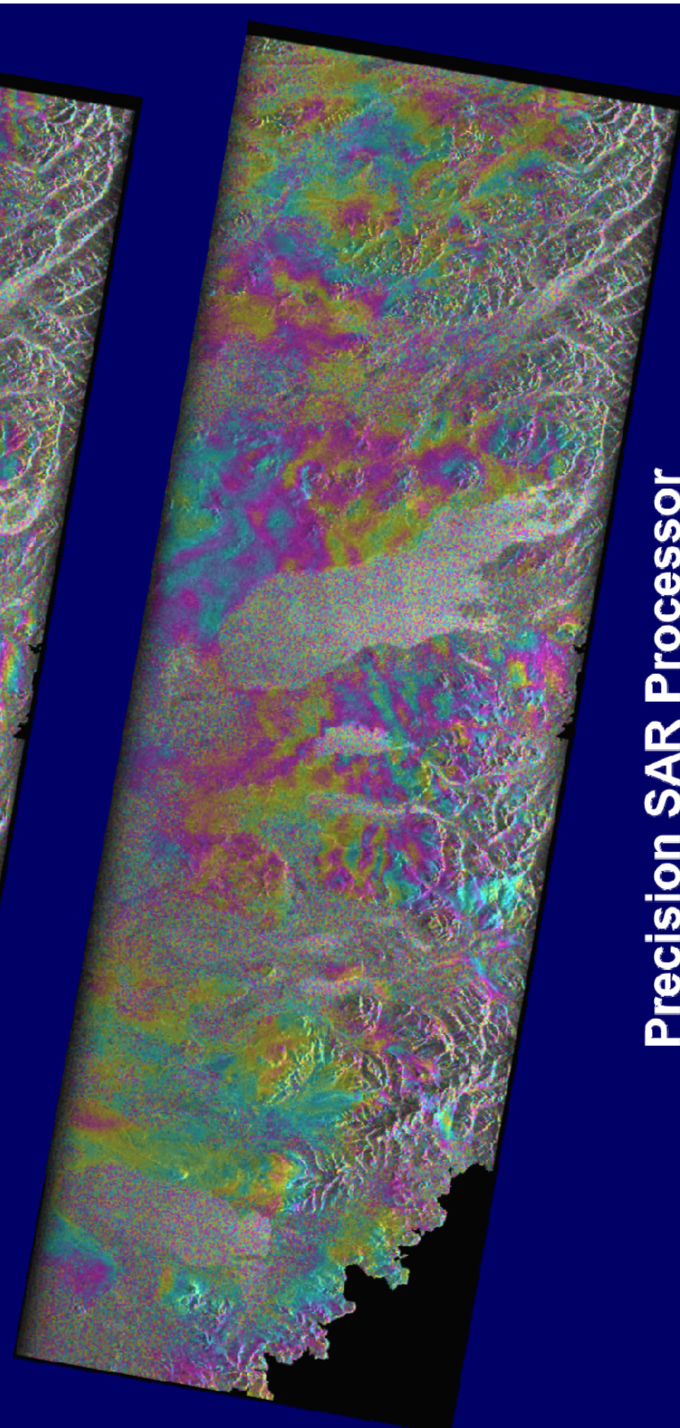

Multi-interferogram InSAR Processing

Improve deformation measurement accuracy of conventional InSAR through the multi-interferogram approach

Multi-interferogram InSAR processing

InSAR Differential Phase Equation

For pixel *n* in interferogram *i:*

$$\phi_{n,i} = \underbrace{\phi_{\varepsilon,n,i}}_{\text{DEM Error Term}} + \underbrace{\phi_{def,n,i}}_{\text{Deformation}} + \underbrace{\phi_{Atm,n,i}}_{\text{Atmospheric Artifact Term}} + \underbrace{\phi_{orbit,n,i}}_{\text{Orbit Error Term}} + \underbrace{\sigma_{n,i}}_{\text{Noise}}$$

Persistent scatterer InSAR

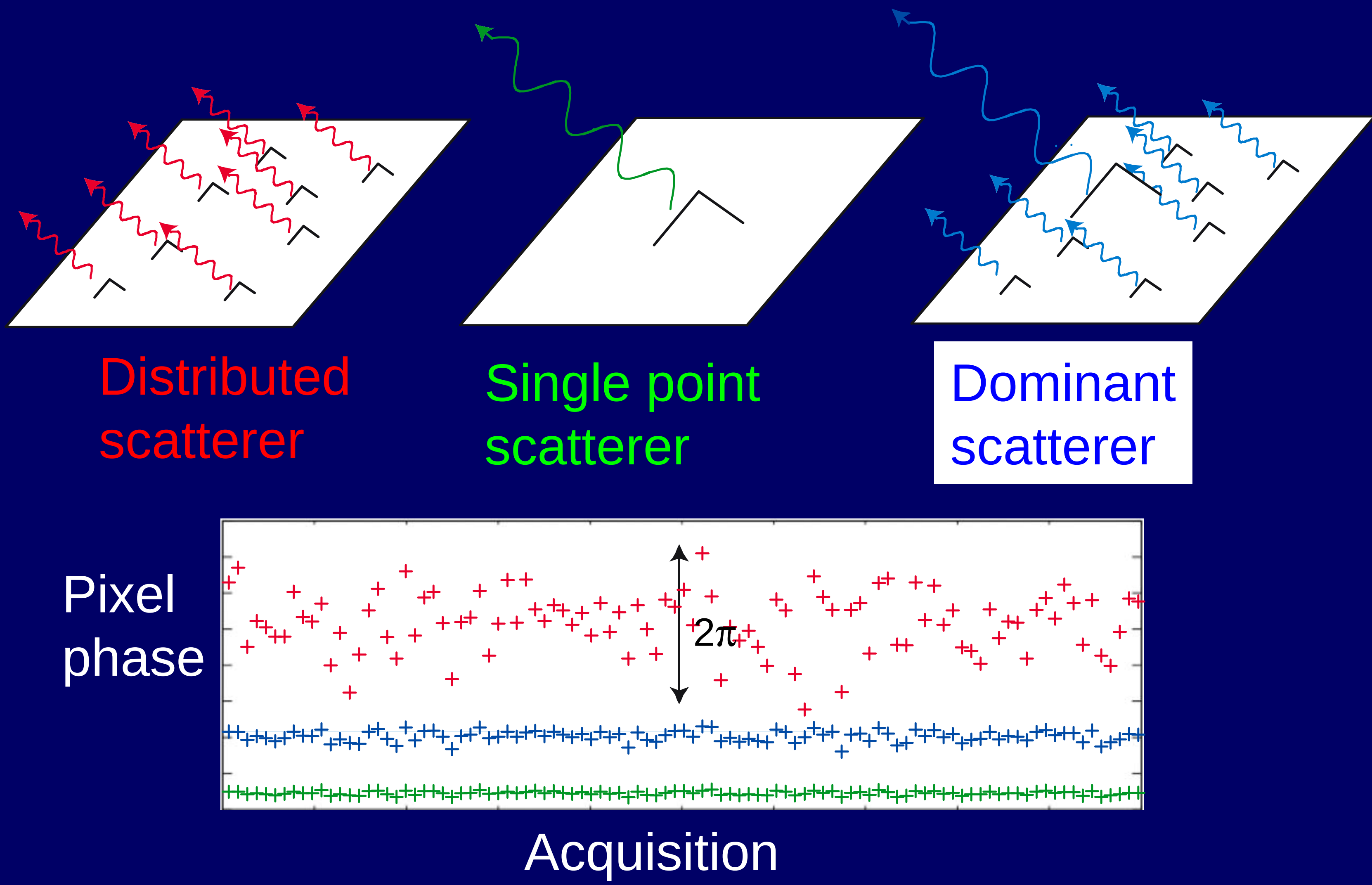

Courtesy of A. Hooper

Persistent Scatterer InSAR (PSInSAR)

• PSInSAR uses unique characteristics of atmospheric delay anomalies and backscattering of certain ground targets to improve the accuracy of the conventional InSAR deformation measurement from 1-2 cm to 2-3 mm.

• The basic idea behind PSInSAR is to separate the different phase contributions (surface deformation, atmospheric delay anomaly, and decorrelation noise) by iterations, taking into account the spatio-temporal data distribution and the correlation between the point target samples which have unique SAR backscattering characteristics.

• Most of the point targets correspond to single buildings or other stable structures. These points can be used as a “natural benchmark” to monitor terrain motion by analyzing the phase history of each target in the image.

Deformation of Augustine Volcano

"Deformation" Images

"Atmospheric artifact" Images

Deformation Images obtained via the multi-interferogram approach

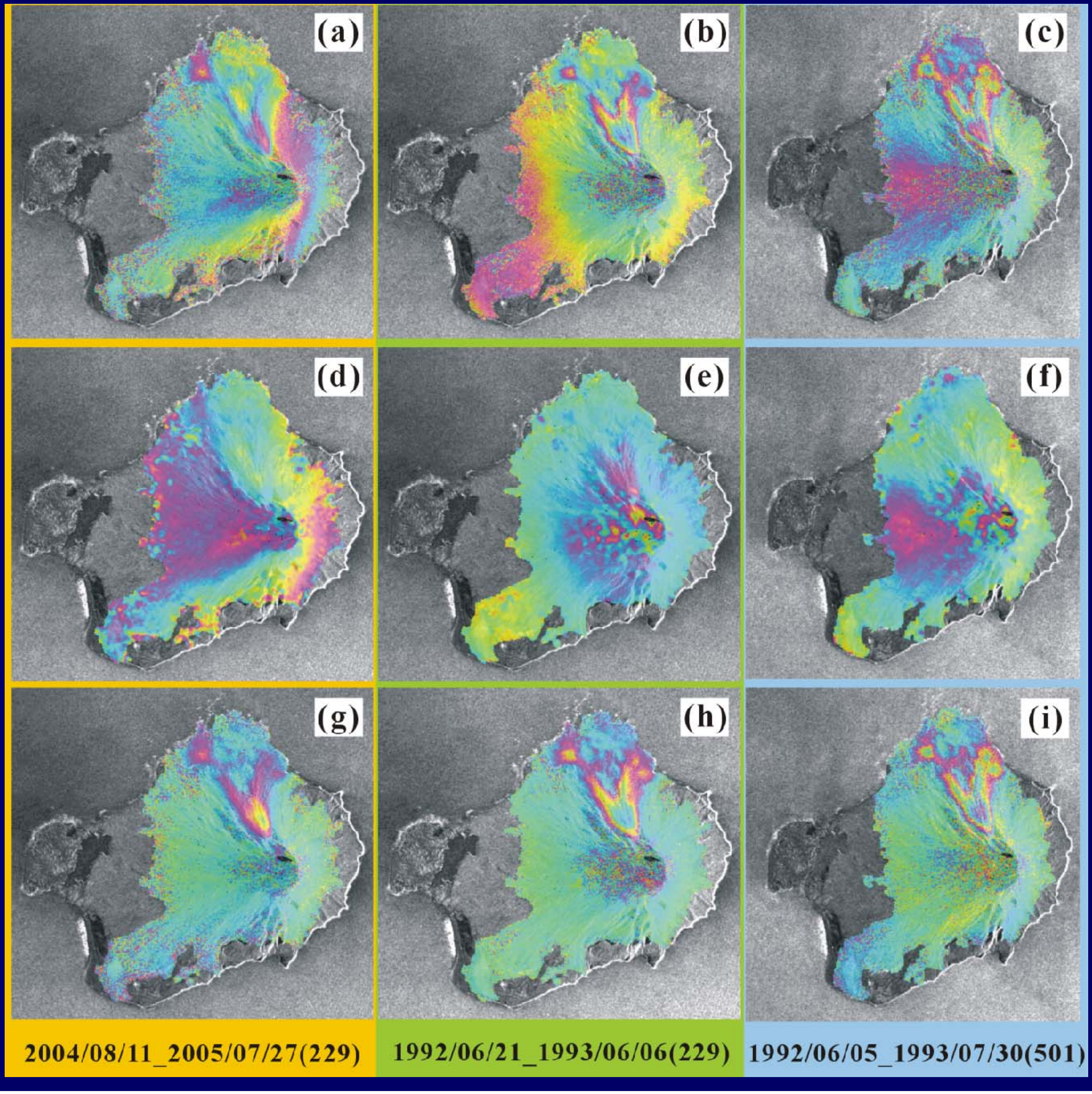

Deformation of Augustine volcano via multi-interferogram approach

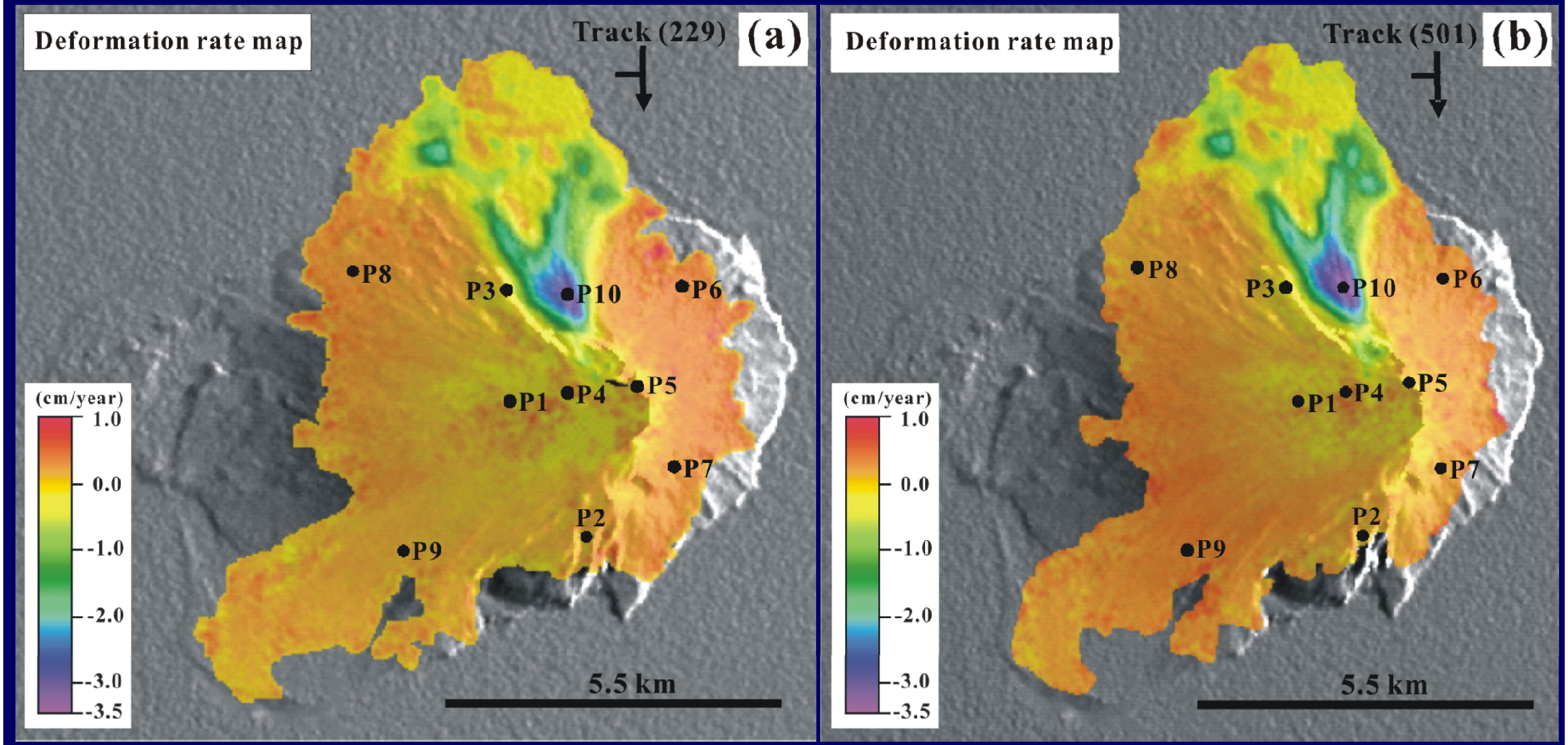

Time-series deformation histories

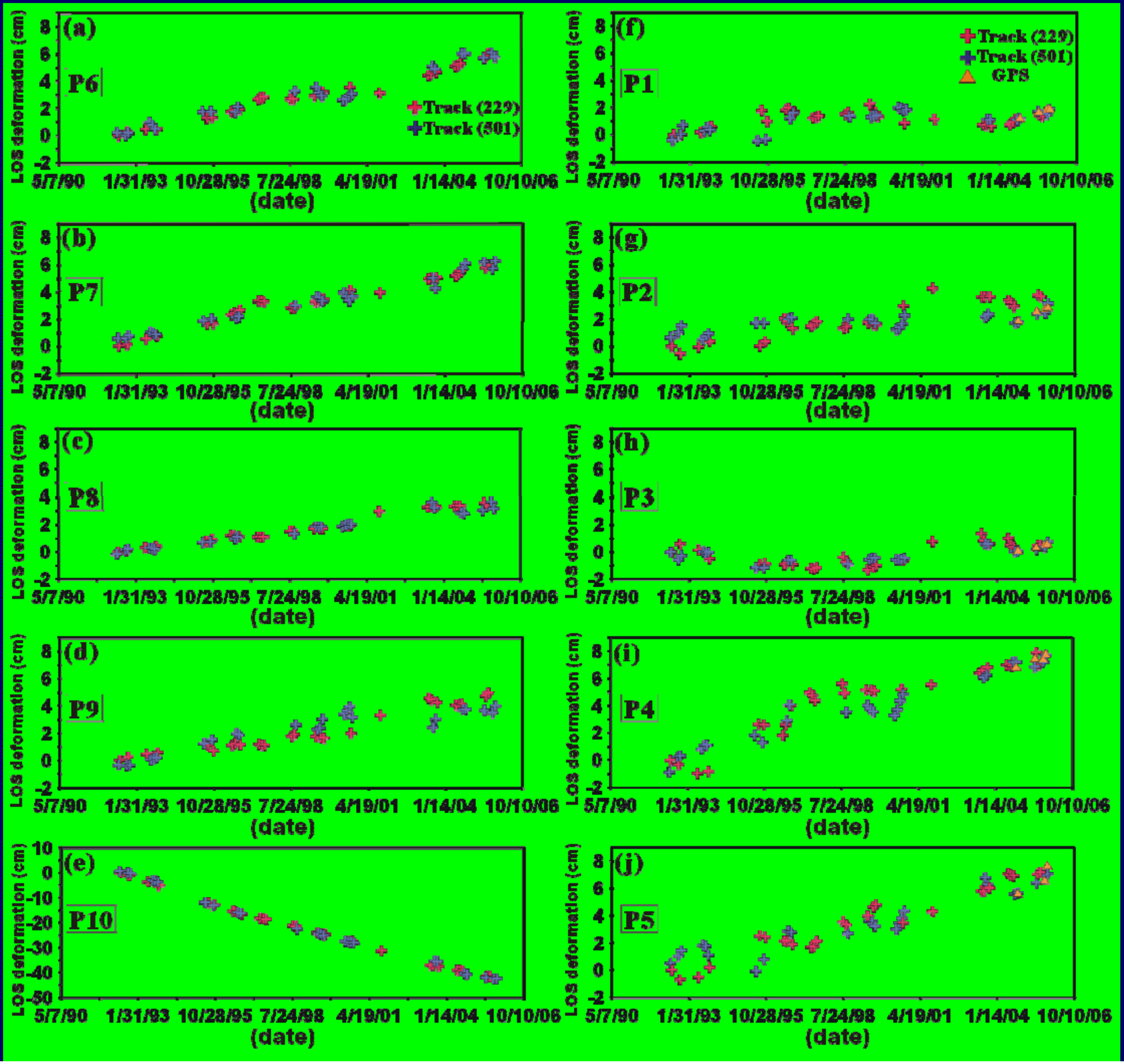

Lee et al., 2010

USGS

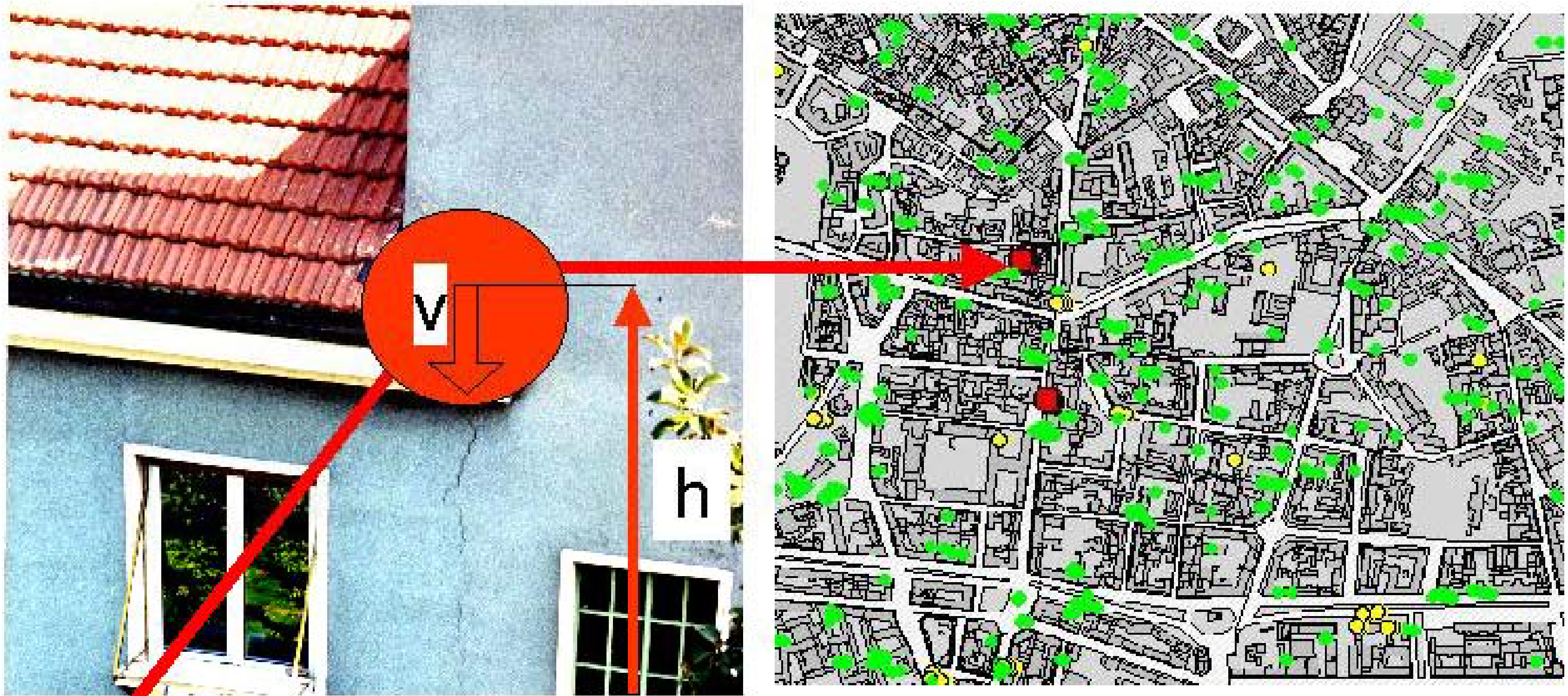

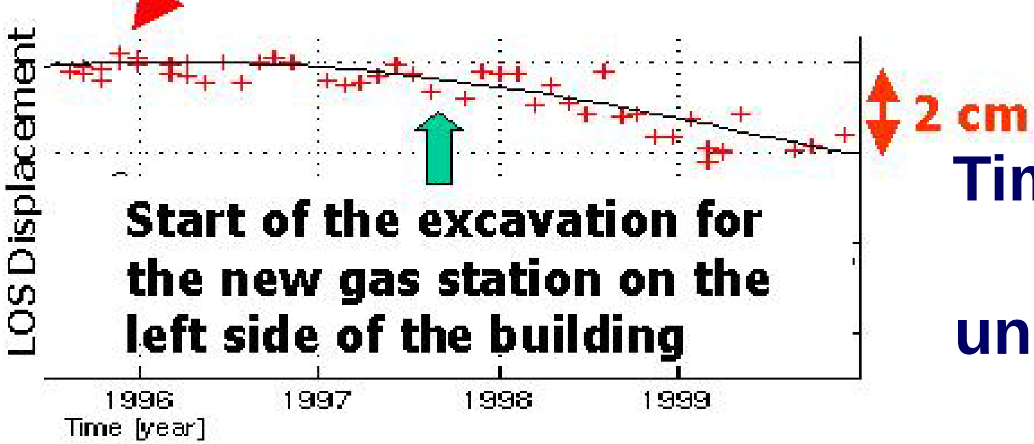

Time-series InSAR detects subsidence due to underground construction

Courtesy of TRE

InSAR Decorrelation Sources

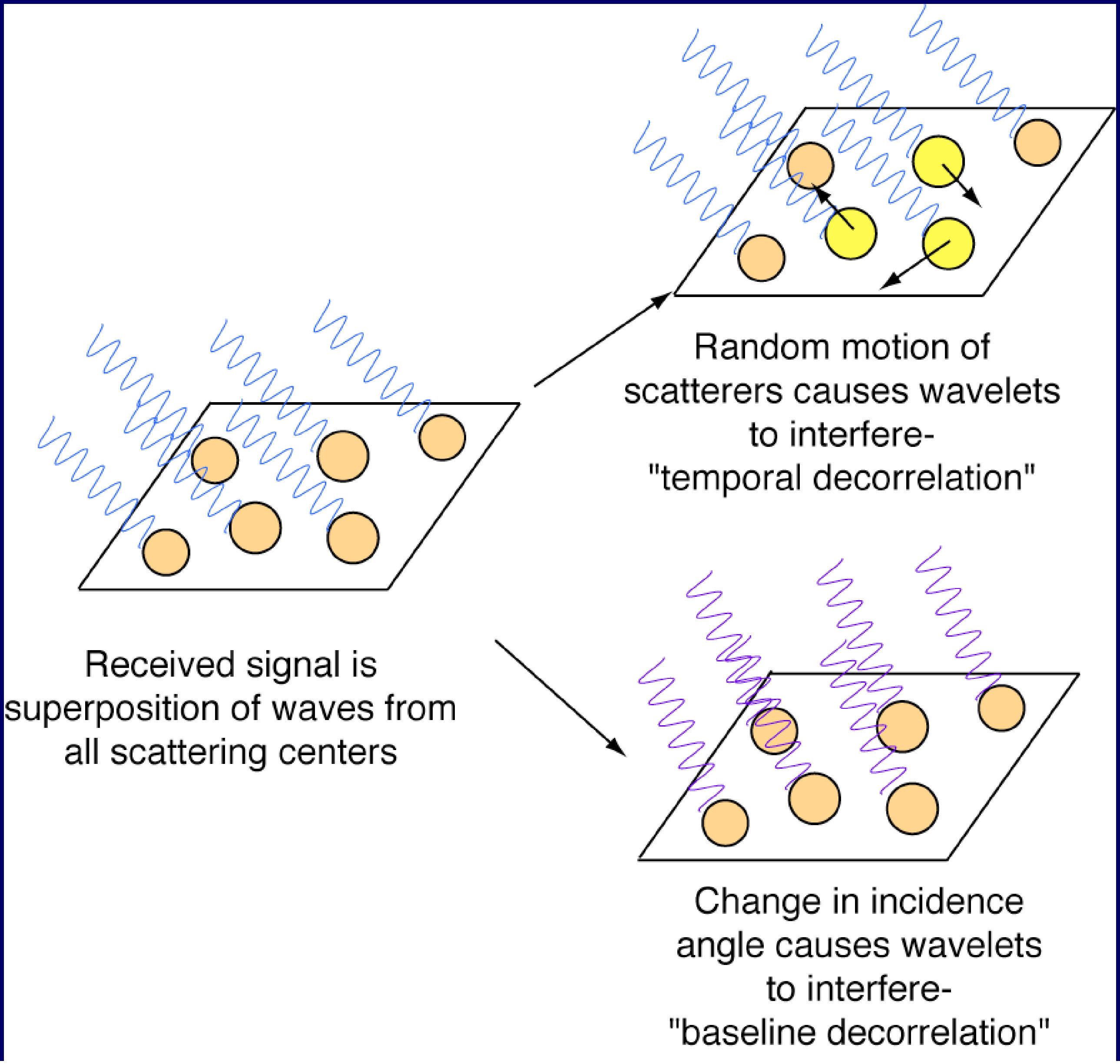

Courtesy of H. Zebker

Loss of InSAR Coherence -Decorrelation

$$Cohrence = \frac{\sum s_1 s_2^*}{\sqrt{\sum s_1 s_1^* \sum s_2 s_2^*}}$$

- Baseline decorrelation
- Temporal decorrelation
- Volume decorrelation
- Rotational decorrelation
- Unspecified noises in system

Coherence image is a by-product of InSAR processing, useful for landscape characterization

Baseline Decorrelation

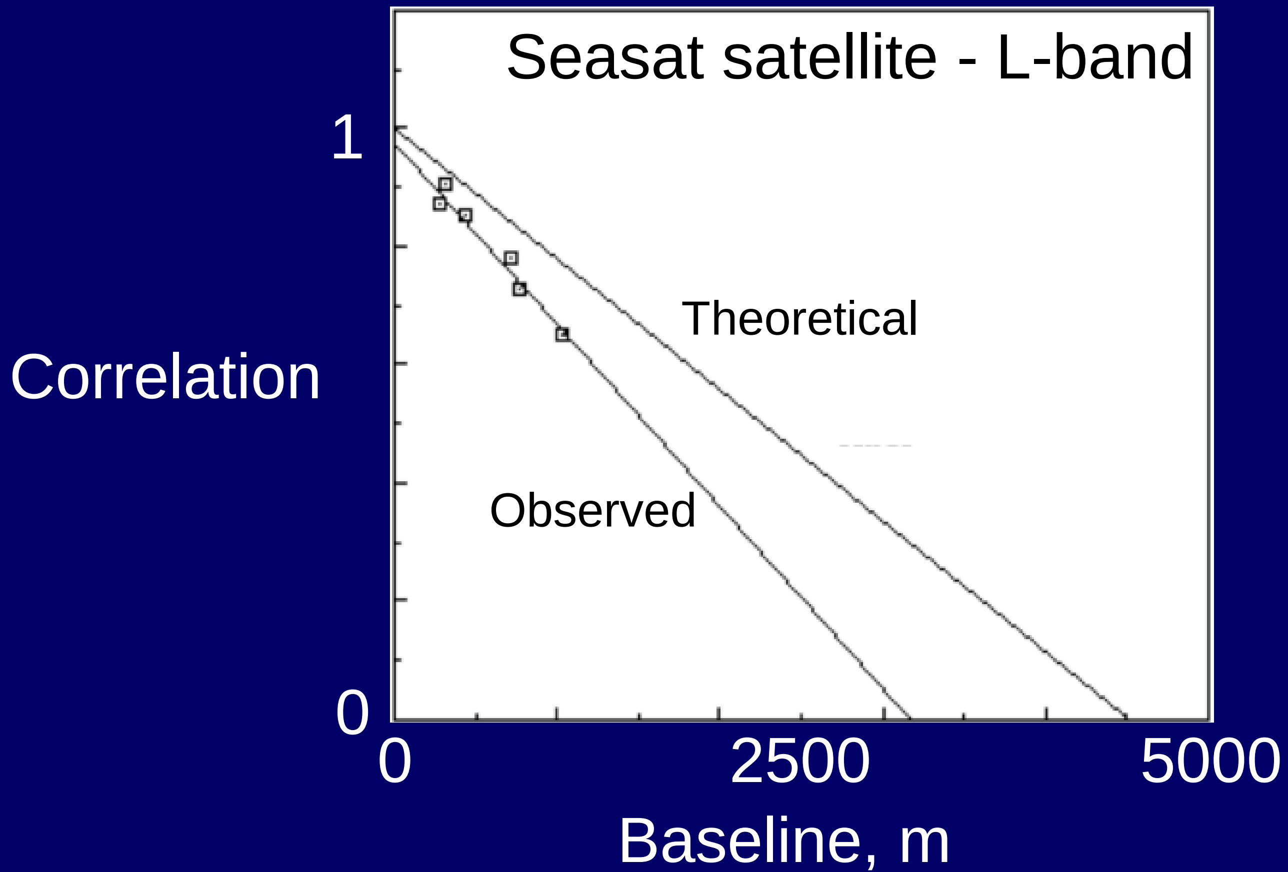

Courtesy of
H. Zebker

Temporal Decorrelation: L-band InSAR

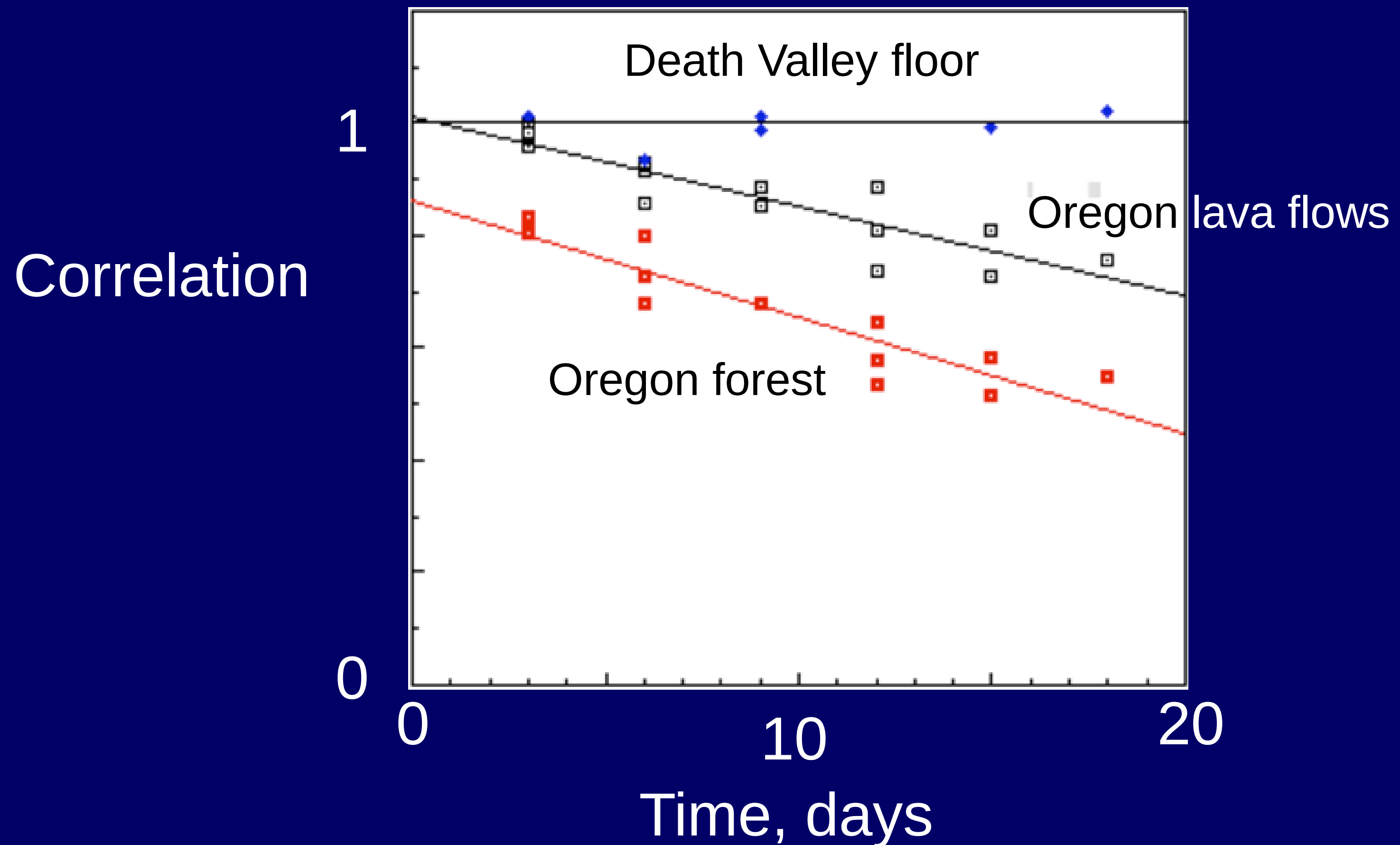

Courtesy of
H. Zebker

Radar Wavelength vs. Coherence

Deformation mapped by ERS (**C-band**, λ = 5.66 cm) InSAR

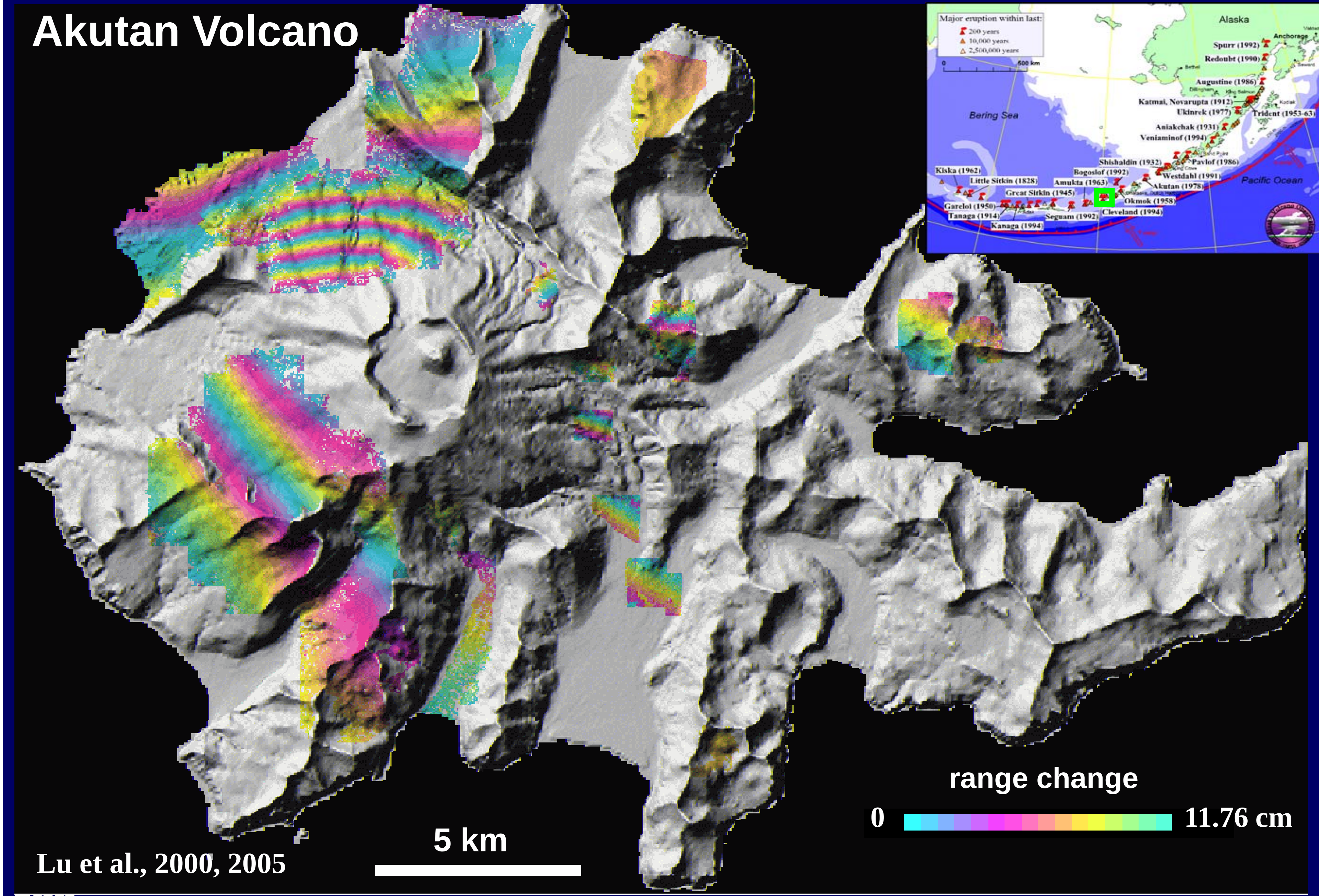

Deformation mapped by JERS (**L-band**, λ = 23.53 cm) InSAR

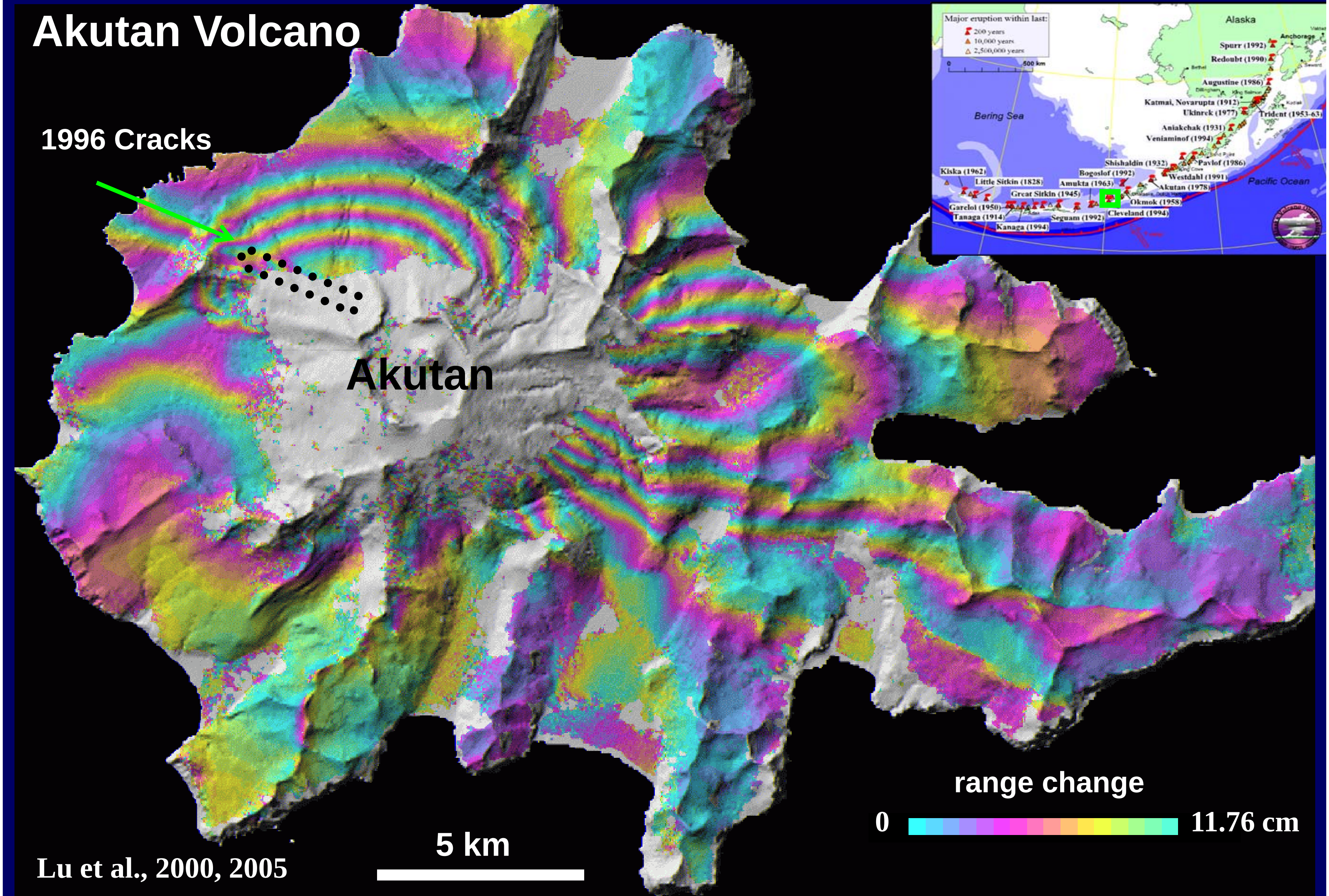

Superior coherence of ALOS over vegetated terrain

C-band Envisat
35-day: 5/14-6/18, 2007
Bp: 36 m

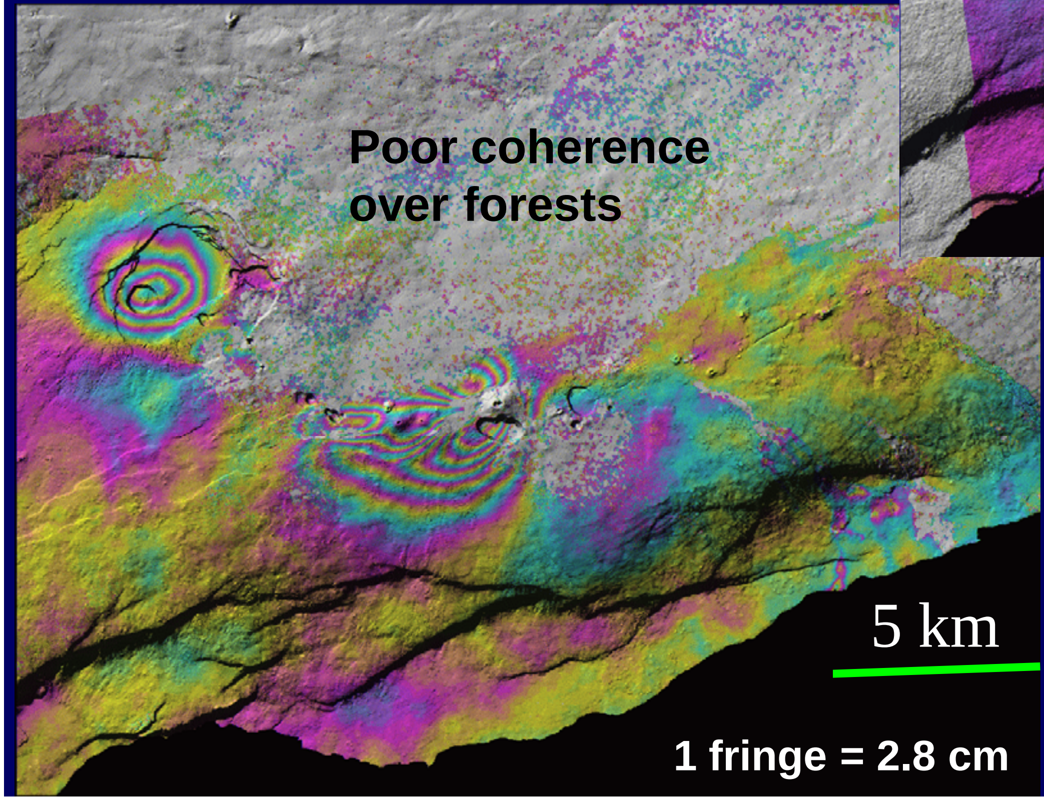

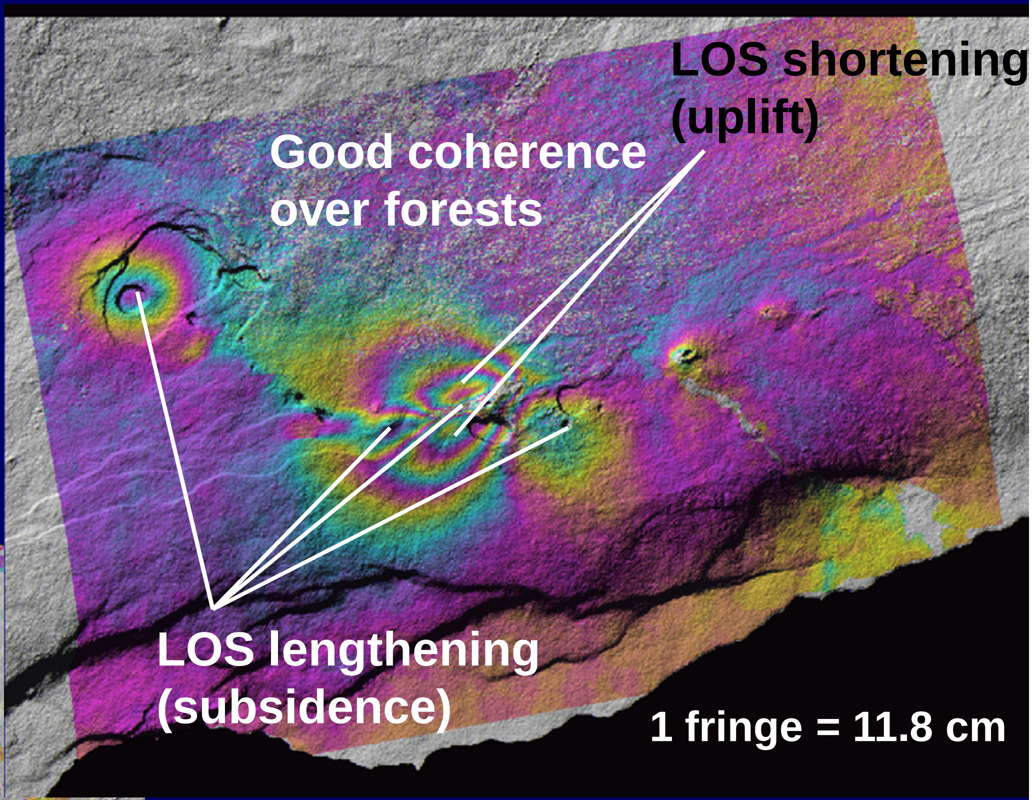

L-band ALOS
46-day: 5/5-6/20, 2007
Bp: 320 m

Lu, 2007

DEM from InSAR

DEM generation from repeat-pass InSAR

- **Issues affecting DEM accuracy**
  - **Baseline uncertainty**
  - **Atmospheric anomalies**
  - **Phase decorrelation**
  - **Surface deformation due to tectonic loading sources**
- **Strategies for accurate InSAR-derived DEM**
  - **Choose interferograms with large baseline within the limit of phase correlation**
  - **Use precision orbit data (DLR, Delft), and refine baseline with GCPs**
  - **Estimate the deformation signal and remove it from the interferograms used for DEM generation**
  - **Average multiple interferograms** $h = \frac{\sum_{i=1}^{4} h_i c_i B_i^2}{\sum_{i=1}^{4} c_i B_i^2}$ **, h – height, c –coherence, B -baseline**

DEM from repeat-pass InSAR

$$\phi = \frac{4\pi}{\lambda} \cdot \frac{B_{\perp} \cdot h}{r \sin\theta} + \phi_{atm} + \phi_{base} + \phi_{def} + \Delta n$$

- Issues affecting DEM accuracy
  - Baseline uncertainty
  - Atmospheric anomalies
  - Phase decorrelation
  - Surface deformation due to tectonic loading sources

$$\Delta\phi_{init} = \frac{4\pi}{\lambda} \frac{B_{\perp}}{H \tan\theta_1} h + \phi_{def} \approx -\frac{2\pi}{9600} B_{\perp} h + \phi_{def}$$

- Strategies for accurate InSAR-derived DEM
  - Choose interferograms with large baseline within the limit of phase correlation
  - Choose interferograms with small temporal baseline
  - Use precision orbit data and refine baseline with GCPs or an existing DEM
  - Estimate the deformation signal and remove it from the interferograms used for DEM generation
  - Fuse multiple interferograms

$$h = \frac{\sum_{i=1}^{4} h_i c_i B_i^2}{\sum_{i=1}^{4} c_i B_i^2}$$

Interfrograms used for DEM generation

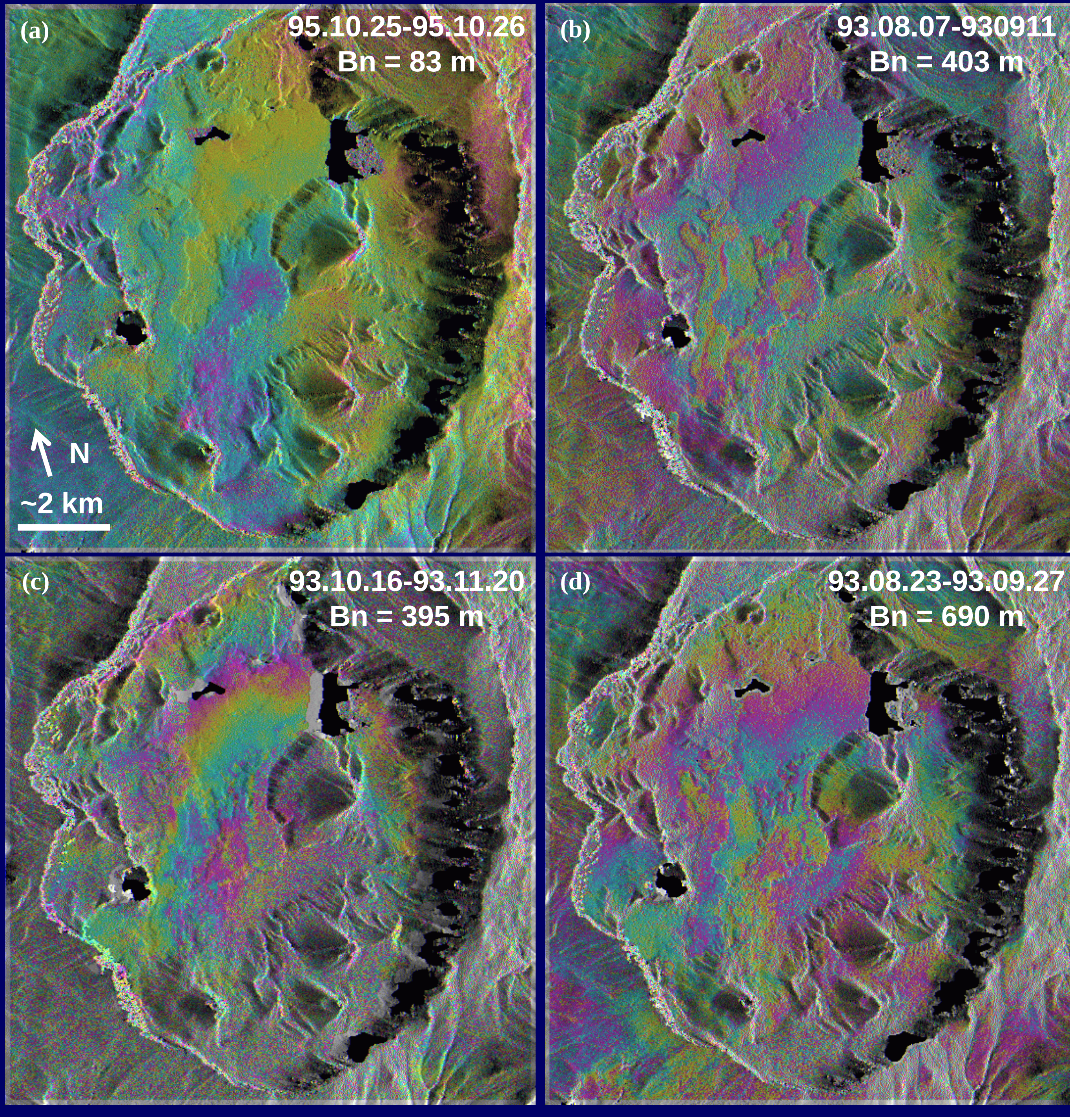

USGS

Pre-eruption DEM of Okmok volcano, Alaska

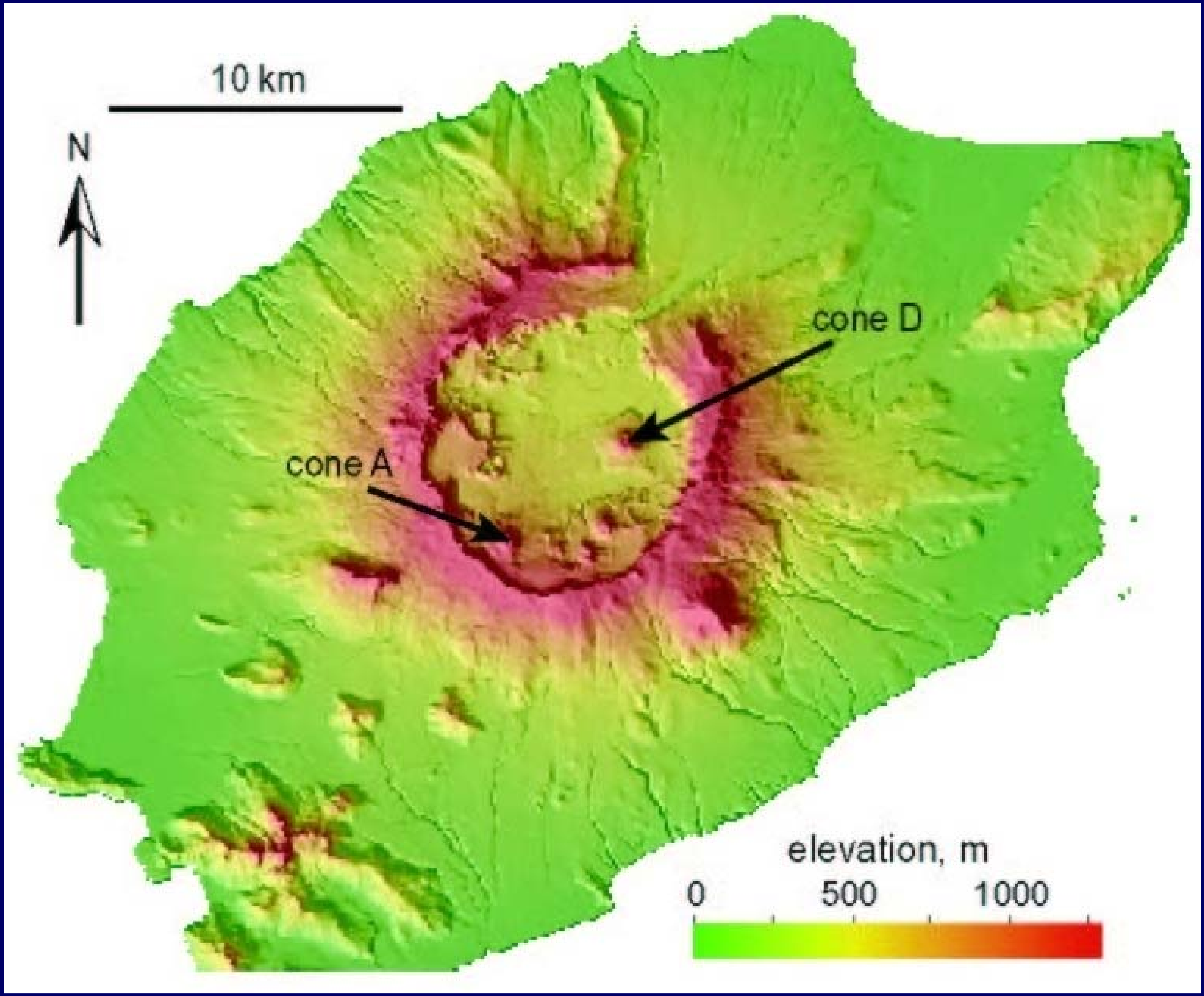

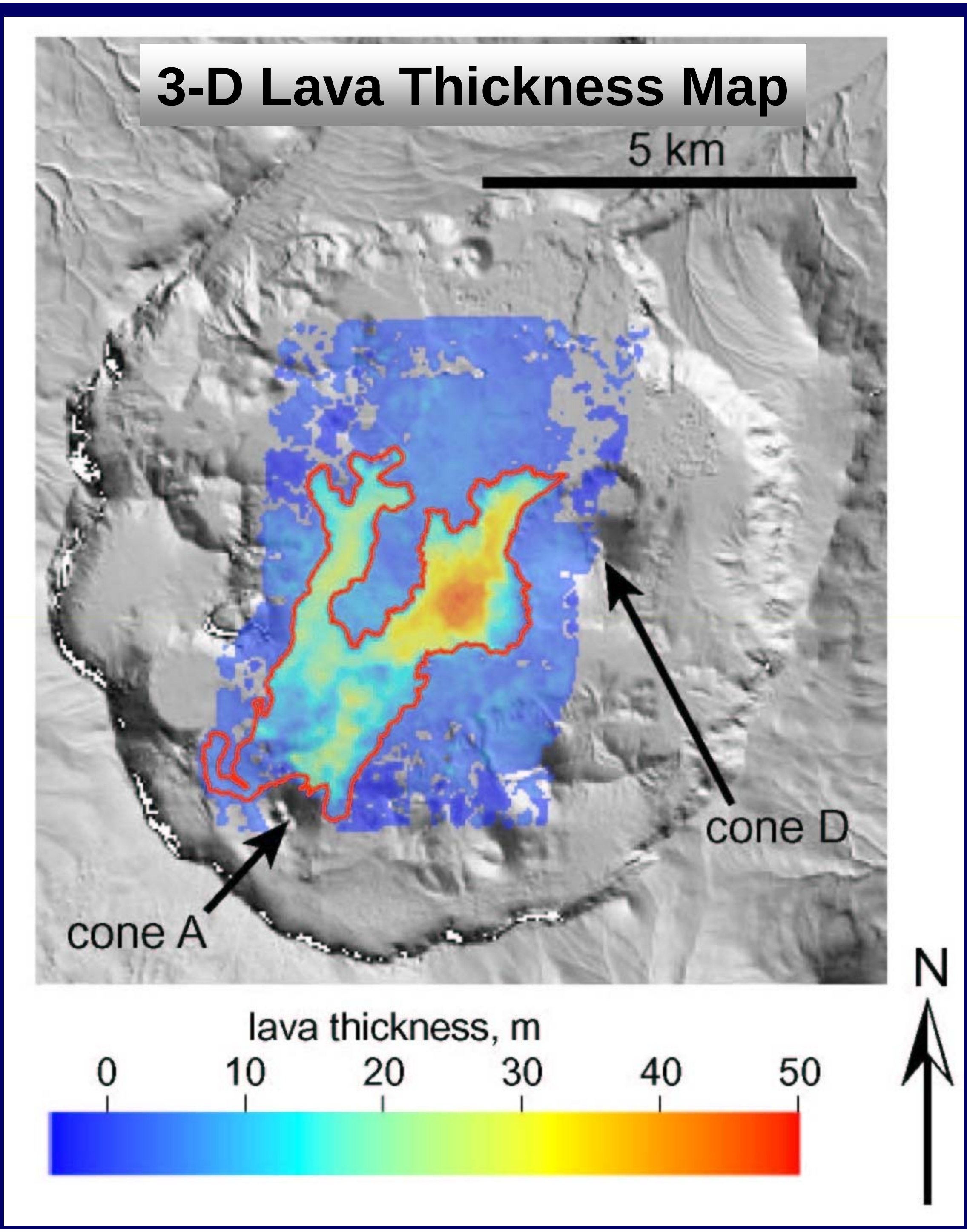
3-D Lava Thickness Map
5 km
cone D
cone A
N
lava thickness, m
0
10
20
30
40
50

Lu et al., 2003

Thickness of lava flows from the 1997 eruption by differencing pre- and post-eruption DEMs

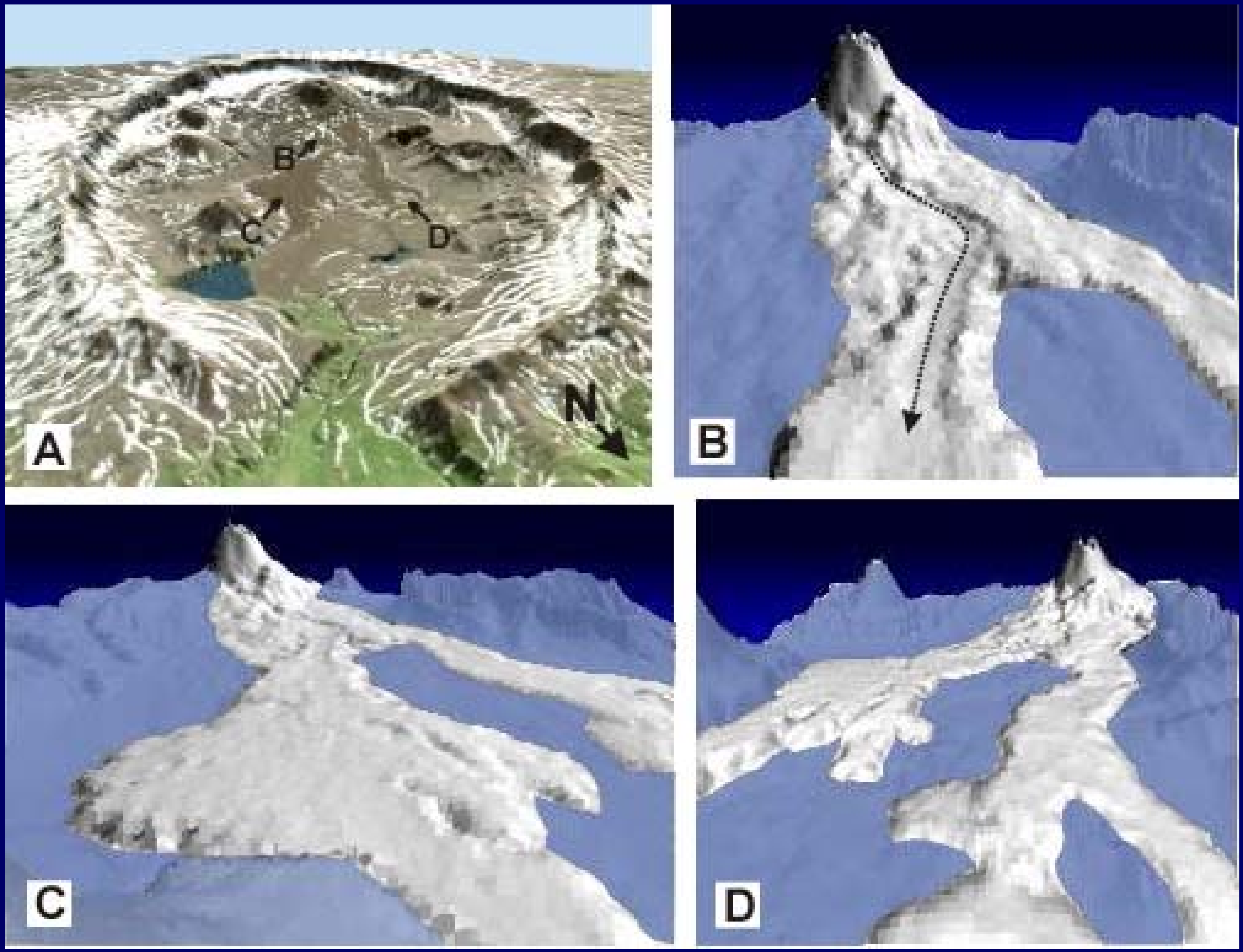

Photo of 1997 Eruption

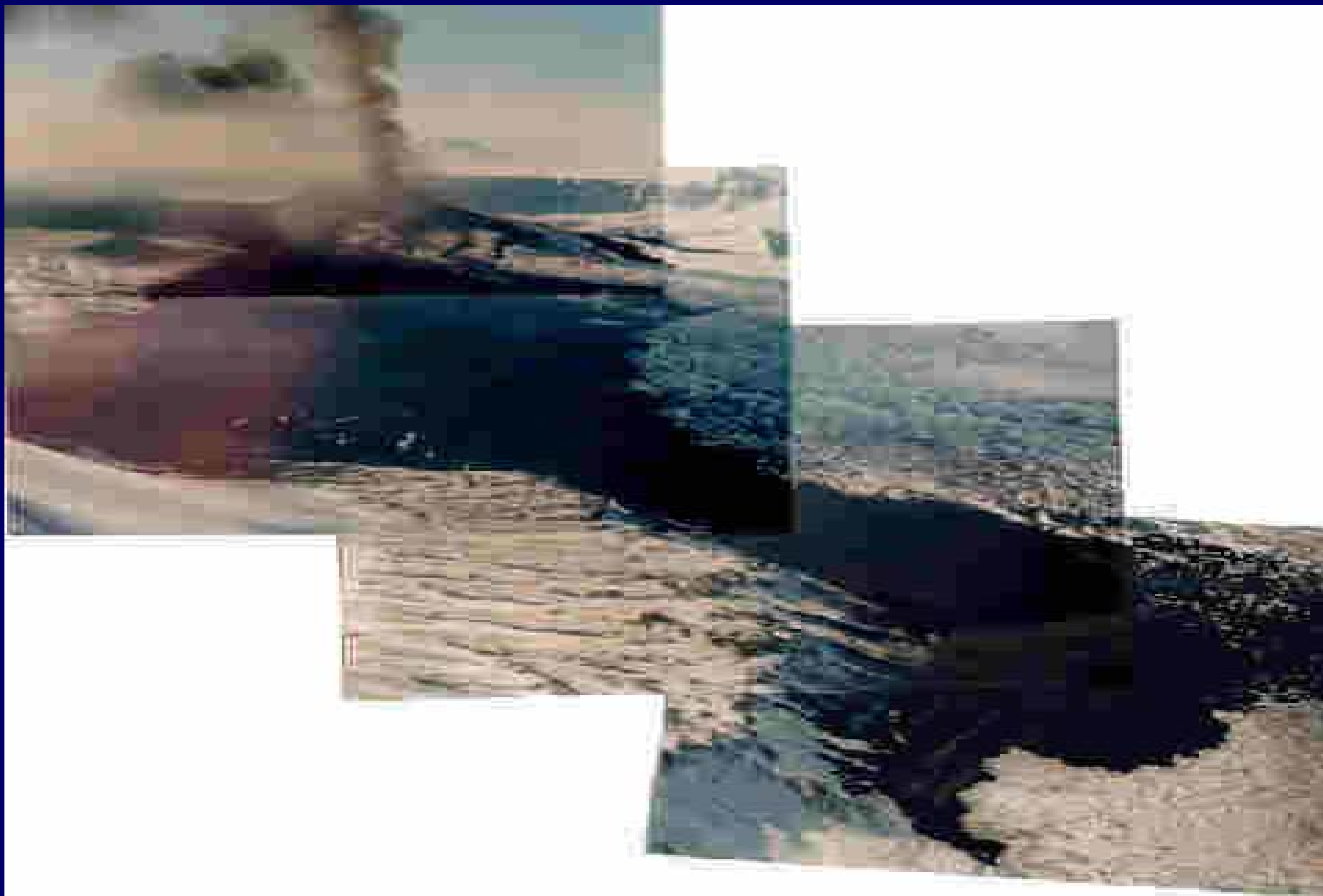

Courtesy of AVO

Photo of New Lava

Courtesy of AVO

3-D Lava Thickness Map

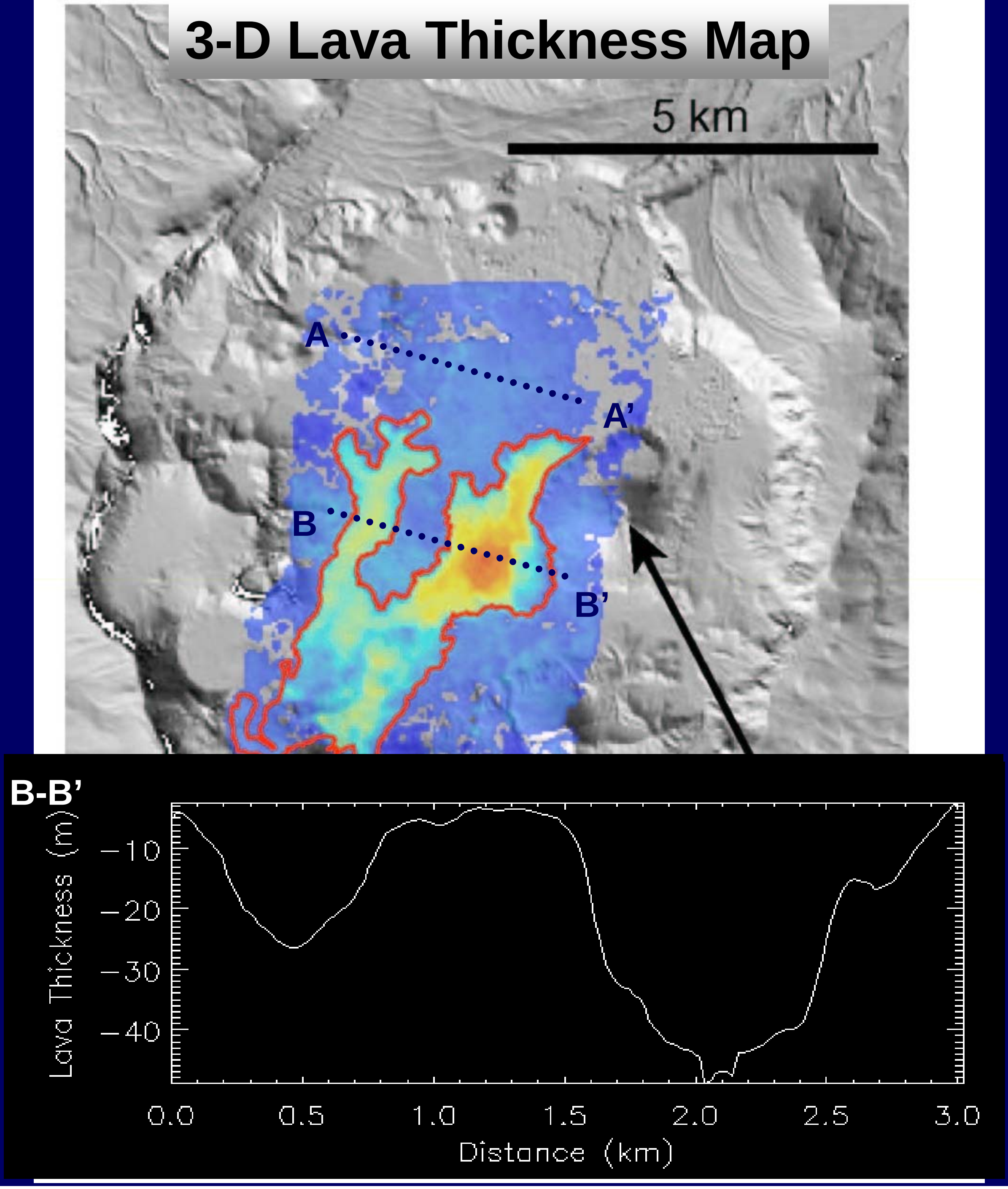

AVHRR Thermal Observations Confirmed Lava Thickness

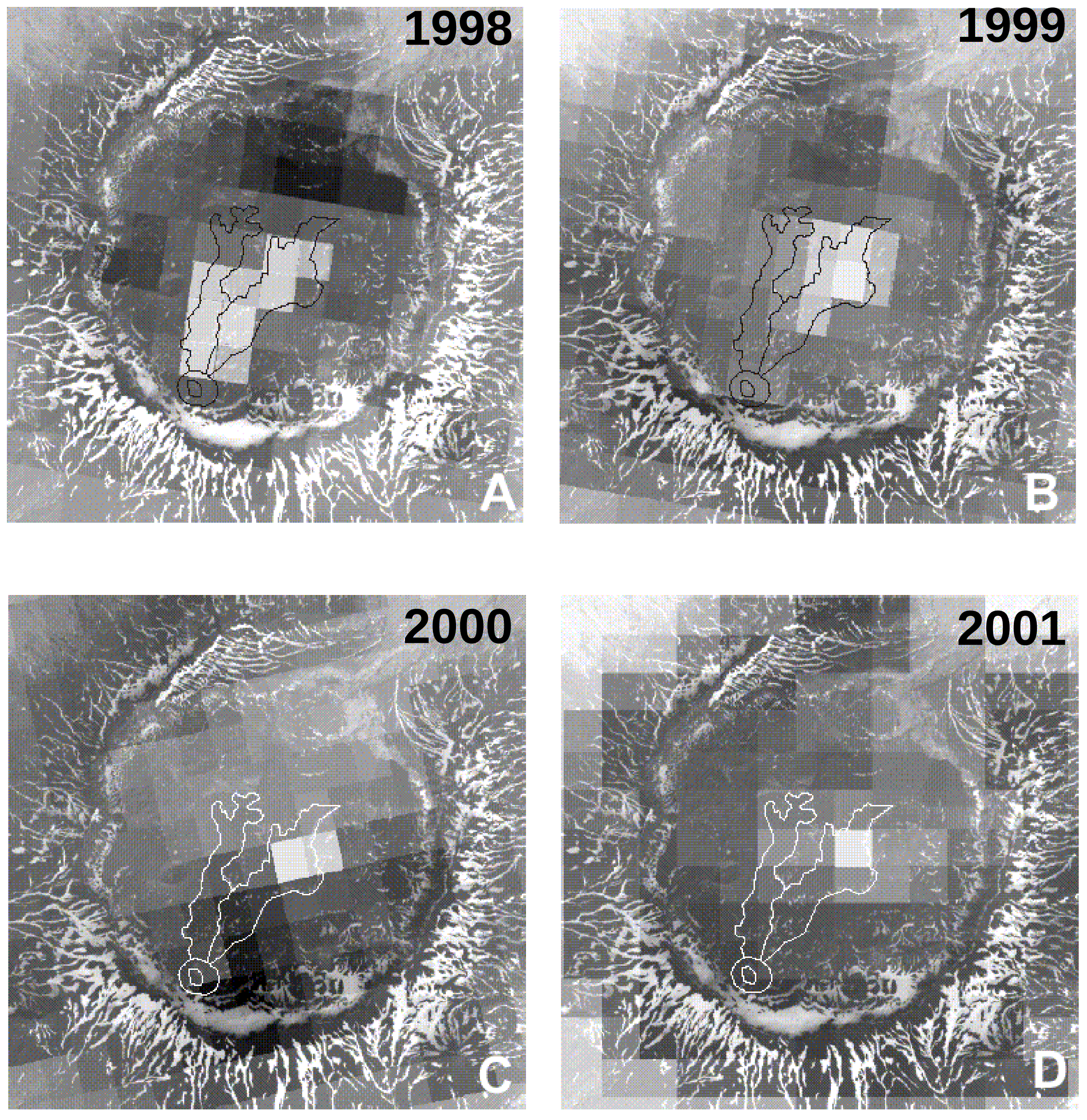

Multi-temporal AVHRR thermal images draped over Landsat-7 Band-8 image

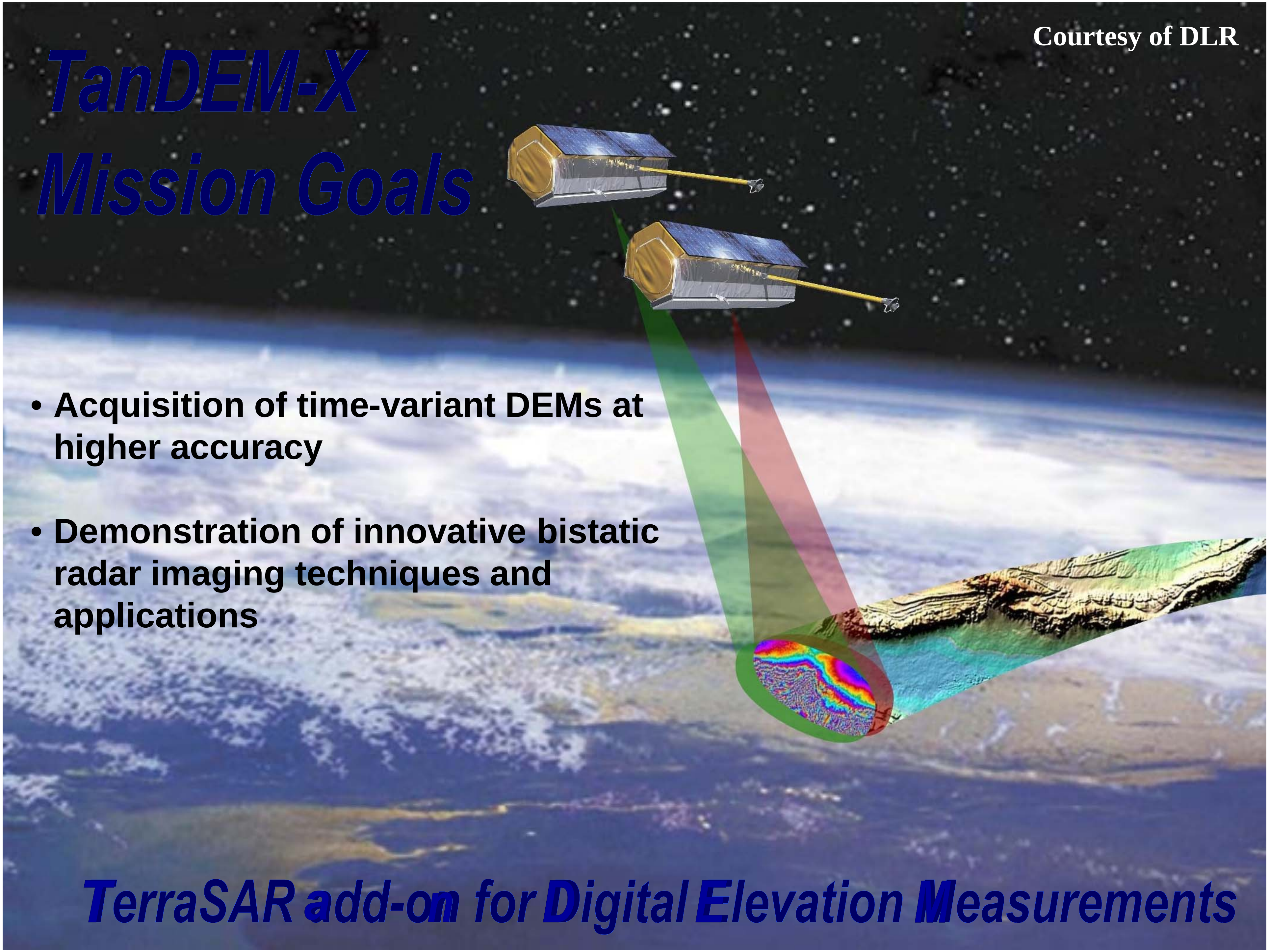
Courtesy of DLR
TanDEM-X
Mission Goals
• Acquisition of time-variant DEMs at higher accuracy
• Demonstration of innovative bistatic radar imaging techniques and applications
TerraSAR add-on for Digital Elevation Measurements

Capabilities of TanDEM-X

Cross-Track Interferometry	Along-Track Interferometry	New Techniques
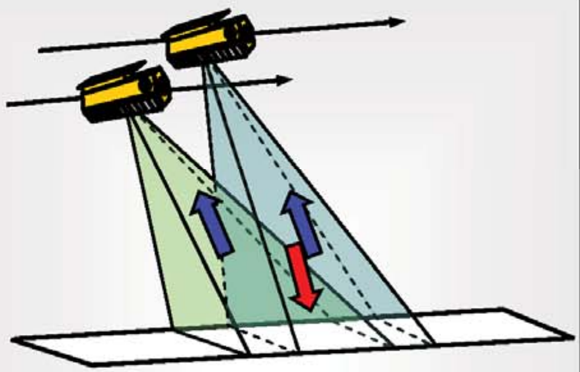	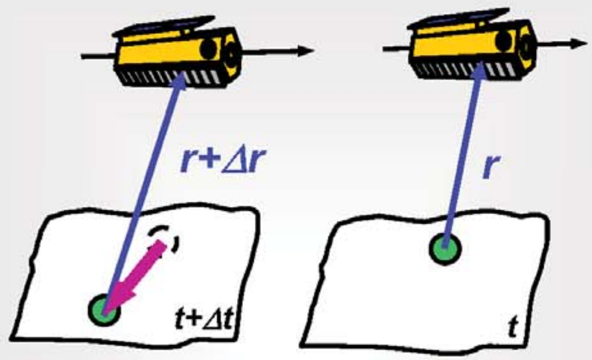	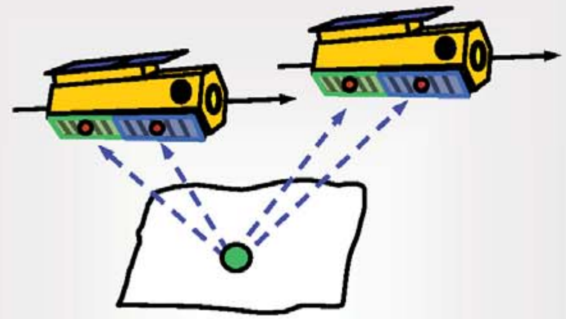
→ **Digital Elevation Models**	→ **Large Scale Velocity Fields** (ocean currents, ice drift, ...)	→ **4 Phase Center MTI** (traffic, ...)
→ **Spatial Coherence** (forest, ...)	→ **Moving Object Detection**	→ **PolInSAR** (vegetation height, ...)
→ **Double DInSAR** (change maps, ..)	→ **Temporal Coherence Maps**	→ **Digital Beamforming** (HRWS, ...)
→ **High Resolution SAR Images**		→ **Bistatic Imaging** (classification, ..)

TanDEM-X is a highly flexible sensor which enables multiple powerful imaging modes

- cross-track baselines (0 km to several km)
- along-track baselines (0 km to several 100 km)
- interferometric modes (bistatic, alternating, monostatic)
- SAR modes (ScanSAR, Stripmap, ...)
- bandwidth / resolution (0 ... 150/300 MHz)
- incident angles (20° ... 55°)
- polarisations (single, dual, quad)
- ...

Safe & Well-Controlled Close Formation Flight

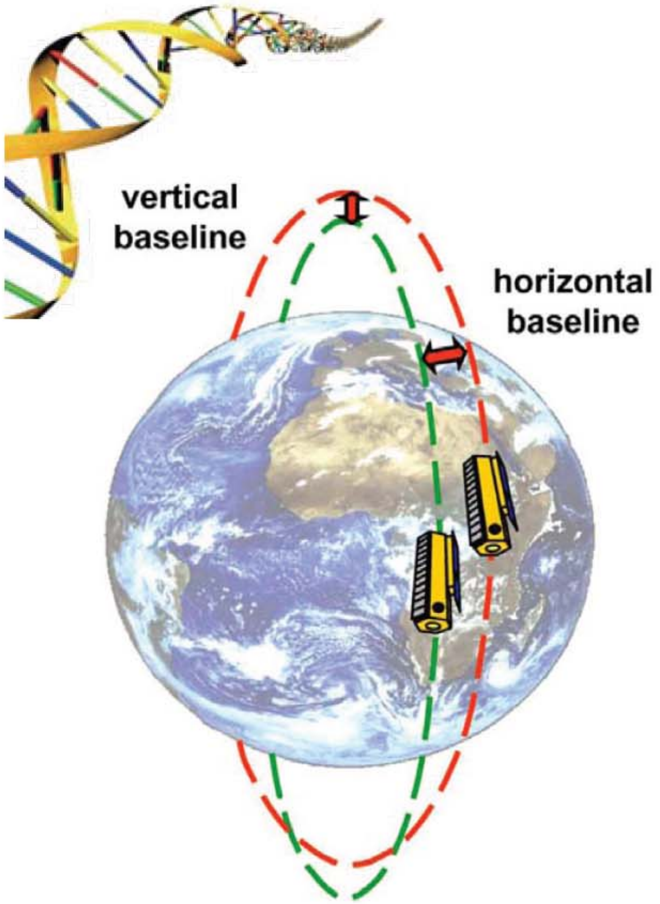

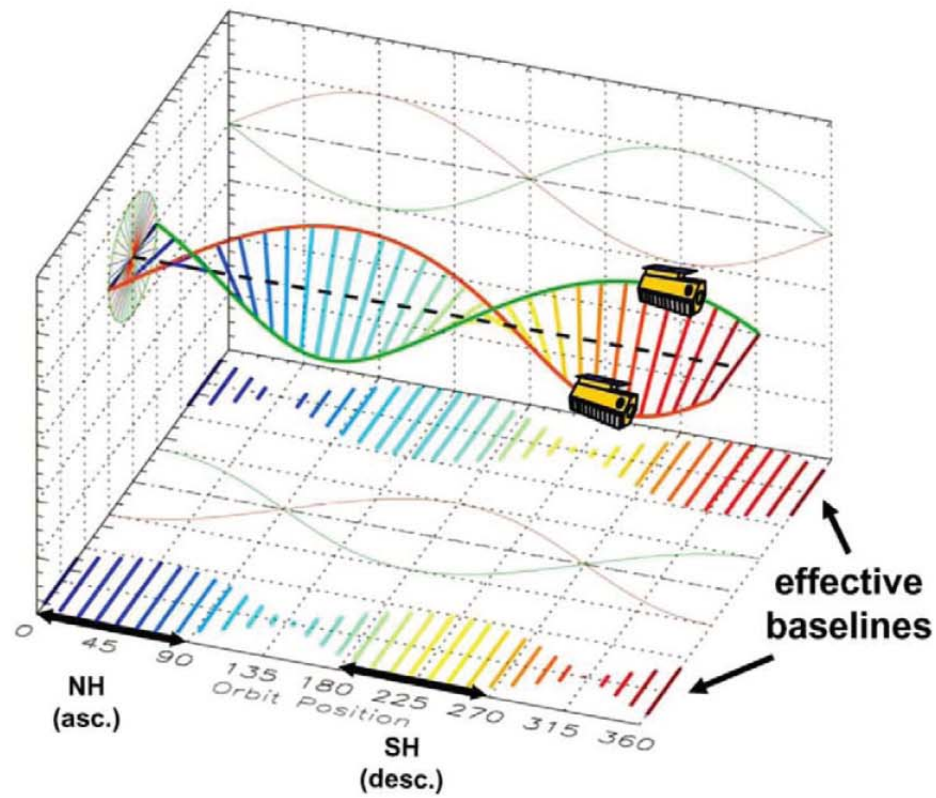

Baseline determination to mm-accuracy

TanDEM-X: DEM Specifications

	Spatial Resolution	Absolute Vertical Accuracy (90%)	Relative Vertical Accuracy (point-to-point in 1° cell, 90%)
DTED-1	90 m x 90 m	< 30 m	< 20 m
DTED-2	30 m x 30 m	< 18 m	< 12 m
HRTI-3	12 m x 12 m	< 10 m	< 2 m
HRTI-4	6 m x 6 m	< 5 m	< 0.8 m

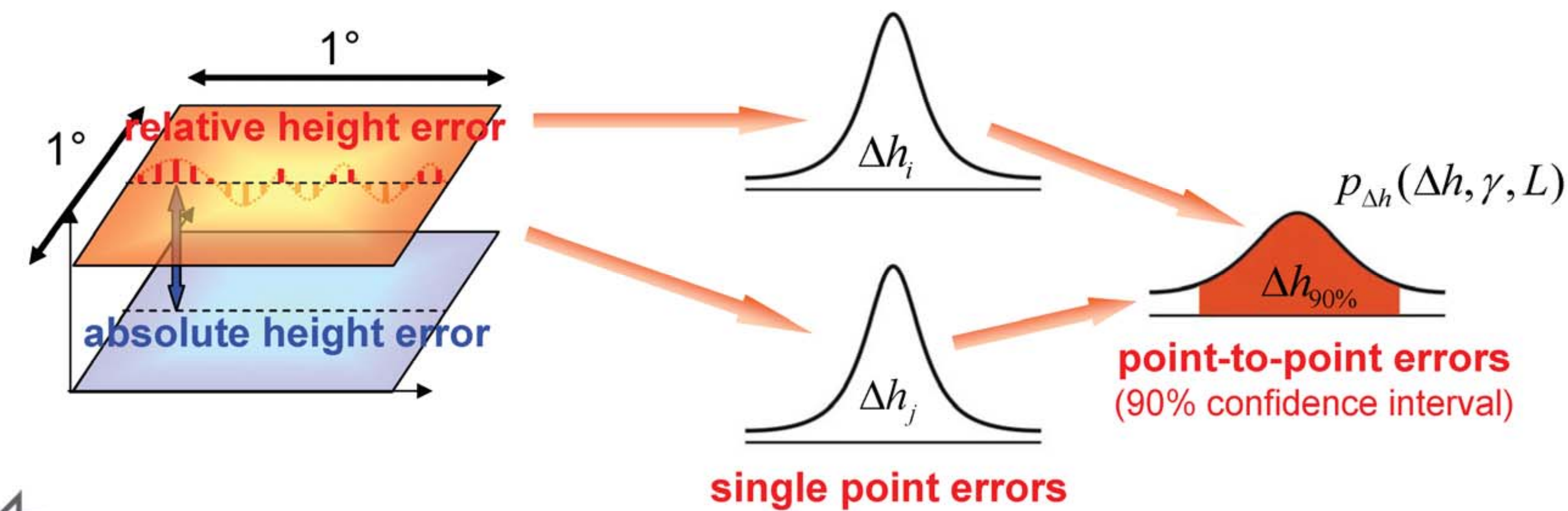

General Outline of the Data Acquisition Plan

	1 year	1 year	6 months	≥ 3 months
Commissioning Phase	1 global DEM acquisition with small baselines + acquisition of approx. 1000 scientific radar data products	1 global DEM acquisition with scaled (larger) baselines + acquisition of scientific radar data products	additional DEM data takes for difficult terrain and filling-in of possible gaps + radar data products	radar data products and customized DEMs with large interferometric baselines

Deutsches Zentrum für Luft- und Raumfahrt e.V.
in der Helmholtz-Gemeinschaft

Courtesy of DLR

ScanSAR InSAR Processing

- Scan-mode SAR (ScanSAR) is achieved by periodically increasing the antenna look angle to illuminate neighboring sub-swaths in the cross-track direction, thereby increasing the size of the accessible image swath to 400–500 km (compared to ~100 km for conventional SAR).

- Because ScanSAR can acquire more frequent observations of a given study area than is possible with strip-mode SAR, ScanSAR InSAR can significantly improve the temporal resolution of deformation mapping.

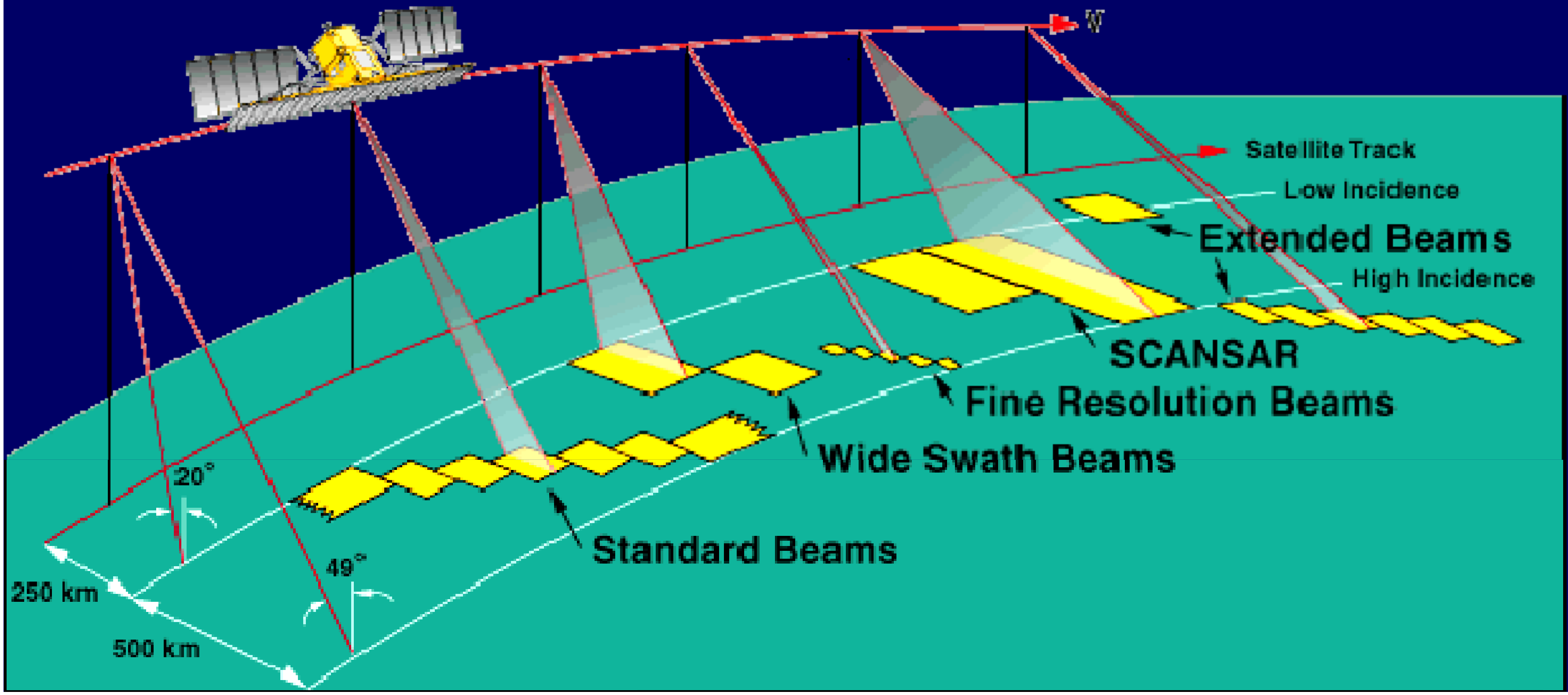

Strip-mode (conventional) InSAR

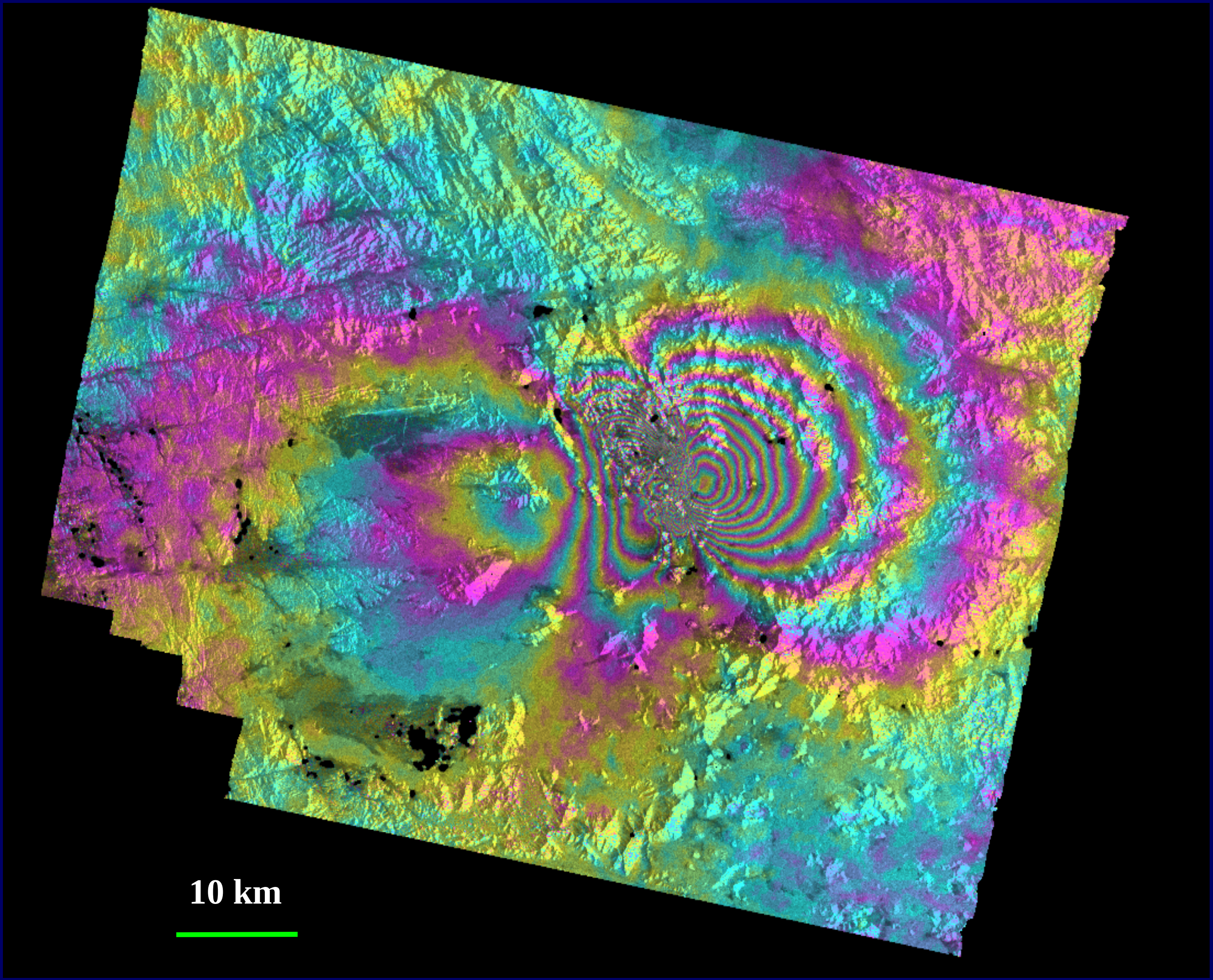

Ground surface deformation over western Saudi Arabia during May 2009 Seismic Swarm

Lu et al., 2010

ScanSAR InSAR

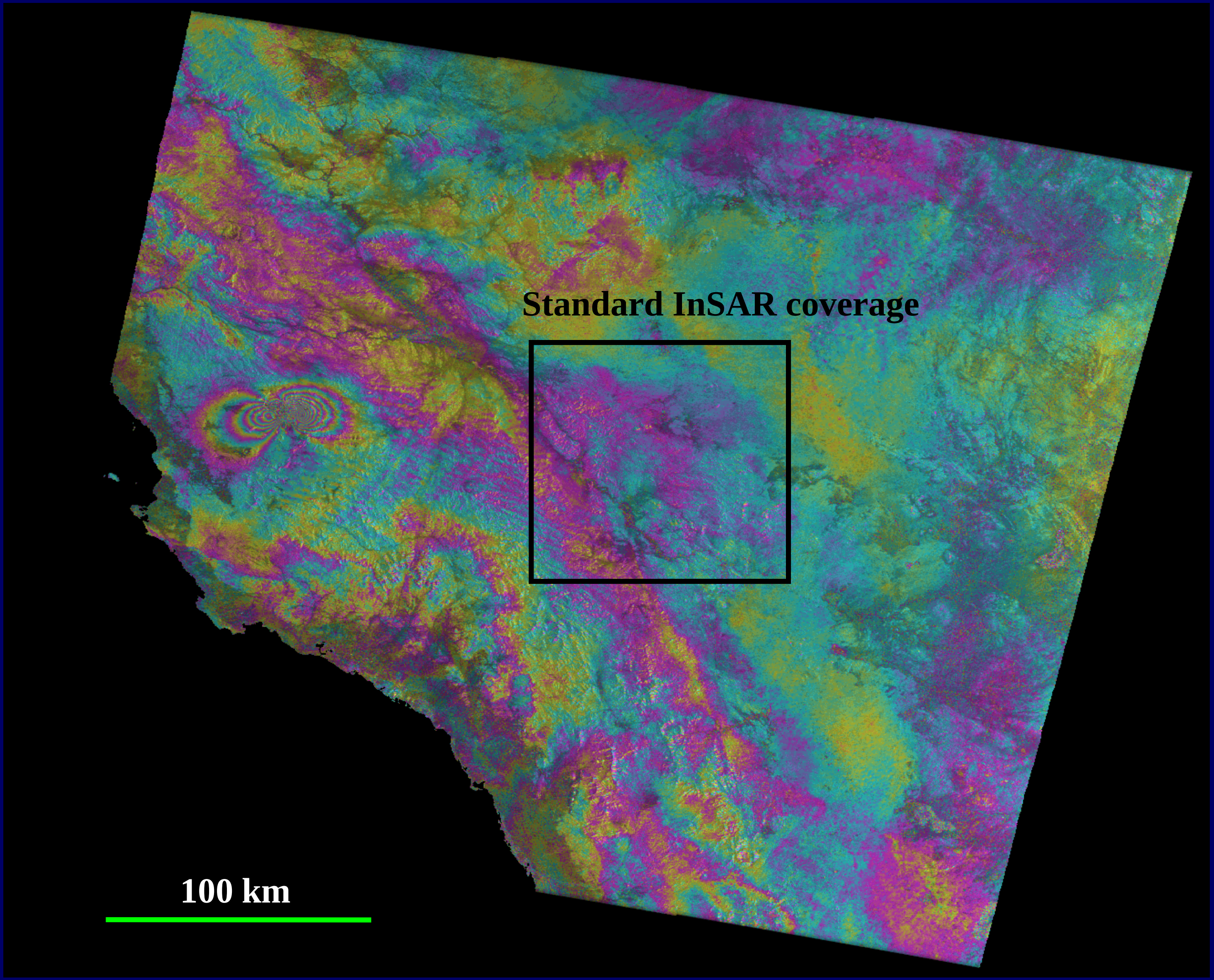

Ground surface deformation over western Saudi Arabia during May 2009 Seismic Swarm

Lu et al., 2010

Summary

About SAR/InSAR

- SAR – all-weather day and night operational imaging capability, sensitive to terrain slope, surface roughness and dielectric constant.

- Interferometric synthetic aperture radar (InSAR) combines phase information from two or more radar images of the same area acquired from similar vantage points at different times to produce an interferogram.

- The interferogram, depicting range changes between the radar and the ground, can be further processed with a digital elevation model (DEM) to image ground deformation at a horizontal resolution of tens of meters over areas of ~100 km x 100 km with centimeter to sub-centimeter precision under favorable conditions.

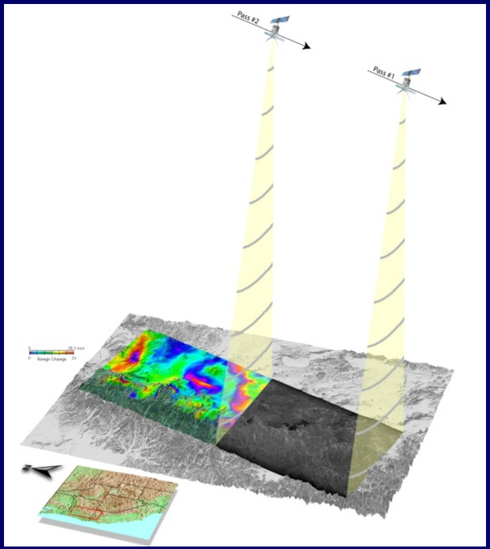

Deflation **Inflation**

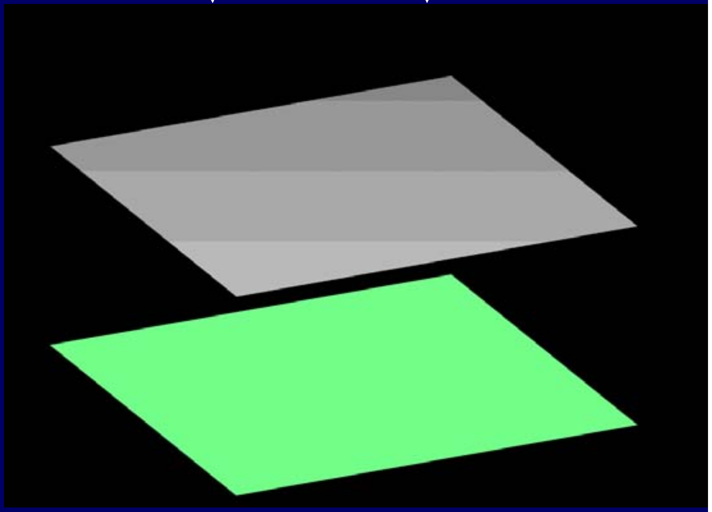

InSAR Products

- SAR intensity images -
  - terrain slope
  - roughness
  - dielectric constant

- InSAR coherence image -
  - change detection

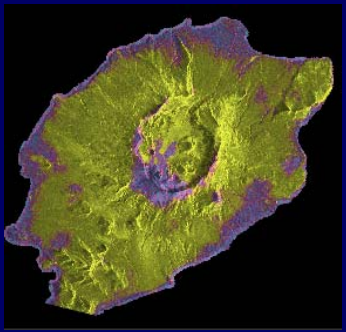

- InSAR deformation image -
  - deformation & modeling

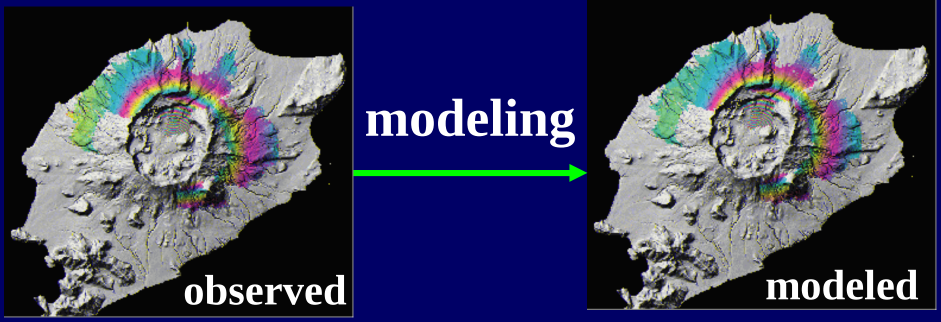

- InSAR DEM

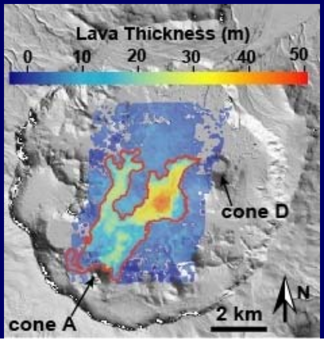

USGS

Synthetic Aperture Radar Satellites

• European ERS-1,	1991-2000,	C-band,	35-day repeat	
• Japanese JERS-1,	1992-1998,	L-band,	44-day repeat	
• European ERS-2,	1995-now,	C-band,	35-day repeat	
• Canadian Radarsat-1,	1995-now,	C-band,	24-day repeat	
• European Envisat,	2002-now,	C-band,	35-day repeat	
• Japanese ALOS,	2006-now,	L-band,	46-day repeat	
• German TerraSAR-X,	2007-now,	X-band,	11-day repeat	⊕
• Italian COSMO-SkyMed,	2007-now,	X-band,	16-day repeat	⊗
• Canadian Radarsat-2,	2007-now,	C-band,	24-day repeat	
• German TanDEM-X	2010-now,	X-band,	11-day repeat	⊕

⊕ **Tandem Missions**

⊗ **Constellations**

Wavelength (λ)
- X-band: λ = ~3 cm
- C-band: λ = ~5.7 cm
- L-band: λ = ~24 cm